Network Solution as a Facilitator for Precise Point Positioning Real-Time Kinematic (PPP-RTK)

Christopher Edward Robert Pearson

Thesis submitted for the degree of

Doctor of Philosophy

School of Engineering

Newcastle University

May 2018

Abstract

Precise Point Positioning (PPP) is a Global Navigation Satellite System (GNSS) processing technique for obtaining decimetre level accuracy in real-time applications within a Kalman filter. PPP is based on knowledge of the GNSS orbits and requires access to precise GNSS ephemerides and clocks. As orbital errors are long-wavelength, GNSS orbits can be predicted with high accuracy, but GNSS clocks are highly variable and not deterministic. The limiting factors of PPP are therefore GNSS clock, as well as inability to fix ambiguities to integer values. The latter is due to Uncalibrated Phase Delays (UPDs), which exist in the hardware of the receivers and satellites, and destroy the integer nature of the undifferenced ambiguities.

In Network Real-Time Kinematic (NRTK) positioning, UPD errors cancel when double differencing the observations. But NRTK requires a dense network of base stations close to the user, which is not practical offshore. However, the stability of the UPDs over large distances and in time can allow a network of receivers to be employed to estimate the UPDs, which can be broadcast to the user. Various models exist to estimate UPDs, enabling a user, ambiguity fixed solution to be produced, in a method known as Precise Point Positioning Real-Time Kinematic (PPP-RTK).

This study will use L1 and L2 frequencies independently in a measurement model capable of estimating the UPD and satellite clock parameters simultaneously. The estimated parameters can be transmitted to the user to acquire an ambiguity fixed position in real time.

A series of tests show how factors such as the number of stations in the network, interstation distances and location of the user with respect to the network affect the accuracy of the user position. Tests show by using satellite clock and UPD corrections at a rover station it is possible to obtain position estimates with a root mean square error of 16 mm in plan and 23 mm in height.

Acknowledgements

This research project was jointly funded by Fugro Intersite and the Engineering and Physical Sciences Research Council (EPSRC).

GNSS data used throughout this project was provided by the Natural Environment Research Council (NERC) British Isles GNSS Facility (BIGF).

I would like to thank my supervisors at Newcastle University, Professor Philip Moore and Dr Stuart Edwards for their support and guidance throughout the PhD, which has been instrumental to the completion of this project.

I would also like to thank Fugro Intersite for their support during the project and in particular the late Dr Kees de Jong, as without his guidance at the beginning of the project, this PhD would not have been possible.

Fellow PhD students within the geomatics group at Newcastle University and members of the geodesy group have also provided invaluable advice and help during the project.

Finally, I wish to thank my family and friends who have supported me throughout the PhD. In particular I must thank my wife Beth who has always been there to offer support, advice and friendship.

Table of Contents

List of Figures & Tables

List of Abbreviations

ANTEX – ANTenna EXchange

BIGF – British Isles GNSS Facility

CNES – Centre National d'Etudes Spatiales

DOY – Day Of Year

DIA – Detection Identification and Analysis

GFZ – GeoForschungsZentrum

GIM – Global Ionospheric Model

GNSS – Global Navigation Satellite System

GPS – Global Positioning System

IAR – Integer Ambiguity Resolution

IGS – International GNSS Service

ILS – Integer Least Squares

JPL – Jet Propulsion Laboratory

LAMBDA – Least-squares AMBiguity Decorrelation Adjustment

NL – Narrow Lane

NRTK – Network Real-Time Kinematic

OMC – Observed Minus Computed

OS Net – Ordnance Survey GNSS base station NETwork

PPP – Precise Point Positioning

PPP-RTK – Precise Point Positioning Real-Time Kinematic

PRN – Pseudo Random Noise

RHCP – Right Handed Circularly Polarised

RMS – Root Mean Square

RTK – Real-Time Kinematic

UPD – Uncalibrated Phase Delay

UT – Universal Time

VRS – Virtual Reference Station

WL – Wide Lane

Chapter 1. Introduction

1.1 Background

In the offshore industry, position is vitally important for many applications in surveying and navigation including; monitoring oil rig subsidence, bathymetric surveys and pipeline route surveys. The main positioning method in recent years has employed Global Navigation Satellite Systems (GNSS) in a variety of modes but increasingly the technique of Precise Point Positioning (PPP) has been employed. This has led to decimetre level accuracy positioning with the use of just a single receiver. However, both time and accuracy are critical for the majority of offshore applications such as pipeline surveys and oil rig monitoring. The cost of an offshore rig is between £500,000 and £1 million per day (Allinson, 2012). Therefore, time and accuracy is essential to deliver a project on budget. Consequently, if PPP accuracies can be further increased and convergence times decreased it would provide improvements for the offshore industry.

One of the main limitations of undifferenced PPP processing is the inability to undertake Integer Ambiguity Resolution (IAR). The ability to correctly fix the ambiguities to integer values has the effect of making the carrier phase observations into a precise range measurement between the satellite and the receiver. IAR is not possible in undifferenced PPP due to the existence of Uncalibrated Phase Delays (UPDs), which corrupt the integer nature of the ambiguities (Geng *et al.*, 2011), making fixing impossible. Therefore, to allow IAR the UPDs need to be either removed or estimated.

Processing strategies that allow IAR exist for onshore or nearshore applications such as relative Real-Time Kinematic (RTK). This method employs double differenced observations to cancel out the UPDs, along with other GNSS errors, such as, the ionosphere and troposphere. Hence, restoring the integer nature of the ambiguities. This method is capable of achieving centimetre level precision with decreased convergence times compared to PPP. However, to achieve these high accuracies the required reference receiver must be within 10-20 km of the rover (Wanninger, 2004). This is not practical for the majority of offshore applications. Therefore, a processing technique that is able to employ more distant reference receivers is required.

Over the past few years, multiple studies such as Ge *et al.* (2008) and Geng *et al.* (2010a) have been conducted into PPP accuracy and convergence time. Some of these studies have been able to show that through the calculation and application of UPDs, the accuracy and convergence time can be significantly improved. The UPDs originate as hardware delays in both the receiver and the satellites, but are potentially stable over time and location. Therefore, there is an opportunity to calculate the UPDs, which are then transmitted to a receiver so that they can be incorporated into the rover solution. The incorporation of UPDs into the solution should remove the fractional part of the non-integer phase offset, which will then allow a fixed integer ambiguity solution to be obtained at the zero difference level. This will provide benefits to the accuracy and the convergence time, allowing Precise Point Positioning Real-Time Kinematic (PPP-RTK) to be a viable alternative to existing offshore processing techniques.

The viability of PPP-RTK has already been demonstrated using the GPS LC frequency, which is a combination of the L1 and L2 frequencies (Geng *et al.*, 2011; Laurichesse, 2011). However, this project will concentrate on using the L1 and L2 frequencies separately. One advantage of calculating the UPDs in this way is that the addition of other satellite systems (e.g. Galileo/GLONASS/Beidou), as well as, additional frequencies on the GPS satellites can be easily accommodated into the calculations. The incorporation of more observations would also allow further redundancy to be incorporated within the system potentially, providing more accurate results.

The use of L1 and L2 frequencies separately to calculate UPDs has previously been studied (Zhang *et al.*, 2011; de Jong *et al.*, 2016). However, existing methods have never been able to estimate UPD parameters and true satellite clock parameters simultaneously. If this is achieved it will lead to improved convergence time, as well as, improved accuracies for a rover receiver in an offshore environment.

1.2 Aim and Objectives

The aim of the project is to design a method of processing GNSS observations in order to simultaneously calculate UPD and satellite clock corrections from a wide ranging network of receivers. These UPDs can then be used to calculate a user's PPP solution with IAR.

In order to achieve the project aim the following objectives are addressed:

1. Literature review of the current methodologies used in the calculation of UPDs.
2. Understand the theoretical differences and challenges of trying to calculate UPDs for L1 and L2 instead of LC.
3. Investigate the parameters required to be broadcast to a user from a network (e.g. satellite clocks and UPDs).
4. Computation of UPDs and pure satellite clock corrections at a high temporal rate.
5. Develop a generic software approach, which is capable of handling GPS and other GNSS data.
6. Test the accuracy and convergence times of a PPP system with UPDs and satellite clocks from data obtained from a range of networks based in the UK.
7. Test the ability to fix ambiguity parameters to integers at the network and rover receivers.

1.3 Thesis Outline

The thesis comprises seven chapters. Chapter 1 sets out the historical background to the research along with the motivation for further research. The aims and objectives are also presented.

Chapter 2 reviews the background to GNSS positioning and its processing techniques. The measurement models for GPS observations are introduced along with the multiple error sources, such as the troposphere, ionosphere and UPDs within the signals. The importance of each error is outlined along with how they will be dealt with within this study. Additionally, several existing GNSS processing techniques capable of varying degrees of accuracy are discussed. Within these techniques, methodologies to estimate UPDs are presented along with their respective advantages and disadvantages

Chapter 3 presents the derived measurement models used throughout the study. The measurement models are derived *a priori* from the original observation equations for both the network and the user. These measurement models can be used to calculate

UPD and satellite clock values from a network of receivers and hence, can enhance estimation of the position of an unknown receiver.

The Kalman filter (Kalman, 1960) is the subject of Chapter 4. In this chapter the Kalman filter equations are outlined, which enable the estimation of the parameters presented in Chapter 3. The Kalman filter uses the weighted observations and different process noise values to produce the best parameter estimation at each epoch.

Chapter 5 outlines the testing methodology that will be been undertaken. This includes the proposed tests to be completed during the study and why each of these is important. This chapter will also use another existing methodology to compare the methods developed in this thesis.

Subsequently, Chapter 6 presents results of the tests outlined in Chapter 5. These results are presented as a series of plots and statistics to show whether the application of UPD and satellite clock corrections improve the position estimates of a rover receiver.

Finally, Chapter 7 outlines conclusions about the estimation of UPDs and satellite clocks from a network and subsequent position estimates at a rover. It identifies how each of the objectives set out in Chapter 1 has been met and also shows how future work could progress the research further.

Chapter 2. GPS Background

2.1 Introduction

It shall be assumed for the purpose of this thesis, that the reader has a basic knowledge of GNSS. Therefore, this will not be presented here. More information on the basic background to GPS can be gained from a number of resources such as Wells (1986), Kleusberg and Teunissen (1998) and Xu (2003) amongst others.

A number of different processing strategies will be outlined within this chapter. These include PPP, RTK and Network Real-Time Kinematic (NRTK). Once these highly developed methods have been outlined, the more recent concept of PPP-RTK will be introduced. All of these approaches will be critically analysed, to show their advantages and disadvantages, leading to the creation of the PPP-RTK approach, which combines the advantages, into a new improved system.

2.1.1 Measurement Model

Prior to detailing various processing strategies, the signals received from GPS satellites and consequently the measurement model created, must be analysed. There are two primary signals received from the GNSS satellites; the pseudorange and carrier phase observations, which are transmitted on all frequencies. The carrier phase observation is more precise, with accuracies in the millimetre range, compared to the metre level precision of the code observations (Hofmann-Wellenhof, 2008). However, the high precision of the carrier phase observations can only be realised once the initial integer ambiguities have been solved. This is one of the key features when comparing processing strategies and is essential for high accuracy positioning.

The measurement model for a code observation p and a carrier observation ϕ at station r to satellite s, s=1,…, n, at frequency i, i=1,…, f, and time t,both expressed in metres, reads:

$$p_{i,r}^{s}(t) = R_r^s(t) + c\delta t_r(t) - c\delta t^s(t) + T_r^s(t) + \gamma_i I_r^s(t) + m_{p_i,r}^s(t) + d_{p_i,r} - d_{p_i}^s + \upsilon_r^s$$

(2.1)

$$\phi_{i,r}^{s}(t) = R_r^s(t) + c\delta t_r(t) - c\delta t^s(t) + T_r^s(t) - \gamma_i I_r^s(t) + m_{\phi_i,r}^s(t) + d_{\phi_i,r} - d_{\phi_i}^s + \lambda_i N_{i,r}^s + \varphi_{i,r} - \varphi_i^s + \upsilon_r^s$$

(2.2)

where R is the geometric distance between the station and satellite, c the speed of light, δt_r the receiver clock bias, δt^s the satellite clock bias, T the tropospheric delay, $\gamma_i = \lambda_i^2 / \lambda_1^2$, λ_i the carrier wavelength at frequency i, I the ionospheric effect, $m_{\phi_i,r}^s$ the multipath effect, d the UPDs (Uncalibrated Code and Phase Delays), N the integer ambiguity, φ the non-integer initial carrier ambiguity and υ the measurement error including orbit error (Leick, 2015).

In the phase observation equation (2.2), the initial carrier biases $\varphi_{i,r}$ and φ_i^s cannot be separated from the UPD terms $d_{\phi_i,r}$ and $d_{\phi_i}^s$ as they are linearly dependent. Therefore, the initial carrier biases are lumped into the UPD terms resulting in the modified phase observation given by equation (2.3).

$$\phi_{i,r}^{s}(t) = R_r^s(t) + c\delta t_r(t) - c\delta t^s(t) + T_r^s(t) - \gamma_i I_r^s(t) + m_{\phi_i,r}^s(t) + d_{\phi_i,r} - d_{\phi_i}^s + \lambda_i N_{i,r}^s + \upsilon_r^s$$

(2.3)

2.1.2 Geometric Distance

The first term within the measurement model, equations (2.1) and (2.3) is R the geometric distance. This range computation is given by equation (2.4).

$$R_r^s = \sqrt{(X^S - X_r)^2 + (Y^S - Y_r)^2 + (Z^S - Z_r)^2}$$

(2.4)

where X^S, Y^S, Z^S are the satellite coordinates and X_r, Y_r, Z_r are the receiver coordinates. Approximate values for the receiver coordinates must be available, as it is these receiver coordinates that are estimated in the linearised observation equations within the GPS processing of a rover site.

2.1.3 Receiver and Satellite Clock Biases

The receiver clock term, $c\delta t_r$, and satellite clock term, $c\delta t^s$, are important parameters to counter mis-synchronization between the clocks. GPS observations rely on exact time measurements to compute the satellite-receiver range. Therefore, even small timing errors can lead to large range errors, when multiplied by the speed of light.

Receiver clocks are not as accurate as satellite clocks as this would be too expensive and energy intensive to each individual user. The receiver clocks still include biases like the satellite clocks, which can be estimated to within 1 μsec or better (Leick, 2015). For high accuracy applications the receiver clock bias must be estimated as a parameter. It is assumed that the bias is white noise and therefore independent at each epoch. Therefore, it does not use previous estimates to predict the value at future epochs.

Satellite clocks are also highly accurate but drift away from standard GPS time. This drift is kept within one millisecond (Wells, 1986; Leick, 2015), which is equivalent to approximately 300 km of range error. The amount of drift is accurately known and corrected for in the broadcast message, which keeps the clock accurate to about 20 nanoseconds. However, there are external factors such as temperature variations and random drift, which also affect the clock and need to be considered. These parameters, like the receiver clocks, are assumed to be independent from one epoch to the next. Therefore, cannot be modelled and must be estimated, unconstrained at each epoch.

2.1.4 Ionosphere

The ionosphere is the layer of the atmosphere from approximately 50 km to 1000 km (Kleusberg and Teunissen, 1998). The electrons present in this part of the atmosphere affect the propagation of the GPS signal. The ionosphere is a dispersive medium, which means waves of different frequency will travel through at different velocities. In terms of GPS observations, this has the effect that carrier phase observations are advanced, making the range shorter, and the pseudorange measurements are delayed, making the range longer. Crucially, the amount the carrier phase is advanced is the same as the amount the pseudorange is delayed. Therefore, it is possible to remove the ionosphere by combining the frequencies.

When using dual frequency data it is possible to remove the effect of the ionosphere, by creating a linear combination of the L1 and L2 observations called LC. The ionosphere free linear combinations for carrier phase and pseudorange respectively are given by equations (2.5) and (2.6) (Sanz Subirana *et al.*, 2011).

$$\Phi_C = \frac{f_1^2 \Phi_{L1} - f_2^2 \Phi_{L2}}{f_1^2 - f_2^2} \tag{2.5}$$

$$p_C = \frac{f_1^2 p_{P1} - f_2^2 p_{P2}}{f_1^2 - f_2^2} \tag{2.6}$$

Alternative methods for removing the effect of the ionosphere include single difference observations and ionosphere models. For baselines of <30-50 km (Awange, 2012) the ionosphere to 1st order will cancel to within a few mm (Dekkiche *et al.*, 2010) when observations are differenced. Alternatively, ionospheric models are capable of removing 50-60% Root Mean Square (RMS), of the ionospheric effect (Kleusberg and Teunissen, 1998). However, single differences are not possible in PPP and the accuracy of ionospheric models are not sufficient for PPP applications. Consequently, ionospheric parameters are estimated in PPP positioning. It is possible to propagate ionosphere values from epoch to epoch, although this may not account for particularly rapid changes in the ionosphere caused by ionospheric scintillations.

2.1.5 Troposphere

Unlike the ionosphere, the troposphere is a non-dispersive medium, and has the same effect for all frequencies. However, the effect of the troposphere is smaller and more predictable than the ionosphere. The tropospheric delay at the zenith is approximately 2 m but increases for satellites at lower elevations up to approximately 20 m (Xu, 2003).

The delay caused by the troposphere "*depends on temperature, pressure, humidity as well as the location of the GPS antenna*" (Xu, 2003). Consequently, the troposphere is more easily modelled as these parameters can be easily measured. It

can be split into wet and dry parts, which depend on water vapour and the dry atmosphere respectively. The dry part which accounts for about 90% of the error can be estimated with an accuracy of about 99.8% (Wells, 1986). However, the wet part is harder to model, as it depends on the atmospheric conditions between the receiver and the satellite. Tropospheric models calculate the zenith delay at a location. Subsequently, mapping functions can be used to estimate the delay at various elevation angles.

The residual tropospheric error that has not been modelled, mainly the wet troposphere, must be estimated in the measurement model. This delay is slowly changing, and therefore can be tightly constrained and propagated from epoch to epoch. When using short baselines of 10-20 km (Dai *et al.*, 2003), the tropospheric delay can be assumed equal at both stations to obtain the cm level accuracy required in many applications. However, in many applications a tropospheric parameter must be estimated for each receiver independently; due to the baseline lengths or significant height differences between the stations.

2.1.6 Multipath

GPS observations rely on uninterrupted and direct signal, between the receiver and the satellite. However, this is not always the case, especially in urban areas or in offshore environments. Multipath is the error caused by the GPS signal reflecting off a surface before reaching the receiver, instead of going direct to the receiver. The additional time it takes to reach the receiver after the reflection, leads to an error in the range observation.

There are only limited ways to mitigate or reduce multipath, but many attempts have been made. Firstly, the location of the GPS receiver must be as far away as possible from obstacles that could cause a reflection, such as buildings. Secondly, the signal to noise ratio of the signal, once reflected, will be about a 1/3 of the direct signal (Xu, 2003). This can be used to try to identify multipath, as they are likely to have much weaker signals. Thirdly, antenna beam shaping can be used to block signals from certain directions (Wells, 1986). Finally, GPS signals are right-hand circularly polarised (RHCP) and consequently antennas are designed to receiver RHCP signals. When a signal is reflected, the polarisation is changed and therefore would not be received by the antenna.

Despite many efforts to mitigate multipath it remains one of the main error sources in GPS observations, as there are few accurate methods to model the expected multipath in real time.

2.1.7 Uncalibrated Code and Phase Delays

The terms $d_{p_i,r}$, $d^s_{p_i}$, $d_{\phi_i,r}$ and $d^s_{\phi_i}$ from equation (2.3) are the receiver and satellite UPDs. These terms originate in the hardware of the antennas and the satellites. These are uncalibrated, meaning the value is unknown and unmonitored. The existence of these components of code and phase delay, have been studied for many years and it is known that "*their presence prevents the resolution of the integer cycle biases*" (Blewitt, 1989). However, it has been shown that they are quite stable over time and space (Ge *et al.*, 2008). The accurate estimation of these parameters could realise the potential to fix ambiguities to their integer values.

2.1.8 Ambiguities

The carrier phase observations (2.3) include ambiguity terms $N^s_{i,r}$. The carrier phase signal from the satellite is sent as a sinusoidal wave. Hence, the difference in phase between when the signal was sent and when it was received can be accurately measured. However, the integer number of cycles, N, between the satellite and the receiver cannot be measured. It is this integer value that is corrupted by the presence of UPDs, but the accurate calculation of the integer ambiguities holds the key to achieving centimetre level precision.

2.1.9 Orbit Errors

Range measurement between the satellite and the receiver depend on knowing the position of the satellite to high accuracy, at the time of the signal transmission. Due to the large number of forces acting on the satellite, it is difficult to precisely know the positon in real time. Consequently, the broadcast ephemeris is accurate to approximately 100 cm (International GNSS Service, 2017b).

However, by using a large network of IGS stations worldwide it is possible to improve the accuracy of the orbit corrections. Ultra-rapid orbits, first computed in November 2000, were developed for use in real time or near real time. The ultra-rapid orbits use

the latest GPS observations to improve the predictions of the orbits, resulting in accuracies of approximately 5 cm (International GNSS Service, 2017b). These orbit products are realised every six hours to ensure the data is as up to date as possible.

In addition to the ultra-rapid orbits, which are used in near real time applications, there are rapid orbits, which are produced with a latency of approximately one day. These products are no longer predicting the orbits ahead of time, but instead use the actual observations to more accurately inform the user where the satellite was over the previous 24 hours. By using the network of base stations to correct the orbits, the rapid orbits are accurate to approximately 2.5 cm (International GNSS Service, 2017b).

Although the rapid orbits, which are available one day after the observations, are accurate estimates of the orbits, the IGS also provides final orbits, which have a latency of approximately two weeks. These orbits are quoted at the same 2.5 cm accuracy as the rapid orbits and for most applications there will be no difference between the applications of the final or rapid orbits (International GNSS Service, 2017b). The accuracies of these orbit products has been independently tested to verify the values given by the IGS (Hadas and Bosy, 2015).

2.1.10 Additional Measurement Errors

There are a number of additional errors that affect GNSS observations including satellite antenna phase centre, phase wind up, solid earth tides and ocean tide loading.

Satellite antenna phase centre errors are caused by a difference in locality of the phase centre of the satellite and its centre of mass. Orbit parameters are referenced to the centre of mass of the satellite, whereas the range measurement, calculated by the receiver is relative to the antenna phase centre. The difference between these values can reach approximately 1 m depending on the phase centre model of the satellite employed. To achieve high accuracy PPP solutions, which are accurate to the cm level in static mode and sub decimetre in kinematic mode (Øvstedal *et al.*, 2006), these errors need to be accounted for. This is done by accessing a satellite antenna phase centre correction in the ANTenna EXchange (ANTEX) file, which is capable of removing the error at the sub millimetre level (Kouba, 2009).

Phase wind up errors result from the satellite or receiver rotating around its vertical axis. The GPS signal is transmitted as a RHCP radio wave. Consequently, if the satellite or receiver rotates relative to the other the carrier phase signal will change by up to one whole cycle (Kouba, 2009). Fixed GPS receivers should not undergo any rotation. However, satellites do slowly rotate to allow the solar panels to face the sun. Therefore, a small error is introduced by this rotation; this error is negligible and will be ignored during this thesis.

The sun and the moon impart large gravitational forces on the Earth, which result in ocean tides and solid earth tides, which can both affect precise positioning. The effect of solid earth tides on an area depends on the latitude and the frequency of the tides. Additionally, "*the periodic vertical and horizontal site displacements caused by tides are represented by spherical harmonics of degree and order (n, m) characterized by the Love number* h_{nm} *and the Shida number* l_{nm} " (Kouba, 2009). Over short baselines the effect of solid earth tides can be ignored but for precise long baseline solutions the effect must be modelled.

As stated above, the sun and moon create ocean tides, which lead to ocean tide loading. This displacement is caused by the ocean tides rising around an area and creating downward pressure on the seafloor. The amount of displacement depends on the location of the receiver, especially its proximity to the ocean as these areas are most affected. For high accuracy applications, in particular for stations near the sea, the effect of ocean tide loading must be modelled. The ocean tides are highly predictable through a series of constituents such as the M2, S2 and K2 (Clarke and Penna, 2010). Each of these constituent parts has a period and amplitude dependant on the latitude and longitude of a given point. From this information an accurate estimation of the tides can be computed and therefore accurate ocean tide loading calculations can be undertaken. A number of models exist to correct for the ocean tides such as Lyard *et al.* (2006) and Matsumoto *et al.* (2000).

2.2 Precise Point Positioning (PPP)

PPP is a common processing method used in GNSS positioning. The approach uses precise satellite orbits and clocks, calculated from a global network of ground stations, which enables accuracies of decimetre to a few centimetre level when

observing in kinematic mode. However, PPP suffers from the limitation that the convergence time to reach decimetre precision levels is typically around 20 - 30 minutes (Li and Zhang, 2014) and can take up to 24 hours to stabilise at the centimetre level in static mode (Kouba and Héroux, 2001).

One of the main advantages of PPP is that there is no requirement for a local base station and therefore it is a reliable and robust method of positioning anywhere in the world. However, the accuracy of the position is limited by the accuracy of satellite clock and orbit estimates received.

2.3 Real-Time Kinematic (RTK)

The second common processing technique is RTK. This differs from PPP as it requires the use of a local base station, which must be within 10–20 km of the rover (Kleusberg and Teunissen, 1998). This reference receiver transmits its raw observations and its known position to the rover in real time, allowing double differenced observations to be created. Double difference observations allow IAR to take place, as the UPDs, which usually prevent this will cancel out in the differencing process.

The most significant disadvantage of RTK is the requirement of a local base station, which may not be possible depending on the location, for example in an offshore environment, or it may be cost prohibitive. Furthermore, if the reference base station exceeds the 10-20 km guideline, ionosphere, troposphere and orbit errors become de-correlated and therefore residual errors will remain following differencing.

2.4 Network Real-Time Kinematic (NRTK)

To overcome the requirement of a second GPS receiver within 10-20 km to act as a reference station, NRTK has been developed. As the name suggests, a network of ground based reference stations are distributed over a large area, often country wide e.g. OS Net (Ordnance Survey, 2017). These stations are permanently installed and run constantly by a third party, allowing a rover user to pay to receive the corrections from the network when required.

The way in which NRTK generates these corrections is quite different to RTK. Firstly, the network of stations must be processed so that all the integer ambiguities are

correctly solved. This is easier than solving ambiguities at a rover in the RTK method, as the reference receiver is stationary at a known point so the receiver coordinates do not have to be simultaneously estimated. Once the ambiguities are solved, each reference station can accurately estimate corrections for parameters, such as the ionosphere, troposphere and orbits.

When the rover wishes to receive these corrections, its approximate position is analysed, to identify which reference stations are nearby. The corrections from a series of nearby reference stations, surrounding the rover, can then be interpolated to create a Virtual Reference Station (VRS) next to the rover. This VRS can then be used in the same way as RTK, to calculate the rover coordinate and solve integer ambiguities.

Unlike PPP, NRTK requires the use of a number of local reference stations. In many applications, such as offshore positioning, this makes the use of NRTK impossible. NRTK on the other hand can achieve cm precision levels, with just a few epochs of data (Odijk *et al.*, 2010) unlike the 10s of minutes required for PPP. Therefore, if the advantages of the two methods could be combined, it could aid fast real-time positioning, particularly in the offshore environment.

2.5 Precise Point Positioning Real-Time Kinematic (PPP-RTK)

PPP-RTK is a relatively new concept (Ge *et al.*, 2008), which combines the advantages of the PPP and the NRTK methods. PPP-RTK does not require additional ‘local’ base stations used in NRTK making the method particularly useful in remote areas or offshore. However, PPP-RTK does require a larger regional network of base stations, to allow the method to achieve accuracies and convergence times closer to that of NRTK. This regional network allows for PPP-RTK IAR to be performed, where IAR is facilitated through the calculation and broadcast of UPDs.

UPDs exist in the hardware of both receivers and satellites and “*destroy the integer nature of undifferenced ambiguities*” (Geng *et al.*, 2012) preventing IAR from being performed. This is only an issue in PPP, as in NRTK the UPD errors cancel in the double differencing of the observations during the processing. However, the stability of the UPDs means a network of receivers can be employed to estimate UPDs, which can then be broadcast to users.

2.6 Recent Developments in PPP-RTK

A number of different methods have been proposed to recover UPDs that can be utilised to obtain a fixed, ambiguity resolved solution (Geng *et al.*, 2011; Zhang *et al.*, 2011; de Jong *et al.*, 2016). A number of these methods are outlined in this chapter along with their advantages, disadvantages and limitations. These limitations will then be examined in more detail, to identify the key objectives required for the development of an improved PPP-RTK system.

In the various PPP-RTK processing techniques, the observations are reparameterised and combined in different ways depending on the method being employed. Equations (2.1) and (2.3) for pseudo range and phase respectively are both singular and rank deficient meaning that all the parameters cannot be solved for individually. The mathematical techniques by which these equations are made non-singular are one of the main differences between the various methods for obtaining a PPP-RTK solution.

2.6.1 GeoForschungsZentrum (GFZ) Method

This method was developed and methodologies proposed by GFZ (Geng *et al.*, 2011) and will be referred to as the GFZ approach throughout this document. In this approach the first step combines the L1 and L2 GPS observations into an ionosphere free combination (LC) as shown in equations (2.5) and (2.6).

The ionosphere free combination has the advantage that ionospheric terms in the observation equations (2.1) and (2.3) are removed. The ionosphere free approach reduces the number of observation equations from four to two for each satellite observed. This is critical in the remainder of the processing as the reduced data availability makes it more difficult to estimate the required UPDs. Furthermore, the GFZ approach cannot directly calculate the UPDs on L1 and L2 because of the use of the ionosphere free combination. Therefore, the Wide lane (WL) and Narrow Lane (NL) combinations are used. The WL and NL combinations are given by equations (2.7) and (2.8).

$$L_{WL} = L_1 - L_2 \tag{2.7}$$

$$L_{NL} = L_1 + L_2$$

(2.8)

The WL and NL UPDs cannot be estimated simultaneously because of the rank deficiencies in the observation equations (Ge *et al.*, 2008). Instead the WL solution is calculated first and subsequently this calculation is used to estimate the NL UPD solution.

Equation (2.7), also known as the Melbourne-Wubbena WL, provides a signal wavelength of 86.2 cm (Melbourne, 1985). This is much longer than the 19 cm and 24 cm for the L1 and L2 frequencies respectively (Sideris, 2009), effectively making the WL UPDs easier to fix than the L1 and L2 UPDs. This is due to the relative levels of measurement noise not being as high, making integer fixing more robust. Additionally, the use of the WL ambiguities reduces the solution convergence time. For example, Geng *et al.* (2011) report that "*at least 10 minutes of observations are required for most receiver types to reliably fix about 90% of wide-lane ambiguities*". A further advantage of the WL UPDs is their superior temporal stability, meaning that once computed they can be predicted for several days allowing for a single daily update rate (Geng *et al.*, 2011).

In contrast the NL ambiguities are harder to determine and therefore, take considerably longer to compute. The narrow 10 cm wavelength results in the requirement for a much longer observation period, to smooth out observation noise. The slowly changing geometry of the satellites further increases the time taken for NL ambiguity resolution (Geng *et al.*, 2011). Additionally, the NL counterparts are much more temporally unstable resulting in the requirement for an update rate of ~15 minutes to achieve high precision results (Geng *et al.*, 2012). A number of studies (Geng *et al.*, 2010a; Geng *et al.*, 2011), have employed NL UPDs estimated once per satellite pass showing it to be "*rather stable*" (Geng *et al.*, 2010b) during this period.

When calculating the UPDs using the GFZ method, it is the NL UPDs that are critical to the positioning accuracy. This is because "*even a slightly biased NL UPD estimate … is likely to deteriorate the positioning accuracy*" (Geng *et al.*, 2012). Therefore, it was proposed (Geng *et al.*, 2012) that these NL UPDs should be derived from an

ambiguity fixed network instead of ambiguity float. In order to achieve this, double differenced ambiguity resolution needs to be carried out over the network. Using this double differenced network, the accuracies of the NL UPDs were improved. The accuracy of the PPP-RTK positions improved the RMS values from 3.6 mm, 2.3 mm and 6.4 mm in the East, North and Up directions respectively for daily positions using a float solution to 2.6 mm, 2.2 mm and 6.1 mm using the fixed solutions (Geng *et al.*, 2012). Hence, using an ambiguity fixed network solution is desirable for highly accurate UPDs, especially "*when only a small number of reference stations are involved*" (Geng *et al.*, 2012).

2.6.1.1 UPD Calculation in the GFZ method

The methodology adopted in the network processing of the GFZ method to calculate the required UPDs is to simply average the fractional parts of all the ambiguity parameters, for all the reference stations within the network. The fractional parts of the UPDs are the critical factors, as the integer parts cannot be separated from the integer ambiguities. These undifferenced ambiguity estimates are then single differenced between satellites, to remove the receiver dependent UPDs, resulting in the remaining UPD being referenced to a satellite pair (Geng *et al.*, 2010b).

$$b_{ck}^{i,j} = \frac{f_1}{f_1 + f_2}\left(n_{nk}^{i,j} - \phi_n^{i,j}\right) + \frac{f_1 f_2}{f_1^2 + f_2^2}\left(n_{nk}^{i,j} - \phi_w^{i,j}\right) \tag{2.9}$$

where b_{ck} is the ionosphere free carrier phase bias, n_{nk} is the NL integer ambiguity, ϕ_n is the between satellite differenced NL UPD and ϕ_w is the between satellite differenced WL UPD.

Once the WL and NL UPDs have been estimated using the network of reference receivers these estimates are transmitted to the user. These estimates are then used to correct the float single difference ambiguities at the user station. Sequential bias fixing and the Least-squares AMBiguity De-correlation Adjustment (LAMBDA) (Teunissen, 1993) method are then used to fix the WL and NL ambiguities in sequence as for the network ambiguities.

2.6.1.2 GFZ Network Testing

Geng *et al.* (2011) used a European-wide network of 91 stations to obtain UPD estimates. They show that by employing more stations, the robustness of the averaging technique increases, with at least 10 stations required to obtain precise results. Using these precise UPD estimates, hourly positional estimates of East, North and Height coordinate components could be improved from 13.7 cm, 7.1 cm and 11.4 cm to 0.8 cm, 0.9 cm and 2.5 cm respectively as a result of the ambiguity resolution.

Additional studies (Ge *et al.*, 2008; Geng *et al.*, 2012) employed a similar network of 180 global International GNSS Service (IGS) stations to calculate UPDs. Using this global network it was found that the density of the network affects the accuracy of the UPDs calculated. In North America and Europe, where the network of ground stations is very dense, the RMS values are small: 0.6 mm on average. In contrast, East Africa and Central Asia, which have sparse networks, have RMS values in the region of 0.8-1.6 mm (Geng *et al.*, 2012). Hence it is important, when developing a system, to consider the density and location of the network to ensure it is capable of obtaining the results that are required for the application.

2.6.1.3 GFZ Review

Liu (2010) reviewed the GFZ approach, making four main observations about the methodology and outlining ways it could be improved. Firstly, the UPD terms being estimated are not pure UPD terms but instead contain additional code delay. Secondly, the single difference observation equations are unnecessary as it can be shown that zero difference measurements can achieve the same results. Thirdly, simple averaging of the fractional parts of the ambiguities to estimate UPDs can lead to errors when the fractional parts are close to ± 1 or 0. For example, averaging the fractional parts of 0.96 and 1.04 gives 0.5, instead of the 0 value required. This is alluded to in the original work by GFZ but the solution is never fully discussed. Finally, the formation of double difference ambiguities between reference stations will not only avoid the incorrect averaging problem but also make the estimate more precise and shorten the convergence time for the user.

2.6.2 Centre National d'Etudes Spatiales (CNES) Method

A method similar to the GFZ method has been developed at the Centre National d'Etudes Spatiales (CNES) in France. The CNES method followed the GFZ methodology in using the LC ionosphere free combination to remove ionospheric delay and then employing the Melbourne-Wubbena combination to solve the WL ambiguities using equation (2.10) (Laurichesse, 2011). However, the methods differ when the GFZ method attempts to solve the NL ambiguities. At this stage the CNES method uses the WL ambiguities to fix the L1 ambiguities. This can be achieved by solving equation (2.11) presented in Laurichesse (2011).

$$Q_c = \frac{\gamma\lambda_1 L_1 - \lambda_2(L_2 + N_w)}{\gamma - 1} \tag{2.10}$$

$$Q_c = D_c + \lambda_c W + h_i - h^j - \lambda_c N_1 \tag{2.11}$$

where Q_c is the ionosphere free combination, γ is $\frac{f_1^2}{f_2^2}$ where f is the GPS frequency, λ is $\frac{c}{f}$ where c is the speed of light, L is the phase measurement in cycles, W is the wind-up effect in cycles, N_w is the WL ambiguity, D_c is the satellite-receiver range, h_i is the receiver clock, h^j is the satellite clock, λ_c is the wavelength of the ionosphere free combination and N_1 is the L1 ambiguity.

When these have been fixed, the UPDs generated through the calculation are broadcast as part of the 'integer' satellite clock. This clock correction is then applied at the user end to fix the L1 ambiguities, "*leading to centimetre level PPP*" (Laurichesse, 2011).

Since the publication of the GFZ and CNES approaches, there have been further attempts to compare the methods. It has been demonstrated that theoretically and practically the two methods are equivalent (Geng *et al.*, 2010b).

2.6.3 Jet Propulsion Laboratory (JPL) Method

In addition to the approaches developed by GFZ and CNES, JPL have developed their own approach, which is compatible with the JPL software package GIPSY-OASIS (Bertiger *et al.*, 2010). JPL use a globally distributed set of GPS receivers to compute orbits and clock products for the IGS. Alongside these products, WL phase biases are estimated and saved in a WLPBLIST file. A WL bias estimate is computed for each GPS satellite arc that is processed in the global solution.

These WL estimates allow single ground receivers, which run the GIPSY-OASIS software to compute an ambiguity resolved solution. In a similar manner to that outlined in section 2.6.2, the WL biases are first used to estimate the WL ambiguities and then subsequently the L1 ambiguities can be fixed to integers. Additionally, the JPL approach only applies a soft constraint to the ambiguities upon fixing rather than a hard constraint. This allows the solution to change its ambiguity fix value as "*the probability of mis-resolution is typically fairly high*" (Bertiger *et al.*, 2010).

2.6.4 Regional Network Method

A fourth approach to PPP-RTK positioning (Teunissen *et al.*, 2010; Zhang *et al.*, 2011) utilises smaller 'regional' networks of reference stations, comprising as few as four receivers in the network with inter-station distances ranging from 60-100 km (Zhang *et al.*, 2011). This approach is similar to the standard network RTK method. However, in standard network RTK, the user requires the network corrections and the raw data from one of the Continuously Operating Reference Stations (CORS) stations. Whereas, in this approach only the network parameter estimates are required to obtain an ambiguity fixed solution.

The key assumption is that both the troposphere and ionosphere remain constant within the network extents, negating the need to use the ionosphere free (LC) combination as employed by the GFZ, CNES and JPL methods. One of the main advantages of not using the LC combination is that it is possible to calculate user

corrections in a single step, instead of the step-wise processing in the GFZ, CNES and JPL methods. This speeds up the process of obtaining UPDs considerably and hence the time to the first ambiguity fixes. However, despite having twice the number of original observation equations in the process, there is still insufficient data to directly solve for all the parameters. Additionally, the small spatial extent of the reference network allows satellite orbit error parameters to be ignored, as the effect of these on each receiver will be similar and therefore common to each station.

2.6.4.1 UPD Calculation in the Regional Network Method

In these approaches, a number of reparameterisation steps are required to make the equations non-singular. In this reparameterisation, the UPD and satellite clock term equations are modified, so that they are no longer pure UPD and satellite clock terms. For example, the satellite clock terms have receiver clock and troposphere parameters lumped into the solution (Zhang *et al.*, 2011). For the UPD terms, additional receiver biases and integer ambiguity terms are integrated (Zhang *et al.*, 2011). Thus, the UPD and satellite clock terms are said to be biased in order to distinguish them from the pure terms. Using these biased UPD and satellite clock terms instead of the pure corrections should not affect results, so long as the user observations are reparameterised in the same manner. However, it does mean that the corrections obtained from this method will not be directly comparable or interchangeable with the corrections from an alternative method, for example GFZ.

Despite the reparameterisation of the satellite clock and UPD terms not affecting the results directly, it can impact on the area the corrections can be used in. For example, the satellite clock term has been reparameterised to include the troposphere from the reference network receiver (Zhang *et al.*, 2011). In theory, when the user solution is calculated, the troposphere parameter at the user will be relative to the troposphere at the network reference receiver. However, if the network is sufficiently distant from the user, the mapping functions will be significantly different. Therefore, the troposphere values will not fully cancel out in the user solution. This limits the applications of the method, as the network stations must be relatively (100 km in this study) close to the user, which is often not possible in an offshore application.

To further improve the IAR speed of this approach the ionosphere is interpolated using the Kriging method (Zhang *et al.*, 2011). This interpolation method provides a relatively precise value for the ionospheric delay due to the small size of the network. However, Kriging could not be successfully extended to larger networks due to the spatial variability of the ionosphere. For example, when the method was tested in Perth, Australia, where interstation distances reached up to 180 km, the IAR success rate fell from 99.7% to 92.4% (Zhang *et al.*, 2011).

Other corrections sent to the user in this processing strategy are the biased satellite clock correction and the biased satellite UPD. These corrections are subsequently applied to the user's observation equations. Finally, the linear dependence between the receiver UPD and the receiver ambiguity must be addressed through reparameterisation. This results in full-rank observation equations with double difference integer ambiguity terms, which can be solved for, to obtain precise positions.

The accuracies achieved through this process were of the order of 1 cm and 5 cm for the horizontal and vertical coordinate components when positioning in kinematic mode (Zhang *et al.*, 2011). These results are comparable to those obtained by the GFZ method. However, the method achieved IAR in under 5 minutes on the majority of occasions and always under 15 minutes (Zhang *et al.*, 2011), which is considerably faster than the GFZ approach.

2.6.5 Global Ionospheric Map (GIM) Method

A fifth method only recently developed also deals directly with the L1 and L2 UPDs (Li *et al.*, 2013). This PPP-RTK algorithm uses the raw L1 and L2 observations in conjunction with a Global Ionospheric Map (GIM) to provide *a priori* estimates of the ionospheric effect. This GIM approach is capable of producing "*real time ionospheric products with an accuracy of a few decimetres*" (Li *et al.*, 2013). While insufficiently accurate to solve for the ionosphere, the approach is accurate enough to tightly constrain the ionospheric parameters in the observation equations. This allows the Kalman filter process noise values to be reduced and consequently allows a solution to be determined.

Combining the raw observations with the GIM data, real-time orbits and clocks, a PPP float solution is obtained for all stations in the network. The coordinates of all reference stations are held fixed, allowing the undifferenced L1 and L2 float ambiguities to be obtained. Once the ambiguities are known, one UPD is fixed to zero and the other UPDs can be estimated through a least squares computation. These UPDs can then be used to correct the undifferenced ambiguities, allowing ambiguity fixing over the network to be attempted. This fixing will improve the accuracies of the UPDs obtained, allowing more ambiguities to be fixed in the next iteration. Once sufficient iterations have been completed, the UPDs can be broadcast to the user together with precise orbits, clocks and GIMs to allow PPP ambiguity fixing at that location. The UPD estimates are updated epoch-by-epoch and broadcast at five second intervals.

2.6.5.1 GIM Network Testing

In the method outlined in 2.6.1 it was found that the accuracy to which the UPDs could be estimated was dependent on the density of the reference station network in the region that the user was obtaining the correction. The problem of network density has also been found to be an issue in the GIM method, because of the lack of reference stations in some areas. A sparse reference network is the limiting factor on the accuracy of the GIM as small scale ionospheric variations cannot be estimated (Li *et al.*, 2013). The GIM accuracy not only affects the convergence time for IAR but also the ability to adopt this method successfully.

To test the method, 80 IGS stations were used globally to estimate UPDs and 150 IGS stations to generate the GIMs. When compared to the GFZ method this new method appeared to provide results with better accuracies and faster convergence times. The time required for ambiguity fixing is decreased by 25% from 20 to 15 minutes (Li *et al.*, 2013).

2.6.6 Fugro Intersite Methodology

Current methods employed by Fugro Intersite to compute UPDs are based on the direct estimation of the hardware delays on the L1 and L2 frequency in a program called E-HP (de Jong, 2013). These UPDs are computed by employing a relatively sparse reference station network of four or five stations. Test networks capable of

estimating UPDs are currently running for the North Sea and the Gulf of Mexico. These networks are larger than those in the regional method outlined above, where inter-station distances ranged from 100-1000 km. Therefore, atmospheric errors such as the troposphere and the ionosphere cannot be ignored, but must be incorporated into the parameter list for estimation. However, it is assumed the stations are sufficiently close for the satellite orbit errors to be equal at each of the reference stations.

As in previous approaches (e.g. Teunissen *et al*., 2010), it is not possible to solve for all the parameters in the observation equations and again the equations require reparameterisation. At this stage, it is assumed that the major part of the satellite clock and satellite orbit parameters can be removed through the use of precise orbit and clock data obtained from Fugro Intersite's G2 service (Fugro, 2017). The G2 service employs a global network of receivers and transmits the estimated values to receivers allowing just a slowly changing residual part of the parameter to remain: $\varepsilon^s(t)$ and $v_r^s(t)$ for clocks and orbits respectively. A model is also used to estimate the troposphere whilst multipath terms are ignored. This results in the reparameterisation given by equations (2.12) and (2.13). In these equations, a reference satellite and reference station are used to remove singularities from the measurement model. A full description of how reference satellites and stations are introduced is shown in section 3.2.1.

$$p_{i,r}^{s}(t) = R_r^s(t) + \mathrm{T}_r^s(t) + \mathrm{b}_{pi,r}^{ref}(t) + d_{p_i,p_1,r}^{s,ref}(t) - \gamma_i I_r^{s,ref}(t) \tag{2.12}$$

$$\phi_{i,r}^{s}(t) = R_r^s(t) + \mathrm{T}_r^s(t) + \mathrm{b}_{\phi i,r}^{ref}(t) + d_{\phi 1,\phi 1,r}^{s,ref}(t) - \gamma_i I_r^{s,ref}(t) \tag{2.13}$$

where $\mathrm{b}_{\phi i,r}^{ref}(t)$ and $\mathrm{b}_{pi,r}^{ref}(t)$ are the biased receiver clocks and $d_{\phi 1,\phi 1,r}^{s,ref}(t)$, along with $d_{p_i,p_1,r}^{s,ref}(t)$, are the biased UPD parameters.

Using these equations it is possible to obtain estimates for the UPDs by assuming the reference station position is known and held fixed. The UPD parameters, together with tropospheric and ionospheric terms, are transmitted to the user. However, these

atmospheric parameters only provide improved *a priori* values, thus reducing convergence times. The application of the UPD term should however allow the ambiguities to be fixed to integer values.

2.6.7 Proposed Methodology

The aim of this study will be to develop and test a new method that will provide further improvements on those outlined above to yield a fast, reliable and precise PPP-RTK position. To achieve this, a combination of a number of other proposed methodologies will be employed. This will be developed in section 3.2. The overarching aim will be to estimate UPDs from a sparse global network of reference stations allowing an IAR solution to be obtained anywhere on the globe. The difference between the proposed method and the methods in use at GFZ and CNES will be that the UPDs will be estimated directly on the L1 and L2 frequencies.

Data from stations globally is processed by the IGS to calculate the satellite orbit parameters, which will be removed from the observations processed in this method in accordance with the Fugro Intersite methodology shown in section 3.2.1. Alternative stations over a regional network can then be used to obtain the UPD and satellite clock estimates. These UPD and satellite clock parameters can then be sent to the user, together with the precise satellite orbits, allowing accurate IAR after 10s of minutes at the user location.

Chapter 3. Measurement Model

3.1 Introduction

To create a system capable of calculating UPDs and satellite clocks for all GNSS simultaneously, a different measurement model to the ones given in equations (2.12) and (2.13) must be developed. This measurement model will use the raw GNSS observations shown in equations (2.1) and (2.3) from a number of reference stations, combining them such that the system is non-singular and therefore solvable. While creating this measurement model it is important to keep in mind the stochastic nature of the parameters being combined. For example, combining parameters such as tropospheric errors with receiver clock errors will destroy the slowly changing stochastic property of the troposphere, as the receiver clock will change in value significantly quicker. Consequently, this would make the parameters more difficult to solve for within a Kalman filter.

Currently there are a number of differing approaches to solve for UPDs and satellite clocks as outlined in Chapter 2. A number of papers such as Ge *et al.* (2008) create the ionosphere free combination frequency LC. This allows the UPDs to be estimated on the wide-lane frequency and then the narrow lane as discussed in section 2.6.1. Whereas, the regional network method outlined in Teunissen *et al.* (2010) uses a small dense network with only single troposphere and ionosphere terms calculated for the network.

Current approaches employed by Fugro Intersite to calculate satellite clocks and UPDs involve two separate programs. Firstly, the G2 service provides satellite clock corrections along with satellite orbits. This data is subsequently employed to estimate the UPDs separately in the E-HP program. As stated in de Jong (2013), '*it would be more efficient if the UPDs could be estimated together with the satellite clock corrections*'. The satellite orbits can be accurately predicted through various services such as the IGS. These orbit parameters are compatible with the measurement model so do not need to be estimated alongside the UPDs and satellite clock corrections. This chapter outlines the theoretical development of a methodology to accomplish this.

3.2 Standard Measurement Model

The standard measurement model for all GPS observations is given in section 2.1.1 in equations (2.1) and (2.3).

However, equations (2.1) and (2.3) must be reparameterised to be solved. An existing reparameterisation developed by Fugro Intersite is outlined in section 3.2.1. Section 3.2.2 then further develops this reparameterisation into a proposed measurement model, which will be used in this thesis to simultaneously compute satellite clocks and UPDs.

3.2.1 Fugro Reparameterisation

The reparameterisation developed by Fugro Intersite starts by using equations (2.1) and (2.3). However, to simplify these equations and all further equations in this thesis multipath will be ignored.

In equations (2.1) and (2.3) the receiver UPD parameters $d_{p_i,r}$ and $d_{\phi_i,r}$ cannot be separated from the receiver clock parameter $c\delta t_r$ and are therefore combined as seen in equations (3.3) and (3.4). Additionally, the parameters $d^s_{\phi_i}$ cannot be separated from the ambiguity parameters $N^s_{i,r}$ and also combined as shown in equation (3.5). This results in equations (3.1) and (3.2):

$$p^s_{i,r}(t) = R^s_r(t) + c\delta\tilde{t}_{p_i r}(t) - c\delta t^s(t) + T^s_r(t) + \gamma_i I^s_r(t) - d^s_{p_i} + \upsilon^s_r \tag{3.1}$$

$$\phi^s_{i,r}(t) = R^s_r(t) + c\delta\tilde{t}_{\phi_i,r}(t) - c\delta t^s(t) + T^s_r(t) - \gamma_i I^s_r(t) + \lambda_i\tilde{N}^s_{i,r} + \upsilon^s_r \tag{3.2}$$

where

t is the current epoch,

$$c\delta\tilde{t}_{p_i r} = c\delta t_r + d_{p_i,r} \tag{3.3}$$

$$c\delta\tilde{t}_{\phi_i,r} = c\delta t_r + d_{\phi_i,r}$$

(3.4)

$$\tilde{N}^s_{i,r} = N^s_{i,r} - d^s_{\phi_i}$$

(3.5)

Equations (3.1) and (3.2) are not solvable due to singularities. One such singularity is between the receiver clocks and the satellite clocks. To remove this singularity a reference satellite, ^{n}, is selected and this applies for all satellite dependent parameters. The reference satellite has been taken, for simplicity of notation, to correspond to the nth satellite; in practice the reference satellite would be chosen based on the satellite with the highest elevation at that epoch. This results in equations (3.6) and (3.7):

$$p^s_{i,r}(t) = R^s_r(t) + b^n_{p_i,r}(t) - c\delta\tilde{t}^s(t) + T^s_r(t) + \gamma_i \tilde{I}^s_r(t) - \tilde{d}^s_{p_i} + \tilde{\upsilon}^s_r$$

(3.6)

$$\phi^s_{i,r}(t) = R^s_r(t) + b^n_{\phi_i,r}(t) - c\delta\tilde{t}^s(t) + T^s_r(t) - \gamma_i \tilde{I}^s_r(t) + \lambda_i \hat{N}^s_{i,r} + \tilde{\upsilon}^s_r$$

(3.7)

where

$$b^n_{p_i,r} = c\delta t_r + d_{p_i,r} - c\delta t^n - d^n_{p_i} + \upsilon^n_r + \gamma_i I^n_r$$

(3.8)

$$b^n_{\phi_i,r} = c\delta t_r + d_{\phi_i,r} - c\delta t^n - d^n_{\phi_i} + \upsilon^n_r - \gamma_i I^n_r + \lambda_i N^s_{i,r}$$

(3.9)

$$c\delta\tilde{t}^s = c\delta t^s - c\delta t^n$$

(3.10)

$$\tilde{I}_r^s = I_r^s - I_r^n$$

(3.11)

$$\tilde{d}_{p_i}^s = d_{p_i}^s - d_{p_i}^n$$

(3.12)

$$\tilde{\upsilon}_r^s = \upsilon_r^s - \upsilon_r^n$$

(3.13)

$$\hat{N}_{i,r}^s = \tilde{N}_{i,r}^s - \tilde{N}_{i,r}^n$$

(3.14)

The reparameterised form given in equations (3.6) and (3.7) is still not solvable. There is a linear dependency between the satellite clock term $c\delta\tilde{t}^s$ and the orbit error term $\tilde{\upsilon}_r^s$.Therefore, the orbit errors are combined into the satellite clock terms. Additionally, there is a linear dependency between the satellite clocks $c\delta\tilde{t}^s$, the code satellite UPDs $\tilde{d}_{p_i}^s$ and the ambiguities $\hat{N}_{i,r}^s$. To remove the linear dependency a separate code satellite clock parameter and phase satellite clock parameter are created. Both of these changes are shown in equations (3.17) and (3.18). The resultant equations are shown in equations (3.15) and (3.16):

$$p_{i,r}^s(t) = R_r^s(t) + b_{p_i,r}^n(t) - k_{p_{i,r}}^{s,n}(t) + T_r^s(t) + \gamma_i \tilde{I}_r^s(t)$$

(3.15)

$$\phi_{i,r}^s(t) = R_r^s(t) + b_{\phi_i,r}^n(t) - d_{\phi_i,r}^{s,n}(t) + T_r^s(t) - \gamma_i \tilde{I}_r^s(t)$$

(3.16)

where

$$k_{p_{i,r}}^{s,n} = c\delta\tilde{t}^s - \tilde{d}_{p_i}^s + \tilde{\upsilon}_r^s$$

(3.17)

$$d_{\phi_i,r}^{s,n} = c\delta\tilde{t}^{s} + \tilde{\upsilon}_r^s + \hat{N}_{i,r}^s$$

(3.18)

The final stage to make the equations solvable is to remove the linear dependency between the ionosphere terms $\tilde{I}_r^s$ and the satellite clock terms $k_{p_i,r}^{s,n}$ and $d_{\phi_i,r}^{s,n}$. This can be removed by selecting a reference frequency on the code observations as shown in equations (3.21), (3.22) and (3.23). Therefore, the full rank observation equations developed by Fugro Intersite are given as equations (3.19) and (3.20):

$$p_{i,r}^s(t) = R_r^s(t) + b_{p_i,r}^n(t) - k_{p_i,p_1,r}^{s,n}(t) + T_r^s(t) + \gamma_i \overline{I}_r^s(t)$$

(3.19)

$$\phi_{i,r}^s(t) = R_r^s(t) + b_{\phi_i,r}^n(t) - d_{\phi_i,p_1,r}^{s,n}(t) + T_r^s(t) - \gamma_i \overline{I}_r^s(t)$$

(3.20)

where

$$k_{p_i,p_1,r}^{s,n} = k_{p_i,r}^{s,n} - \gamma_i k_{p_1,r}^{s,n}$$

(3.21)

$$d_{\phi_i,p_1,r}^{s,n} = d_{\phi_i,r}^{s,n} + \gamma_i k_{p_1,r}^{s,n}$$

(3.22)

$$\overline{I}_r^s = \tilde{I}_r^s + k_{p_1,r}^{s,n}$$

(3.23)

3.2.2 New Reparameterisation

The approach developed in this thesis and outlined here uses a reparameterised set of observation equations, as it is not possible to solve the equations (2.1) and (2.3), as previously discussed. The measurement model, equations (3.19) and (3.20), developed by Fugro Intersite, is designed to be a theoretical reparameterisation and is not practically solvable due to the stochastic properties of the equations. For

example, the slowly varying ionosphere parameter is lumped in with the rapidly varying satellite clock parameters. Therefore, the Fugro Intersite measurement model will be further reparameterised in this chapter to create a new measurement model.

To aid readability and completeness the elements in equations (3.19) and (3.20) derived in section 3.2.1 are defined by:

$$b^{n}_{p_i,r}(t) = c\delta t_r(t) + d_{p_i,r} - d^{n}_{p_i} - c\delta t^{n}(\mathrm{t}) + \upsilon^{n} + \gamma_i I^{n}_{r}$$

(3.24)

$$k^{s,\mathrm{n}}_{p_i,p_1,r}(t) = k^{s,\mathrm{n}}_{p_i,r}(t) - \gamma_i k^{s,\mathrm{n}}_{p_1,r}(t)$$

(3.25)

where $k^{s,\mathrm{n}}_{p_i,r}(t) = -d^{s}_{p_i} + d^{n}_{p_i} - c\delta t^{s}(t) + c\delta t^{n}(t) + \upsilon^{s}(t) - \upsilon^{n}(t)$

(3.26)

$$b^{n}_{\phi_i,r}(t) = c\delta t_r(t) + d_{\phi_i,r} - d^{n}_{\phi_i} - c\delta t^{n}(t) + \upsilon^{n}(t) + \lambda_i N^{n}_{i,r} - \gamma_i I^{n}_{r}(t)$$

(3.27)

$$d^{s,\mathrm{n}}_{\phi_i,p_1,r}(t) = d^{s,\mathrm{n}}_{\phi_i,r}(t) + \gamma_i k^{s,\mathrm{n}}_{p_1,r}(t)$$

(3.28)

where $d^{s,n}_{\phi_i,r}(t) = -d^{s}_{\phi_i} + d^{n}_{\phi_i} - c\delta t^{s}(t) + c\delta t^{n}(t) + \upsilon^{s}(t) - \upsilon^{n}(t) + \lambda_i N^{s}_{i,r} - \lambda_i N^{n}_{i,r}$

(3.29)

$$\overline{I}^{s,\mathrm{n}}_{r}(t) = I^{s}_{r}(t) - I^{n}_{r}(t) + k^{s,n}_{p_1,r}(t)$$

(3.30)

By employing equations (3.19) and (3.20) at a single reference station, denoted as station, $_{\mathrm{a}}$, it is theoretically but not practically possible to determine a float solution. From a theoretical basis, the measurement model for one epoch of data, assuming

the station position is known, and the tropospheric delay consists of a zenith delay (ZD) only, is given by equation (3.31).

In equation (3.31), the vectors $p_{1,a}-R_a$, $\phi_{1,a}-R_a$ etc. contain Observed Minus Computed (OMC) distances. These are computed by inputting RINEX files into a program called GenOMC provided by Fugro Intersite for the purpose of this thesis. These are used instead of raw GPS observations in this thesis, to allow errors, such as cycle slips to be ignored.

$$\begin{pmatrix} p_{1,a}-R_a \\ p_{2,a}-R_a \\ \phi_{1,a}-R_a \\ \phi_{2,a}-R_a \end{pmatrix} = \begin{pmatrix} e_n & 0 & 0 & 0 & f_{n,a} & \gamma_1 I_{nx(n-1)} & 0 & 0 & 0 \\ 0 & e_n & 0 & 0 & f_{n,a} & \gamma_2 I_{nx(n-1)} & I_{nx(n-1)} & 0 & 0 \\ 0 & 0 & e_n & 0 & f_{n,a} & -\gamma_1 I_{nx(n-1)} & 0 & I_{nx(n-1)} & 0 \\ 0 & 0 & 0 & e_n & f_{n,a} & -\gamma_2 I_{nx(n-1)} & 0 & 0 & I_{nx(n-1)} \end{pmatrix} \begin{pmatrix} b^n_{p_{1,a}} \\ b^n_{p_{2,a}} \\ b^n_{\phi_{1,a}} \\ b^n_{\phi_{2,a}} \\ ZD_a \\ \overline{I}^{s,n}_a \\ k^{s,n}_{p_2,p_1} \\ d^{s,n}_{\phi_1,p_1,a} \\ d^{s,n}_{\phi_2,p_1,a} \end{pmatrix}$$

(3.31)

where e_n is n-vector of all unity values, the matrix $I_{nx(n-1)}$ is given by equation (3.32) and the vectors $p_{1,a}-R_a$ are given by equation (3.33).

$$I_{nx(n-1)} = \begin{pmatrix} 1 & & & \\ & . & & \\ & & . & \\ & & & . \\ & & & 1 \\ 0 & . & . & . & 0 \end{pmatrix}$$

(3.32)

$$p_{1,a}-R_a = \begin{bmatrix} p^1_{1,a}-R^1_a \\ p^2_{1,a}-R^2_a \\ \cdots \\ p^n_{1,a}-R^n_a \end{bmatrix}$$

(3.33)

The vector $f_{n,a}$ has the tropospheric mapping function for each satellite. Throughout this thesis, the tropospheric mapping function is computed within the Fugro OMC program.

The zeroes in the final row of equation (3.32) are associated with the usage of the final satellite as the reference. As stated previously, this choice is for the simplicity of the notation only.

3.2.3 Satellite Clocks

In the measurement model provided in section 3.2.2, the parameters in equation (3.25) are estimated. When using GPS data the frequency, i, is equal to either 1 or 2. However, when i = 1 the parameter $k^{s,n}_{p_i,p_1,r}(t)=0$. Therefore, $k^{s,n}_{p_i,p_1,r}(t)$ is just a single parameter per satellite provided by $k^{s,n}_{p_2,p_1,r}(t)$.

The orbit errors, υ^s_r, included in this and other parameters in the measurement model are considered to be small and will therefore be ignored for the remainder of this thesis. This results in the parameter, $k^{s,n}_{p_2,p_1,r}(t)$ becoming receiver independent. Therefore, it will be now written as $k^{s,n}_{p_2,p_1}(t)$.

Expanding the parameter $k^{s,n}_{p_2,p_1}(t)$ from equation (3.25) with the use of equation (3.26) results in equation (3.34):

$$k^{s,n}_{p_2,p_1}(t)=-d^s_{p_2}+d^n_{p_2}-(1-\gamma_2)c\delta t^s+(1-\gamma_2)c\delta t^n+\gamma_2 d^s_{p_1}-\gamma_2 d^n_{p_1} \tag{3.34}$$

Therefore, the parameter $k^{s,n}_{p_2,p_1}(t)$ is a biased satellite clock. However, in equation (2) of Zhang *et al.* (2011) the satellite clock parameter provided by the IGS is given by equation (3.35):

$$dt^s_I(t)=c\delta t^s(t)+\frac{\gamma_2}{\gamma_2-1}d^s_{p_1}-\frac{1}{\gamma_2-1}d^s_{p_2} \tag{3.35}$$

The biased satellite clock equation (3.34) can be rearranged using equation (3.35) to give:

$$\frac{k^{s,n}_{p_2,p_1}(t)}{\gamma_2 - 1} = dt^s_l(t) - dt^n_l(t)$$

(3.36)

Thus, the parameter $k^{s,n}_{p_2,p_1}(t)$ can be written in terms of the IGS products.

If the measurement model is adapted to include this biased satellite clock parameter in the phase observations, it will be possible to estimate unbiased satellite clocks and UPDs simultaneously.

3.2.4 UPD Estimation

The calculation of UPDs in the previous model, outlined in section 3.2.1, is performed by the estimation of the parameters provided by equation (3.28). Using equations (3.29) and (3.26) this can be expanded and simplified to give equation (3.37):

$$d^{s,n}_{\phi_i,p_1,r}(t) = -d^s_{\phi_i} + d^n_{\phi_i} + \lambda_i N^s_{i,r} - \lambda_i N^n_{i,r} - \gamma_i d^s_{p_1} + \gamma_i d^n_{p_1} - (1+\gamma_i)(c\delta t^s(t) - c\delta t^n(t))$$

(3.37)

The parameter $d^{s,n}_{\phi_i,p_1,r}(t)$ is a biased UPD, transmitted to the user to correct the observations. However, the UPD includes the terms $c\delta t^s(t)$ and $c\delta t^n(t)$, which would destroy the slowly changing stochastic property of the UPD. Equation (3.34) can however be rearranged to give equation (3.38):

$$c\delta t^s(t) - c\delta t^n(t) = \frac{1}{\gamma_2 - 1}(\mathrm{k}^{s,n}_{p_2,p_1}(t) + \mathrm{d}^s_{p2} - \mathrm{d}^n_{p2} - \gamma_2\,\mathrm{d}^s_{p1} + \gamma_2\,\mathrm{d}^n_{p1})$$

(3.38)

This rearrangement can then be utilised to substitute in the biased satellite clock parameter from equation (3.37), namely:

$$d^{s,n}_{\phi_i,p_1,r}(t) = -d^s_{\phi_i} + d^n_{\phi_i} + \lambda_i N^s_{i,r} - \lambda_i N^n_{i,r} - \gamma_i d^s_{p_1} + \gamma_i d^n_{p_1} - \frac{(1+\gamma_i)}{(\gamma_2 - 1)}(d^s_{p_2} - d^n_{p_2} - \gamma_2 d^s_{p_1} + \gamma_2 d^n_{p_1}) - \frac{(1+\gamma_i)}{(\gamma_2 - 1)} k^{s,n}_{p_2,p_1}(t)$$

(3.39)

It is now possible to calculate the biased satellite clock alongside a biased UPD, although the UPD is now biased in an alternative way, specifically:

$$d^{s,n}_{\phi_i,p_1,r}(t) = \tilde{d}^{s,n}_{\phi_i,p_1,r} - (1+\gamma_i)(dt^s_l(t) - dt^n_l(t))$$

(3.40)

where

$$\tilde{d}^{s,n}_{\phi_i,p_1,r} = -d^s_{\phi_i} + d^n_{\phi_i} + \lambda_i N^s_{i,r} - \lambda_i N^n_{i,r} - \gamma_i d^s_{p_1} + \gamma_i d^n_{p_1} - \frac{(1+\gamma_i)}{(\gamma_2 - 1)}(d^s_{p_2} - d^n_{p_2} - \gamma_2 d^s_{p_1} + \gamma_2 d^n_{p_1})$$

(3.41)

Using IGS products as shown in equation (3.36) it is possible to write equation (3.40) as equation (3.42):

$$d^{s,n}_{\phi_i,p_1,r}(t) = \tilde{d}^{s,n}_{\phi_i,p_1,r} - \frac{1+\gamma_i}{\gamma_2 - 1} k^{s,n}_{p_2,p_1}(t)$$

(3.42)

The parameterisation of equation (3.40) can be employed in a new measurement model that can be theoretically used to calculate the satellite clocks and UPDs simultaneously, using a single reference receiver or a network of receivers. The new measurement model is given by equations (3.43) and (3.44) using the original satellite clock definition and equations (3.19), (3.20) and (3.40):

$$p^s_{i,r}(t) = R^s_r(t) + T^s_r(t) + b^n_{p_i,r}(t) + k^{s,n}_{p_i,p_1}(t) + \gamma_i \bar{I}^{s,n}_r(t)$$

(3.43)

$$\phi_{i,r}^{s}(t)=R_r^s(t)+T_r^s(t)+b_{\phi_i,r}^{n}(t)-\frac{(1+\gamma_i)}{(\gamma_2-1)}k_{p_2,p_1}^{s,\mathrm{n}}(t)+\tilde{d}_{\phi_i,\mathrm{p}_1,r}^{s,\mathrm{n}}(t)-\gamma_i\overline{I}_r^{s,\mathrm{n}}(t)$$

(3.44)

The matrix form of the observation equations on the L1 and L2 frequency for the single station, a, can be written as equation (3.45):

$$\begin{pmatrix} p_{1,a}-R_a \\ p_{2,a}-R_a \\ \phi_{1,a}-R_a \\ \phi_{2,a}-R_a \end{pmatrix} = \begin{pmatrix} e_n & 0 & 0 & 0 & f_{n,a} & \gamma_1 I_{nx(n-1)} & 0 & 0 & 0 \\ 0 & e_n & 0 & 0 & f_{n,a} & \gamma_2 I_{nx(n-1)} & I_{nx(n-1)} & 0 & 0 \\ 0 & 0 & e_n & 0 & f_{n,a} & -\gamma_1 I_{nx(n-1)} & -\frac{(1+\gamma_1)}{\gamma_2-1} I_{nx(n-1)} & I_{nx(n-1)} & 0 \\ 0 & 0 & 0 & e_n & f_{n,a} & -\gamma_2 I_{nx(n-1)} & -\frac{(1+\gamma_2)}{\gamma_2-1} I_{nx(n-1)} & 0 & I_{nx(n-1)} \end{pmatrix} \begin{pmatrix} b_{p_{1,a}}^{n} \\ b_{p_{2,a}}^{n} \\ b_{\phi_{1,a}}^{n} \\ b_{\phi_{2,a}}^{n} \\ ZD_a \\ \overline{I}_a^{s,\mathrm{n}} \\ k_{p_2,p_1}^{s,\mathrm{n}} \\ \tilde{d}_{\phi_1,p_1,a}^{s,\mathrm{n}} \\ \tilde{d}_{\phi_2,p_1,\mathrm{a}}^{s,\mathrm{n}} \end{pmatrix}$$

(3.45)

Although the measurement model, equation (3.45), is theoretically solvable, the stochastic properties of the ionosphere parameter still prevent the model being optimised practically.

3.2.5 Ionospheric Issues

In the measurement model, equation (3.45), the ionospheric parameter, $\overline{I}_a^{s,\mathrm{n}}$,contains satellite clock terms. Theoretically, this may not be a problem and all the parameters can be estimated. However, in practice, as the ionospheric parameters will be considered as slowly varying, they can be calculated with the use of a Kalman filter, to predict and correct the values. This will currently not be possible in this case as the introduction of a satellite clock value into the parameterisation will cause the parameter to vary stochastically in response to the satellite clock. To rectify this, the satellite clock values must be taken out of the reparameterised form and placed within another parameter. Equation (3.30) can be written as:

$$\bar{I}_r^{s,n}(t) = I_r^s(t) - I_r^n(t) - d_{p_1}^s + d_{p_1}^n - c\delta t^s + c\delta t^n$$

(3.46)

Within equation (3.46) the satellite clocks, $c\delta t^s$ and $c\delta t^n$, cause difficulties stochastically. By using equation (3.38) we can rewrite equation (3.46) as:

$$\bar{I}_r^{s,n}(t) = I_r^s(t) - I_r^n(t) - d_{p_1}^s + d_{p_1}^n - \frac{1}{\gamma_2 - 1}(k_{p_2,p_1}^{s,n}(t) + d_{p2}^s - d_{p2}^n - \gamma_2 d_{p1}^s + \gamma_2 d_{p1}^n)$$

(3.47)

which reduces to:

$$\bar{I}_r^{s,n}(t) = I_r^s(t) - I_r^n(t) + \frac{1}{\gamma_2 - 1} d_{p_1}^s - \frac{1}{\gamma_2 - 1} d_{p_1}^n - \frac{1}{\gamma_2 - 1} d_{p2}^s + \frac{1}{\gamma_2 - 1} d_{p2}^n - \frac{1}{\gamma_2 - 1} k_{p_2,p_1}^{s,n}(t)$$

(3.48)

The satellite clocks are contained within the parameter, $k_{p_2,p_1}^{s,n}(t)$, but this is being estimated separately within the measurement model. Therefore, this term can be removed from the estimated ionospheric parameter, by a reconfiguration of the measurement model. This results in a new ionospheric term given as equation (3.49):

$$\tilde{I}_r^{s,n}(t) = I_r^s(t) - I_r^n(t) + \frac{1}{\gamma_2 - 1} d_{p_1}^s - \frac{1}{\gamma_2 - 1} d_{p_1}^n - \frac{1}{\gamma_2 - 1} d_{p2}^s + \frac{1}{\gamma_2 - 1} d_{p2}^n$$

(3.49)

where (c.f. equation(3.47))

$$\bar{I}_r^{s,n}(t) = \tilde{I}_r^{s,n}(t) - \frac{1}{\gamma_2 - 1} k_{p_2,p_1}^{s,n}(t)$$

(3.50)

The final measurement model can now be formulated to estimate satellite clock and UPD values simultaneously. The measurement model works both theoretically as the equations are non-singular and practically as all the parameters within the model

have the correct stochastic properties. From equations (3.43), (3.44) and (3.50) the required measurement model is given as equations (3.51) and (3.52) :

$$p_{i,r}^{s}(t)=R_r^s(t)+T_r^s(t)+b_{p_i,r}^{n}(t)-\frac{1}{\gamma_2-1}k_{p_2,p_1}^{s,\mathrm{n}}(t)+\gamma_i\tilde{I}_r^{s,n}(t)$$

(3.51)

$$\phi_{i,r}^{s}(t)=R_r^s(t)+T_r^s(t)+b_{\phi_i,r}^{n}(t)-\frac{1}{\gamma_2-1}k_{p_2,p_1}^{s,\mathrm{n}}(t)+\tilde{d}_{\phi_i,\mathrm{p}_1,r}^{s,\mathrm{n}}(t)-\gamma_i\tilde{I}_r^{s,\mathrm{n}}(t)$$

(3.52)

where R_r^s is the satellite range, T_r^s is the troposphere, b^n is the effective receiver clock, $k_{p_2,p_1}^{s,\mathrm{n}}$ the effective satellite clock, $\tilde{d}_{\phi_i,\mathrm{p}_1,r}^{s,\mathrm{n}}$ the effective UPDs and $\tilde{I}_r^{s,\mathrm{n}}$ the effective ionosphere.

In matrix form the observation equations in equations (3.51) and (3.52) on L1 and L2 frequencies for a single station can be written as:

$$\begin{pmatrix} p_{1,a}-R_a \\ p_{2,a}-R_a \\ \phi_{1,a}-R_a \\ \phi_{2,a}-R_a \end{pmatrix}=\begin{pmatrix} e_n & 0 & 0 & 0 & f_{n,a} & \gamma_1 I_{nx(n-1)} & -\frac{1}{\gamma_2-1}I_{nx(n-1)} & 0 & 0 \\ 0 & e_n & 0 & 0 & f_{n,a} & \gamma_2 I_{nx(n-1)} & -\frac{1}{\gamma_2-1}I_{nx(n-1)} & 0 & 0 \\ 0 & 0 & e_n & 0 & f_{n,a} & -\gamma_1 I_{nx(n-1)} & -\frac{1}{\gamma_2-1}I_{nx(n-1)} & I_{nx(n-1)} & 0 \\ 0 & 0 & 0 & e_n & f_{n,a} & -\gamma_2 I_{nx(n-1)} & -\frac{1}{\gamma_2-1}I_{nx(n-1)} & 0 & I_{nx(n-1)} \end{pmatrix}\begin{pmatrix} b_{p_{1,a}}^{n} \\ b_{p_{2,a}}^{n} \\ b_{\phi_{1,a}}^{n} \\ b_{\phi_{2,a}}^{n} \\ ZD_a \\ \tilde{I}_a^{s,\mathrm{n}} \\ k_{p_2,p_1}^{s,\mathrm{n}} \\ \tilde{d}_{\phi_1,p_1,a}^{s,\mathrm{n}} \\ \tilde{d}_{\phi_2,p_1,\mathrm{a}}^{s,\mathrm{n}} \end{pmatrix}$$

(3.53)

Equation (3.53) can be extended to a network of receivers by extending the parameter dataset to include: the station clock/hardware parameters, the zenith delay and the ionospheric term from the additional stations. The satellite clock parameters, $k_{p_2,p_1}^{s,\mathrm{n}}$, are station independent and common to all stations to which the satellite is visible. However, multiple stations for UPD estimation, introduces integer arithmetic as from equation (3.41):

$$\tilde{d}^{s,n}_{\phi_i,p_1,r} = \hat{d}^{s,n}_{\phi_i,p_1} + \lambda_i N^s_{i,r} - \lambda_i N^n_{i,r}$$

(3.54)

where

$$\hat{d}^{s,n}_{\phi_i,p_1} = -d^s_{\phi_i} + d^n_{\phi_i} - \gamma_i d^s_{p_1} + \gamma_i d^n_{p_1} - \frac{(1+\gamma_i)}{(\gamma_2 - 1)}(d^s_{p_2} - d^n_{p_2} - \gamma_2 d^s_{p_1} + \gamma_2 d^n_{p_1})$$

(3.55)

and hence

$$\tilde{d}^{s,n}_{\phi_i,p_1,b} = \tilde{d}^{s,n}_{\phi_i,p_1,a} + \lambda_i N^{s,n}_{i,b,a}$$

(3.56)

where $N^{s,n}_{i,b,a}$ is the integer double difference

$$N^{s,n}_{i,b,a} = N^s_{i,b} - N^n_{i,b} - N^s_{i,a} + N^n_{i,a}$$

(3.57)

Thus, for two stations the extended UPDs' state vector includes $\tilde{d}^{s,n}_{\phi_i,p_1,a}$, for example and the double differences, $N^{s,n}_{i,b,a}$, for i=1, 2. The equations for stations a and b can be represented in matrix form as:

$$
\begin{pmatrix} p_{1,a}-R_a \\ p_{2,a}-R_a \\ \phi_{1,a}-R_a \\ \phi_{2,a}-R_a \\ p_{1,b}-R_b \\ p_{2,b}-R_b \\ \phi_{1,b}-R_b \\ \phi_{2,b}-R_b \end{pmatrix} = \begin{pmatrix}
e_n & 0 & 0 & 0 & 0 & 0 & 0 & 0 & f_a & 0 & \gamma_1 I_{nx(n-1)} & 0 & -\frac{1}{\gamma_2-1} I_{nx(n-1)} & 0 & 0 & 0 & 0 \\
0 & e_n & 0 & 0 & 0 & 0 & 0 & 0 & f_a & 0 & \gamma_2 I_{nx(n-1)} & 0 & -\frac{1}{\gamma_2-1} I_{nx(n-1)} & 0 & 0 & 0 & 0 \\
0 & 0 & e_n & 0 & 0 & 0 & 0 & 0 & f_a & 0 & -\gamma_1 I_{nx(n-1)} & 0 & -\frac{1}{\gamma_2-1} I_{nx(n-1)} & I_{nx(n-1)} & 0 & 0 & 0 \\
0 & 0 & 0 & e_n & 0 & 0 & 0 & 0 & f_a & 0 & -\gamma_2 I_{nx(n-1)} & 0 & -\frac{1}{\gamma_2-1} I_{nx(n-1)} & 0 & I_{nx(n-1)} & 0 & 0 \\
0 & 0 & 0 & 0 & e_n & 0 & 0 & 0 & 0 & f_b & 0 & \gamma_1 I_{nx(n-1)} & -\frac{1}{\gamma_2-1} I_{nx(n-1)} & 0 & 0 & 0 & 0 \\
0 & 0 & 0 & 0 & 0 & e_n & 0 & 0 & 0 & f_b & 0 & \gamma_2 I_{nx(n-1)} & -\frac{1}{\gamma_2-1} I_{nx(n-1)} & 0 & 0 & 0 & 0 \\
0 & 0 & 0 & 0 & 0 & 0 & e_n & 0 & 0 & f_b & 0 & -\gamma_1 I_{nx(n-1)} & -\frac{1}{\gamma_2-1} I_{nx(n-1)} & I_{nx(n-1)} & 0 & \lambda_1 I_{nx(n-1)} & 0 \\
0 & 0 & 0 & 0 & 0 & 0 & 0 & e_n & 0 & f_b & 0 & -\gamma_2 I_{nx(n-1)} & -\frac{1}{\gamma_2-1} I_{nx(n-1)} & 0 & I_{nx(n-1)} & 0 & \lambda_2 I_{nx(n-1)}
\end{pmatrix}
\begin{pmatrix} b^n_{p_{1,a}} \\ b^n_{p_{2,a}} \\ b^n_{\phi_{1,a}} \\ b^n_{\phi_{2,a}} \\ b^n_{p_{1,b}} \\ b^n_{p_{2,b}} \\ b^n_{\phi_{1,b}} \\ b^n_{\phi_{2,b}} \\ ZD_a \\ ZD_b \\ \tilde{I}^{s,n}_a \\ \tilde{I}^{s,n}_b \\ k^{s,n}_{p_2,p_1} \\ \tilde{d}^{s,n}_{\phi_1,p_1,a} \\ \tilde{d}^{s,n}_{\phi_2,p_1,a} \\ N^{s,n}_{1,b,a} \\ N^{s,n}_{2,b,a} \end{pmatrix}
$$

(3.58)

3.3 Mobile Receiver Solution

The reference network of receivers can be utilised to estimate the relative biased satellite clocks, $k^{s,n}_{p_2,p_1}$, as well as the new biased UPDs, $\tilde{d}^{s,n}_{\phi_1,p_1,a}$ and $\tilde{d}^{s,n}_{\phi_2,p_1,a}$. These are subsequently transmitted to the mobile receiver, to allow an integer ambiguity resolved solution to be achieved.

At the mobile receiver, in addition to the remaining parameters: receiver clocks, troposphere, ionosphere and ambiguities, the position of the receiver must be calculated. To achieve this, three parameters, X, Y and Z, must be solved for at each epoch. The partial derivative value for the A matrix, μ_r^s, is computed using the position of each satellite at the given epoch and the approximate position of the mobile receiver. The position of the satellite must be taken at the time of signal transmission and not signal received, as the satellite is moving during the time the signal is travelling. For the X partial relating to the ^{s} satellite the partial can be calculated using equation (3.59):

$$\mu_r^s = \sqrt{\frac{(X_r - X^s)}{(X_r - X^s)^2 + (\mathrm{Y}_r - Y^s)^2 + (\mathrm{Z}_r - Z^s)^2}} \tag{3.59}$$

where X_r, Y_r and Z_r are the coordinates of the mobile receiver and X^s, Y^s and Z^s are the coordinates of the ^{s} satellite.

By transmitting the UPDs from the network, it should allow integer ambiguity resolution at the mobile receiver. Due to the stable nature of the UPDs over time and space, the UPDs at the network should be the same as at the mobile receiver. Therefore, double difference ambiguities can be created in the same manner as those in the network when a second receiver was introduced in section 3.2.5 and equation (3.56).

The resulting user measurement model can be seen in equation (3.60) where μ_r^s is the partial derivative of the distance between the satellite and the receiver and Δx is a vector of the unknown corrections to the initial position estimate in X, Y and Z.

$$\begin{pmatrix} p_{1,\mathrm{u}} - R_u + \dfrac{1}{\gamma_2 - 1} k^{s,\mathrm{n}}_{p_2,p_1} I_{nx(n-1)} \\ p_{2,\mathrm{u}} - R_u + \dfrac{1}{\gamma_2 - 1} k^{s,\mathrm{n}}_{p_2,p_1} I_{nx(n-1)} \\ \phi_{1,\mathrm{u}} - R_u + \dfrac{1}{\gamma_2 - 1} k^{s,\mathrm{n}}_{p_2,p_1} I_{nx(n-1)} - \tilde{d}^{s,\mathrm{n}}_{\phi_1,p_1,\mathrm{a}} I_{nx(n-1)} \\ \phi_{2,\mathrm{u}} - R_u + \dfrac{1}{\gamma_2 - 1} k^{s,\mathrm{n}}_{p_2,p_1} I_{nx(n-1)} - \tilde{d}^{s,\mathrm{n}}_{\phi_2,p_1,\mathrm{a}} I_{nx(n-1)} \end{pmatrix} = \begin{pmatrix} \mu^s_u & e_n & 0 & 0 & 0 & f_{n,\mathrm{u}} & \gamma_1 I_{nx(n-1)} & 0 & 0 \\ \mu^s_u & 0 & e_n & 0 & 0 & f_{n,\mathrm{u}} & \gamma_2 I_{nx(n-1)} & 0 & 0 \\ \mu^s_u & 0 & 0 & e_n & 0 & f_{n,\mathrm{u}} & -\gamma_1 I_{nx(n-1)} & \lambda_1 I_{nx(n-1)} & 0 \\ \mu^s_u & 0 & 0 & 0 & e_n & f_{n,\mathrm{u}} & -\gamma_2 I_{nx(n-1)} & 0 & \lambda_2 I_{nx(n-1)} \end{pmatrix} \begin{pmatrix} \Delta x \\ b^n_{p_{1,\mathrm{u}}} \\ b^n_{p_{2,\mathrm{u}}} \\ b^n_{\phi_{1,\mathrm{u}}} \\ b^n_{\phi_{2,\mathrm{u}}} \\ ZD_u \\ \tilde{I}^{s,\mathrm{n}}_u \\ N^{s,\mathrm{n}}_{1,\mathrm{u,a}} \\ N^{s,\mathrm{n}}_{2,\mathrm{u,a}} \end{pmatrix} \tag{3.60}$$

3.4 Measurement Model Conclusion

This chapter has presented a theoretical method for estimating satellite clocks and UPDs in a single step. Neither the satellite clock parameters nor the UPDs are pure corrections, but instead are a biased form of the parameter. However, as long as the same biased forms of the corrections are used at the mobile receiver as were used in the network, this will not affect the results.

The satellite clocks and UPDs estimated through this method can be obtained using a single receiver and a float solution as shown in equation (3.53). However, if a network of reference receivers is available, it is possible to combine the observations to create a more robust system. Therefore, improving the accuracy of the system.

3.5 Alternative Measurement Model

In section 6.12, comparisons will be made between the measurement models presented in this study and those in the approach outlined in section 2.6.4 (Zhang *et al.*, 2011). For comparison, the equations and measurement models used in this alternative approach will now be outlined.

The reparameterised code and phase observations used to compute satellite clocks and UPDs with a reference network are given in equations (3.61) and (3.62) respectively:

$$p^s_{i,r}(t) = R^s_r(t) + mf^s_r \tilde{T}_r + d\tilde{t}_r - d\tilde{t}^s_l + \gamma_i \bar{l}^s_r$$

(3.61)

$$\phi^s_{i,r}(t) = R^s_r(t) + mf^s_r \tilde{T}_r + d\tilde{t}_r - d\tilde{t}^s_l - \gamma_i \bar{l}^s_r + \lambda_i N^{s1}_{r1,i} + \tilde{\phi}_{i,r} - \tilde{\phi}^s_i$$

(3.62)

The elements of equations (3.61) and (3.62) are defined by:

$$\tilde{T} = T_r - T_1$$

(3.63)

$$d\tilde{t}_r = d\bar{t}_r - d\bar{t}_1$$

(3.64)

where $d\bar{t}_r = dt_r + \frac{\gamma_2}{\gamma_2 - 1} d_{r,1} - \frac{1}{\gamma_2 - 1} d_{r,2}$

(3.65)

$$d\tilde{t}^s_l = dt^s_l - d\bar{t}_1 - mf^s_r T_1$$

(3.66)

where $dt^s_l = dt^s + \frac{\gamma_2}{\gamma_2 - 1} d^s_{,1} - \frac{1}{\gamma_2 - 1} d^s_{,2}$

(3.67)

$$\bar{l}^s_r = l^s_r - \frac{1}{\gamma_2 - 1}(D^S - D_r)$$

(3.68)

where $D^S = d^s_{,2} - d^s_{,1}$

(3.69)

and $D_r = d_{r,2} - d_{r,1}$

(3.70)

$$\tilde{\phi}_{i,r} = \bar{\phi}_{r1,i} + \lambda_i N^1_{r1,i}$$

(3.71)

where $\bar{\phi}_{r1,i} = \bar{\phi}_{r,i} - \bar{\phi}_{1,i}$

(3.72)

and $\bar{\phi}_{r,i} = \phi_{r,i} - \frac{\gamma_2 d_{r,1} - d_{r,2}}{\gamma_2 - 1} + \frac{\gamma_i}{\gamma_2 - 1} D_r$

(3.73)

$$\tilde{\phi}^s_i = \bar{\phi}^s_{,i} - \bar{\phi}_{1,i} - \lambda_i N^s_{1,i}$$

(3.74)

where $\bar{\phi}^s_{,i} = \phi^s_{,i} - \frac{\gamma_2 d^s_{,1} - d^s_{,2}}{\gamma_2 - 1} + \frac{\gamma_i}{\gamma_2 - 1} D^s$

(3.75)

In this approach, the elements given in equations (3.66) and (3.74) are the satellite clock and UPD parameters, respectively. These will subsequently be transmitted to the user as corrections as is done in this study. Equations (3.61) and (3.62) can be used to develop a measurement model for a network of reference receivers, similar to the one developed for this study, as shown in equation (3.58). The measurement model for a network of two stations is presented in equation (3.76):

$$\begin{pmatrix} p_{1,a}-R_a \\ p_{2,a}-R_a \\ \phi_{1,a}-R_a \\ \phi_{2,a}-R_a \\ p_{1,b}-R_b \\ p_{2,b}-R_b \\ \phi_{1,b}-R_b \\ \phi_{2,b}-R_b \end{pmatrix} = \begin{pmatrix} 0 & 0 & \gamma_1 I & 0 & -I & 0 & 0 & 0 & 0 & 0 & 0 \\ 0 & 0 & \gamma_2 I & 0 & -I & 0 & 0 & 0 & 0 & 0 & 0 \\ 0 & 0 & -\gamma_1 I & 0 & -I & 0 & 0 & I & 0 & 0 & 0 \\ 0 & 0 & -\gamma_2 I & 0 & -I & 0 & 0 & 0 & I & 0 & 0 \\ e_n & mf_b & 0 & \gamma_1 I & -I & 0 & 0 & 0 & 0 & 0 & 0 \\ e_n & mf_b & 0 & \gamma_2 I & -I & 0 & 0 & 0 & 0 & 0 & 0 \\ e_n & mf_b & 0 & -\gamma_1 I & -I & 1 & 0 & I & 0 & \lambda_1 I_{nx(n-1)} & 0 \\ e_n & mf_b & 0 & -\gamma_2 I & -I & 0 & 1 & 0 & I & 0 & \lambda_1 I_{nx(n-1)} \end{pmatrix} \begin{pmatrix} d\tilde{t}_b \\ \tilde{T} \\ \overline{I}_a^s \\ \overline{I}_b^s \\ d\tilde{t}_l^s \\ \tilde{\phi}_{1,\mathrm{b}} \\ \tilde{\phi}_{2,\mathrm{b}} \\ \tilde{\phi}_1^s \\ \tilde{\phi}_2^s \\ N_{r1,1}^{s1} \\ N_{r1,2}^{s1} \end{pmatrix}$$

(3.76)

where I is the unit matrix, $I_{nx(n-1)}$ and e_n are the same as previously described in section 3.2.2.

The satellite clock and UPD corrections computed from this measurement model are used to compute a user solution in which IAR is possible. The equations developed in this alternative approach, developed by Zhang *et al.* (2011), for the user receiver are given in equations (3.77) and (3.78):

$$p_{i,\mathrm{u}}^s(t) - R_u^s(t) + d\tilde{t}_l^s = \mu_u^s \Delta x + mf_u^s \tilde{T}_u + d\tilde{t}_u + \gamma_i \overline{I}_u^s$$

(3.77)

$$\phi_{i,\mathrm{u}}^s(t) - R_u^s(t) + d\tilde{t}_l^s + \tilde{\phi}_i^s = \mu_u^s \Delta x + mf_u^s \tilde{T}_u + d\tilde{t}_u - \gamma_i \overline{I}_u^s + \lambda_i N_{u1,i}^{s1} + \tilde{\phi}_{i,\mathrm{u}}$$

(3.78)

where $\tilde{T}_u$, $d\tilde{t}_u$, $\overline{I}_u^s$ and $\tilde{\phi}_{i,\mathrm{u}}$ are similar to those presented in the network equations.

These equations can be written as a measurement model, equation (3.79), to allow comparisons with the measurement model given in this study, as shown in equation (3.60):

$$\begin{pmatrix} p_{1,u} - R_u + d\tilde{t}_l^s \\ p_{2,u} - R_u + d\tilde{t}_l^s \\ \phi_{1,u} - R_u + d\tilde{t}_l^s + \tilde{\phi}_i^s \\ \phi_{2,u} - R_u + d\tilde{t}_l^s + \tilde{\phi}_i^s \end{pmatrix} = \begin{pmatrix} \mu_u^s & e_n & mf_u^s & \gamma_1 & 0 & 0 & 0 & 0 \\ \mu_u^s & e_n & mf_u^s & \gamma_2 & 0 & 0 & 0 & 0 \\ \mu_u^s & e_n & mf_u^s & -\gamma_1 & \lambda_1 & 0 & 1 & 0 \\ \mu_u^s & e_n & mf_u^s & -\gamma_2 & 0 & \lambda_2 & 0 & 1 \end{pmatrix} \begin{pmatrix} \Delta x \\ d\tilde{t}_u \\ \tilde{T}_u \\ \overline{I}_u^s \\ N_{u1,1}^{s1} \\ N_{u1,2}^{s1} \\ \tilde{\phi}_{1,u} \\ \tilde{\phi}_{2,u} \end{pmatrix} \tag{3.79}$$

Chapter 4. Kalman Filter

4.1 Introduction

GNSS observations contain a series of errors, which have been outlined previously in Chapter 2. Some of these are systematic errors that change slowly over time and can be modelled or estimated, while other errors are random errors that vary with a normal distribution with a mean of zero. At each epoch, least squares could be used to estimate a series of parameters, with the aim of achieving the smallest mean square error possible in all the observations.

This process could be expanded and improved by applying weighted least squares. This has the advantage of applying different weights to the input observations depending on their relative accuracies. For example, phase observations are significantly more precise than code observations from GNSS satellites. Additionally, observations from satellites at higher elevations are, in general, more accurate than lower elevation satellites, as the signal must pass through less of the Earth's atmosphere. The weighted least squares can take these differences into account to estimate the best solution for all the parameters.

The least squares methodology is good at achieving a solution at any given epoch of data. However, the results from each epoch are independent of each other and therefore do not utilise the stochastic properties of the estimated parameters to improve the estimation process. To utilise previous epochs of data into the current epoch the Kalman filter must be implemented.

The Kalman filter is an algorithm developed to estimate a series of unknowns from measurements over a period of time. It allows measurement accuracies and statistical noise to be incorporated to achieve the best possible solution at each epoch (Kalman, 1960). The filter is widely used within engineering and other disciplines, but particularly within the field of navigation.

Estimation using a Kalman filter is a two-step process at each epoch. Firstly, the current estimates of the parameters along with their accuracies are used to create a prediction of the parameters at the next epoch. New observations are then incorporated into the filter along with their accuracies and statistical noise. This

allows the second step, the estimation, to take place where a weighted solution of the predicted state and new observations are used to calculate a new set of values for the variables. This process is recursive as each new set of observations becomes available meaning the solution at each epoch uses all the data beforehand to calculate the best solution possible. This process is illustrated in the flowchart in Figure 4-1.

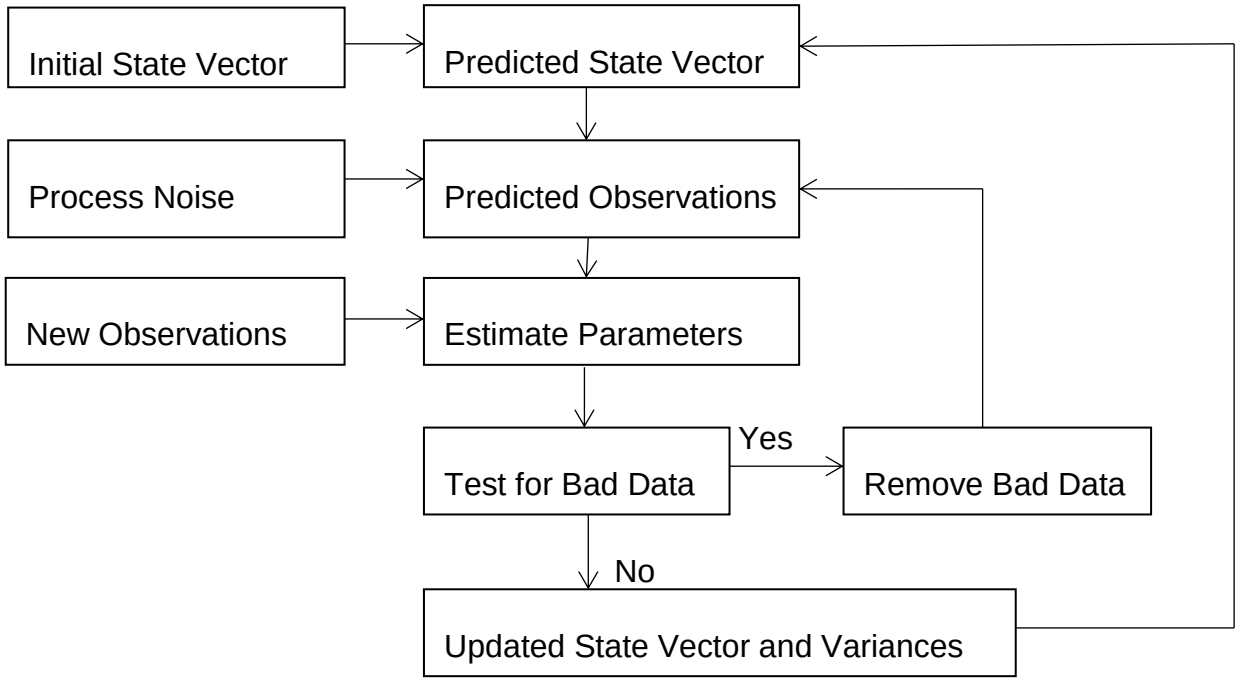

Figure 4-1 - Kalman Filter Process

4.2 Kalman Filter Equations

The filter consists of a vector of observations, y, and a vector of parameters, x, known as the state vector. These are combined into a measurement model at epoch, k, given by:

$$y_k = A_k x_k + \varepsilon_k \tag{4.1}$$

where ε is the random measurement error and A the design matrix of dimension (m x n), where m is the number of observations and n is the number of parameters.

To begin a Kalman filter, an initial state vector and corresponding variances must be created. In the majority of applications, the initial state vector is likely to consist of all zeros, as there is no information about each parameter to improve the estimate. Additionally, the corresponding variance-covariance matrix is likely to have large values along the leading diagonal, representing a high uncertainty in the current state vector, with zeros elsewhere, representing unknown levels of covariance. Exceptions to this are, for example, the XYZ position of a receiver in GNSS positioning, where it may be possible to estimate the position in the initial state vector. However, the corresponding variances are still likely to remain high, as the accuracy of the initial estimate is limited. The initial values used in this work will be discussed later in the chapter.

Once an initial state vector has been established for the epoch k-1, it can be used to calculate the predicted state vector and corresponding predicted variance-covariance matrix at epoch k. To convert the previous epoch's state vector into a predicted state vector, a transition matrix, $\Phi_{k,k-1}$, must be used. This transition matrix accounts for any velocities and accelerations estimated by the Kalman filter, to accurately predict the value of the parameters one epoch later. In many cases, where velocities are not measured or do not exist, the transition matrix is taken to be the unit matrix, as the predicted state will be assumed equal to the previously estimated state vector. The formula to estimate the predicted state vector is given by:

$$\hat{x}_{k|k-1} = \Phi_{k,k-1}\hat{x}_{k-1|k-1} \tag{4.2}$$

The predicted matrix, $Q_{\hat{x}_{k|k-1}}$, consists of two components. Firstly, with the use of the transition matrix, the previous variance-covariance matrix, $Q_{\hat{x}_{k-1|k-1}}$, is used to calculate the accuracies of predicted parameters. Secondly, statistical process noise, Q_{w_k}, is added to the variances in the matrix. This noise is added to allow each variance to change in value between each epoch. The stochastic properties of each parameter dictate the amount of process noise that is added at each epoch. For example, parameters, which change rapidly, such as the satellite clock, will have a large process noise, whereas, slowly varying parameters, such as the troposphere will

have smaller process noise values added. The formula for the predicted variance-covariance matrix is given by:

$$Q_{\hat{x}_{k|k-1}} = \Phi_{k,k-1} Q_{\hat{x}_{k-1|k-1}} \Phi_{k,k-1}^T + Q_{w_k}$$

(4.3)

Once the predicted state vector has been calculated it is possible to compute predicted observations, $y_{k|k-1}$. To compute these observations the design matrix is used to turn the predicted parameters into observations as can be seen in equation (4.4). With the introduction of the actual new observations, y_k, it becomes possible to obtain the innovation residuals, N, which are the difference between the true observations and the predicted observations as shown in equation (4.5).

$$y_{k|k-1} = A_k \hat{x}_{k|k-1}$$

(4.4)

$$N = y_k - A_k \hat{x}_{k|k-1}$$

(4.5)

The next stage within the Kalman filter is to estimate the parameters, $\hat{x}_{k|k}$, using the new observations and predicted parameters. The first step is to calculate the Kalman gain matrix, K_k. This is calculated using the design matrix, predicted variance-covariance matrix and finally the observation weight matrix, Q_{y_k}, which gives more weight to higher precision observations. This observation weight matrix, Q_{y_k}, is a diagonal matrix consisting of weighted variance and will be discussed in more detail in section 4.3.3.2. The Kalman gain equation is given by equation (4.6). The Kalman gain matrix can subsequently be used to calculate the update to the predicted state vector and therefore achieve the new state vector, $\hat{x}_{k|k}$, as shown in equation (4.7):

$$K_k = Q_{\hat{x}_{k|k-1}} A_k^T (Q_{y_k} + A_k Q_{\hat{x}_{k|k-1}} A_k^T)^{-1}$$

(4.6)

$$\hat{x}_{k|k} = \hat{x}_{k|k-1} + K_k(y_k - A_k\hat{x}_{k|k-1})$$

(4.7)

To correspond with the new state vector, a new variance-covariance matrix must be computed to give variances and covariances to the newly estimated parameters. This matrix is computed using:

$$Q_{\hat{x}_{k|k}} = (I - K_k A_k)Q_{\hat{x}_{k||k-1}}$$

(4.8)

Once a new state vector and new variance-covariance matrix have been computed it is possible to determine the post fit residuals. These residuals show how well the observations fit the new estimate of the parameters. Post fit residuals, v, can be computed using:

$$v_k = y_k - A_k\hat{x}_{k|k}$$

(4.9)

4.2.1 Error Detection

At each epoch during the Kalman filter, there are errors in the observations, which contribute to the solution. In the majority of cases, the size of these errors are consistent with the accuracy of the observations. However, in some cases the errors can be large and consequently start to negatively affect the overall accuracy of the solution. In these instances the observations need to be removed so as not to deteriorate the solution. The method for statistically removing these observations is the Detection, Identification and Adaptation (DIA) procedure (Kleusberg and Teunissen, 1998).

The first step of this procedure is the detection. The post fit residuals must be analysed to see if any epoch is anomalous and a statistical outlier. To test for outliers, a T_k value must be calculated. This value is a weighted average of all the post fit residual values, to assess, as a whole, if the parameters fit the epoch of data.

A critical value must then be chosen by the user, which dictates at what point the T value is considered anomalous. The T_k value can be computed using equation (4.10) .

$$T_k = \frac{v_k{}^T Q_{y_k}{}^{-1} v_k}{m-n} \tag{4.10}$$

where m is the number of observations and n is the number of parameters.

The result of the overall model test is given by the value T_k . Hypothesis can then be set up to decide if, as a whole, the epoch of observations will be accepted or not. The null hypothesis is that the T value has a central F distribution with m-n and ∞ degrees of freedom. This is tested using α as the level of significance. The alternative hypothesis is therefore:

$$T_k > F_{\alpha,m-n}(m-n,\infty,0). \tag{4.11}$$

The critical value for accepting the null hypothesis is dependent on the application and the accuracy of the observations being used. If the T_k value computed fails the critical value test, then the epoch of data has been labelled as anomalous and the alternative hypothesis must be accepted. In this situation, it is essential to locate the anomalous observation(s) that are the root cause and to remove them. This second step is the identification stage and is known as the slippage test.

In the slippage test a ω value or the normalised residuals is computed for each observation at the epoch and is calculated as:

$$\omega = \frac{|v_k|}{\sqrt{Q_{y_k}}} \tag{4.12}$$

where v_k is given in equation (4.9) and Q_{y_k} is first used in equation (4.6).

These ω values will follow a normal distribution. Therefore, it is the observation with the largest ω value that is most erroneous. In the final adaptation stage, the observation that has the largest ω value is considered for removal. The Kalman filter may then be rerun at the current epoch to obtain a new solution without this observation. If the observation removed is the reference satellite then a new reference satellite must be selected and the transformations discussed in section 4.3.2 applied. This whole process is then repeated with the new solution until the T_k value passes the null hypothesis.

4.3 Applied Kalman Filter

The Kalman filter described above can be applied to the measurement models presented in the previous chapter. MATLAB was used to develop the Kalman filter.

4.3.1 Observation Files

Before the Kalman filter was developed, observation files are required. For this Fugro Intersite developed a small program that created OMC files to speed up the creation of the Kalman filter program. The program requires RINEX, satellite orbit, satellite clock and antenna files as inputs and outputs a single OMC file per station per day. The OMC file consists of phase and code observations on the L1 and L2 frequencies, the elevation angle of the satellite, the partial derivative values of the troposphere and the partials of the X, Y and Z position if required. The advantage of the OMC program is that factors such as cycle slips, dry tropospheric error and poor signal to noise ratio observations are already removed and therefore could be ignored in the later stages of program development. This allowed more time to be committed to developing the novel ideas presented in this thesis, instead of recreating existing code.

4.3.2 Reference Satellite

Once the OMC residual observations have been read in by the program at each epoch, a reference satellite needs to be selected. This reference satellite is important to set up the measurement model presented in the previous chapter. The reference satellite is selected per epoch as the satellite at the highest elevation, as

theoretically, this will be the most accurate observation due to it travelling through the fewest slant distances in the Earth's atmosphere.

If the reference satellite at any epoch is different from the previous epoch, further actions must be performed. The majority of the parameters calculated in the measurement model use this satellite as reference. Therefore, if this reference satellite changes, all the parameters will change in value. However, this change can be accurately calculated by combining existing parameters. For example, if the reference satellite was satellite 1 at the previous epoch and the new reference is satellite 2 then the parameters for satellite 3 will be calculated using

$$k^{3,2} = k^{3,1} - k^{2,1} \tag{4.13}$$

where the first superscript refers to the satellite and the second the reference satellite.

Calculating the change in the estimated parameters means the parameters can still be accurately predicted in the Kalman filter and the process noise does not have to be increased. The receiver clock parameters cannot be updated in the same way as they are not a difference between two satellites. However, an accurate prediction of the receiver clock is not important as the process noise is high and therefore is unconstrained by the Kalman filter.

In addition to the predicted state vector being updated when a reference satellite change occurs, the corresponding variance-covariance matrix must also be transformed. To achieve this, the variance-covariance matrix computed at the previous epoch, $Q_{\hat{x}_{k-1|k-1}}$, must be pre and post multiplied by the matrix M and M^T respectively in a variance propagation process. This matrix M is a series of 1's and -1's, which transforms the state variance covariance matrix so that it denotes the new parameter set, which are referenced to the changed reference satellite.

There is one exception to the rule that the reference satellite is always the satellite with the highest elevation, as will be further discussed in section 4.3.4. Double difference ambiguities are not fixed to integers instantaneously and in some cases not fixed at all. If some of the double difference ambiguities have been fixed to

integers, but the highest satellite has not, then that satellite cannot become the reference. Instead the highest satellite that has been fixed to an integer is selected. This is required because if the reference satellite is changed to a satellite with a floating ambiguity then when the updated predictions are computed for ambiguities that have already been fixed, they will no longer be integer values so will have to be recomputed as integers.

4.3.3 Kalman Filter Settings

During the development of the Kalman filter a number of settings must be applied, which affect how the Kalman filter works. These settings include the initial values, the process noise and the observation weighting. The settings have variable effects on the results, with some having more effect than others. The following sections will outline the values, which were used throughout this project and the rationale behind the selection of those values.

4.3.3.1 Initial Values

As described in section 4.2, at the first epoch, initial values for all the parameters must be chosen. As there is no prior information about the value of any of the parameters, it is impossible to accurately predict these values. Therefore, all the parameters usually have initial values of zero. Along with initial values, the initial variance covariance matrix must be set, which gives the confidence level of the initial values. As discussed, the initial values are imprecise and consequently the variance values in the matrix must be high. These high values will apply a low weight to the predicted parameter values, thus letting the Kalman filter calculate the parameters to whatever value fits the data best. The variances, , selected for the initial variance covariance matrix in the network and user Kalman filter programs are shown in Table 4-1 and Table 4-2 respectively.

Table 4-1 - Network Initial Variances

Network Initial Variances	σ (m)	σ^2 (m^2)
Receiver Clock	9	81
Troposphere	0.1	0.01
Ionosphere	9	81
UPD	9	81
Satellite Clock	9	81
Ambiguity	9	81

Table 4-2 - User Initial Variances

User Initial Variances	σ (m)	σ^2 (m^2)
XYZ Position	9	81
Receiver Clock	9	81
Troposphere	0.1	0.01
Ionosphere	9	81
Ambiguity	9	81

4.3.3.2 Observation Weighting

The observation weight matrix, Q_{y_k}, allows multiple observations, each with different levels of precision to be integrated simultaneously. For GPS there are two types of observations as outlined in section 2.1.1, the precise phase and the coarse code measurements. Additionally, each observation is transmitted from a satellite at a different elevation angle, which also has an impact on the accuracy of the observations. Signals from low elevation satellites will have to pass through more of the Earth's atmosphere, such as the troposphere. Therefore, these signals will be less accurate than those at high elevations and must be weighted accordingly. The

standard deviation and variances for satellites at 90° elevation can be seen in Table 4-3. The values in the table have been found to be the maximum residual values for the respective observations over a range of receiver types (Bona, 2000). These values are then adapted for all elevation angles using equation (4.14) where e is the elevation angle.

Table 4-3 - Observation Weights

Observation Weights	σ (m)	σ^2 (m)
Code	0.5	0.25
Phase	0.005	0.000025

$$\sigma_e = \frac{\sigma}{\sin(e)^2} \tag{4.14}$$

Low elevation satellites are much less reliable, not only because they travel through more of the Earth's atmosphere, but also due to loss of lock as the line of sight is often obscured. Nearby buildings and trees can frequently block the signal reaching the receivers for a period of time. Therefore, it is common to apply an elevation mask to the data, which excludes all the observations from satellites below a certain elevation. For the purpose of this thesis the elevation mask was set at 7° to mask the majority of this poor data and for accurate comparisons with similar research studies (Fang *et al.*, 1998).

Another factor that can affect the accuracy and reliability of observations is signal to noise ratio. Each GNSS receiver measures the signal to noise ratio of the data from every satellite. The ratio measures how much of the signal is coming directly from the satellite and how much is from a reflected source or interfered version of the direct signal. The ratio is given in the RINEX file and has a value between 1 and 9, where 9 is the maximum signal strength and 1 the weakest. A value of 5 is seen as the threshold value for good signal to noise ratio (Gurtner, 2007). Therefore, all data with

a signal to noise ratio of below 5 is excluded from the observations to prevent that data from corrupting the solution.

4.3.3.3 Process Noise

Within the measurement model, the different parameters that are being estimated have different stochastic properties. These stochastic properties dictate the probability of random movement in the parameter over time. For example, the receiver clock parameters can change rapidly and randomly from one epoch to the next. Conversely, the troposphere is a slowly varying parameter that stays quasi stationary from one epoch to the next. Hence, the Kalman filter can make use of these stochastic properties to bias certain parameters towards their predicted or previous value instead of the incoming observations.

The process noise, Q_{w_k}, is added into the Kalman filter as shown in equation (4.3). The amount of process noise is dictated by the parameter's stochastic properties. Firstly, parameters likely to vary greatly will have a very large σ value, resulting in those parameters being essentially unconstrained. These parameters can be considered as unconstrained because the noise applied results in the solution being so biased towards the new observations, that the effect of the predicted parameters value can be considered negligible. Secondly, parameters which are fairly stable over time are given lower process noise values. Consequently, the predicted parameters values have a larger effect on the result.

The values chosen for each parameter were determined based on literature from similar existing programs and through the initial testing phases of the program. As previously discussed, the receiver and satellite clock parameters can vary rapidly and consequently should be unconstrained in the Kalman filter, resulting in the value of 9 $ms^{-1/2}$ being assigned. The value of 9 $ms^{-1/2}$ was found to be significantly large to consider the parameter as unconstrained, whilst not being so large that it reduced computational efficiency. Likewise, the user position is a parameter that can change rapidly and unpredictably so needs to be unconstrained, with the same value of 9 $ms^{-1/2}$.

The zenith ionosphere value can change rapidly especially in areas close to the equator. Additionally, the ionosphere parameter varies with elevation so both these

factors must be considered in the process noise value. Previous work has shown that maximum changes in the slant ionosphere values are approximately 0.3 $mmin^{-1/2}$, although this could potentially treble in size during years of high solar activity (Doherty *et al.*, 1994). As a result, a value of 0.01 $ms^{-1/2}$ or 0.6 $mmin^{-1/2}$ was chosen to take into account potential solar activity.

The UPD and ambiguity process noise values must be low to tightly constrain the Kalman filter and consequently keep the UPD and ambiguity values stable. Studies have found the UPD values are stable, up to 0.1 of a cycle per day (Zhang *et al.*, 2017). Therefore, a value of $1x10^{-6}$ $ms^{-1/2}$ was decided upon for both the UPD and ambiguity parameters.

Finally, the troposphere varies slowly and has been found to vary approximately 1 $cmh^{-1/2}$ (Leick, 2015), which equates to $3x10^{-6}$ $ms^{-1/2}$. This value has also been validated during testing by comparing the wet zenith tropospheric delay obtained using the approach outlined in this thesis with the values obtained from the GIPSY-OASIS v6.4 PPP software package. The same RINEX files were processed by both software packages over the same 24 hour period to compare the wet troposphere values.

Figure 4-2 and Figure 4-3 show the results of this test for four different stations within the network on two separate days. The offset between the two sets of the values is caused by the difference in the dry troposphere estimates, but this will not affect the amount the two data sets are correlated. The tests were repeated over various stations and days. After ignoring the first 30 minute stabilisation period, a correlation of between 0.85 and 0.96 was observed between GIPSY-OASIS and the Kalman filter solutions. Therefore, it was concluded that this is the correct process noise value to use in the Kalman filter. The process noise values for the network program and the user program are shown in Table 4-4 and Table 4-5 respectively.

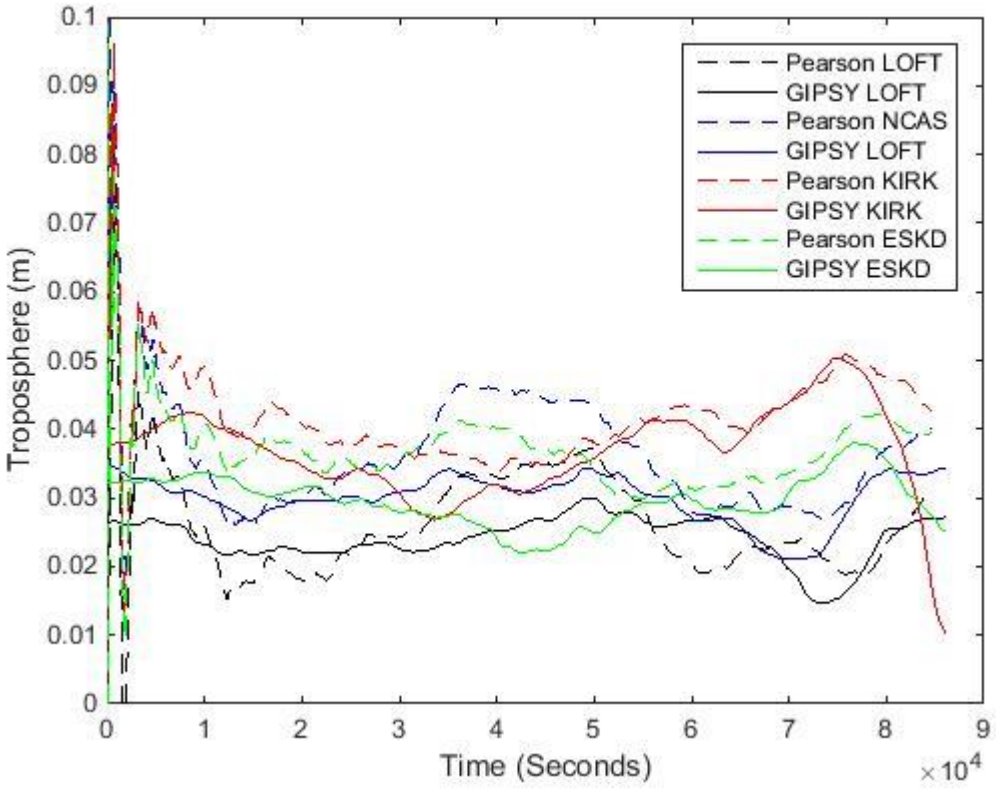

Figure 4-2 - Troposphere Comparison to GIPSY-OASIS for DOY 060

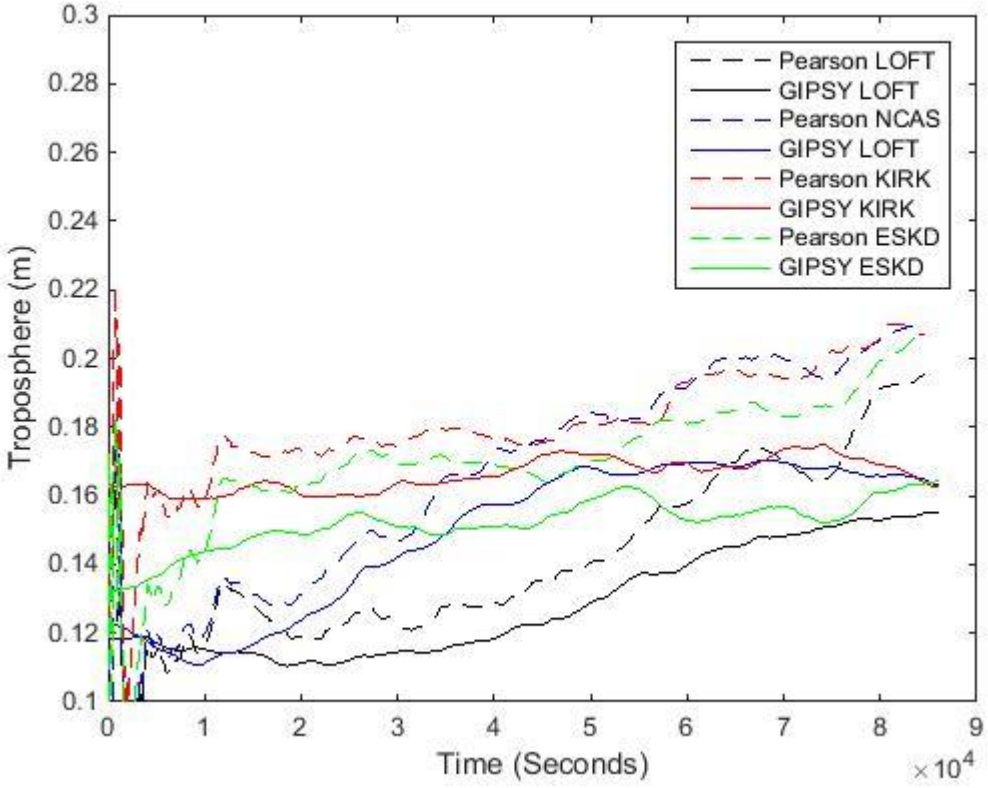

Figure 4-3 - Troposphere Comparison to GIPSY-OASIS for DOY 152

Table 4-4 - Network Process Noise

Network Process Noise	σ (**ms**$^{-1/2}$)	σ^2 (m^{2}s^{-1})
Receiver Clock	9	81
Troposphere	0.000003	9x10^{-12}
Ionosphere	0.01	0.0001
UPD	0.000001	1x10^{-12}
Satellite Clock	9	81
Ambiguity	0.000001	1x10^{-12}

Table 4-5 - User Process Noise

User Process Noise	σ (**ms**$^{-1/2}$)	σ^2 (m^{2}s^{-1})
XYZ Position	9	81
Receiver Clock	9	81
Troposphere	0.000003	9x10^{-12}
Ionosphere	0.01	0.0001
Ambiguity	0.000001	1x10^{-12}

4.3.4 LAMBDA Program

In Chapter 3, the measurement model was presented, in which double difference ambiguities were calculated. These double difference ambiguities are integer in value and will remain at the same integer value throughout the visibility of the satellite, as long as the reference satellite does not change. In reality though, cycle slips can occur where the integer value will change. However, it can be assumed these have been removed during the OMC observation generation.

If it is possible to fix the double difference ambiguities to their correct integer, then this would result in fewer parameters being estimated in the Kalman filter and less

error in the ambiguity parameter. Therefore, in theory, this would result in a more accurate solution due to increased redundancy.

Within the Kalman filter it is not possible to set a certain parameter to an integer value whilst simultaneously estimating other non-integer parameters. Therefore, the double difference ambiguities computed by the Kalman filter at each epoch are floating, non-integer values. These floating ambiguities can subsequently be input to a LAMBDA program, which will attempt to fix the parameters to integers.

The LAMBDA method has been developed since 1993 (Teunissen, 1993; Teunissen, 1994; Teunissen, 1995)). The LAMBDA method has subsequently been implemented in various software packages, including MATLAB (De Jonge and Tiberius, 1996). The latest version of the software in MATLAB is LAMBDA 3.0 and is freely available (Verhagen, 2012). The program requires the floating ambiguity values and the corresponding parts of the variance covariance matrix for each satellite. There are six different options within the LAMBDA program, which decide the method the program will use to try to fix the ambiguities. These six methods are outlined in Verhagen (2012). The method that was chosen for the thesis was the Integer Least Squares (ILS) ratio test as this applies statistical testing to the fixing procedure. This testing allowed some of the ambiguities to be rejected, when it may not be fixing to the correct values. This is critical within the Kalman filter as incorrect ambiguity fixing will result in a significantly worse solution than not fixing at all.

For the ILS ratio test in the LAMBDA program, the float ambiguities, $\hat{a}$, and corresponding variances and covariances, $Q_{\hat{a}\hat{a}}$, are required as inputs. The final state vector, $\hat{x}_{k|k}$, is separated into two parts, the float ambiguities that have just been fixed, $\hat{a}$, and the remaining parameters, $\hat{b}$,. The variance covariance matrix $Q_{\hat{x}_{k|k}}$ is also split into parts corresponding to the float ambiguities and other parameters. This can be represented as:

$$\begin{bmatrix} \hat{a} \\ \hat{b} \end{bmatrix} = \begin{bmatrix} Q_{\hat{a}\hat{a}} & Q_{\hat{a}\hat{b}} \\ Q_{\hat{b}\hat{a}} & Q_{\hat{b}\hat{b}} \end{bmatrix}$$

(4.15)

It is possible to pass all the ambiguities simultaneously to the LAMBDA program to attempt to fix all the ambiguities to integers. However, the statistical test within the ILS ratio test is only capable of accepting the whole solution or rejecting the whole solution. Consequently, this can often result in some ambiguities being fixed incorrectly or no ambiguities being fixed at all. Alternatively, the ambiguities are passed to the LAMBDA program in pairs of L1 and L2 ambiguities for the same satellite-station pair. These two ambiguities are highly correlated with each other and will have been estimated for the same period of time so should be fixed simultaneously.

The L1 and L2 ambiguities are highly correlated, this can cause the LAMBDA program to become inefficient and result in large search times for integer ambiguities. Therefore, the first stage within the LAMBDA program is to undertake a decorrelation. The float ambiguities, $\hat{a}$, are transformed using the Z transformation to create new ambiguities, $\hat{z}$ (Verhagen, 2012).

$$\hat{z} = Z^T \hat{a}$$

(4.16)

The corresponding parts of the variance covariance matrix are also updated within the decorrelation using:

$$Q_{\hat{z}\hat{z}} = Z^T Q_{\hat{a}\hat{a}} Z$$

(4.17)

$$Q_{\hat{b}\hat{z}} = Q_{\hat{b}\hat{a}} Z$$

(4.18)

Once the decorrelation has taken place, an efficient search using ILS can be undertaken. This process uses a least squares solution but with the additional constraint that the ambiguities can only have an integer nature. The value of the fixed ambiguities, $\breve{a}$, are estimated using:

$$\breve{a} = \min_{z \in zn} (\hat{a} - z)^T Q_{\hat{a}\hat{a}}^{-1} (\hat{a} - z)$$

(4.19)

When applying the ILS procedure there may not be a unique solution as there are often multiple integers that the ambiguities could be fixed to. The LAMBDA program is capable of estimating the two most likely solutions that satisfy equation (4.19). The two solutions can subsequently be tested using the ratio test to decide how likely it is that one of the solutions will be correct. Equation (4.20) finds the ratio between the minimised ILS value for the most likely solution, $F(\breve{a})$, and the minimised ILS value for the second most likely solution, $F(\breve{a}')$. This ratio is then tested against a critical value, μ (Verhagen, 2012).

$$\frac{F(\breve{a})}{F(\breve{a}')} \leq \mu$$

(4.20)

where

$$F(\breve{a}) = (\hat{a} - a)^T Q_{\hat{a}\hat{a}}^{-1} (\hat{a} - a)$$

(4.21)

The critical value μ is a user defined value between 0 and 1. This value dictates when the most likely ILS solution is accepted or rejected and therefore the float ambiguities remain. For the purposes of this study a critical value of 0.2 was used, which as a ratio results in the most likely solution needing to be five times more accurate than the second most likely solution. This value of 0.2 is a tight constraint on the LAMBDA program to ensure that incorrect ambiguity fixing is kept to a minimum as this would cause large errors in the solution.

When attempting to fix ambiguities to integer values, it is critical to wait a period of time before the fixing processing begins. As each satellite becomes visible, the parameters (including the ambiguity parameters) must initialise and stabilise. Until this point, the values of the parameters are not reliable and therefore should not be fixed to an integer. During testing carried out using the MATLAB program it was

found that the ambiguities stabilised after approximately 30 minutes, i.e.1800 epochs at 1 Hz. Therefore, a limit was set that each set of floating ambiguities only become eligible for fixing in the LAMBDA program after they have been visible for at least 1800 epochs. Additionally, the elevation of each satellite undergoing IAR must be greater than 30°. This is because observations from satellites at low elevations are less accurate than those at high elevations and therefore the potential for incorrect ambiguity fixing is much greater.

If the LAMBDA program is successful in fixing any ambiguities to integer values then these parameters no longer need to be estimated in the Kalman filter. Therefore, the integer values can be moved to the left hand side of the measurement model and subtracted from the observations. Consequently, there will be increased redundancy in the solution, leading theoretically to a more accurate solution.

When the ambiguities are fixed to integers the change in the value of the ambiguity parameters could be 10's of cm. This sudden change in the value of the ambiguity parameter has to result in a change in other parameters to ensure the solution remains a good fit to the observations. Due to the way the measurement model (described in section 3.2.5) is set up it is not possible to force this change into any single parameter or set of parameters. Instead all parameters must change slightly in order to account for the shift in the ambiguity parameter.

The method for adjusting the parameters when ambiguities have been fixed is outlined in Verhagen (2012). Once the state vector and corresponding variance covariance matrix have been separated using equation (4.15), it is possible to update the remaining parameters, $\hat{b}$. Using the float ambiguities, $\hat{a}$, and the newly computed fixed ambiguities, $\breve{a}$, the updated solution, $\breve{b}$, can be calculated using equation (4.22):

$$\breve{b} = \hat{b} - Q_{\hat{b}\hat{a}} Q_{\hat{a}\hat{a}}^{-1} (\hat{a} - \breve{a}) \tag{4.22}$$

The equation takes into account the difference between the float ambiguities and fixed ambiguities, along with the covariance between all parameters, to adjust all the parameters accordingly. In addition to the state vector being updated, it is essential

to update the variance covariance matrix. The matrix, $Q_{\hat{b}\hat{b}}$, can be updated using equation (4.23) to give the new variance covariance matrix, $Q_{\breve{b}\breve{b}}$:

$$Q_{\breve{b}\breve{b}} = Q_{\hat{b}\hat{b}} - Q_{\hat{b}\hat{a}} Q_{\hat{a}\hat{a}}^{-1} Q_{\hat{a}\hat{b}} \tag{4.23}$$

The newly updated solutions, $\breve{b}$ and $Q_{\breve{b}\breve{b}}$, can then be used at the following epoch to predict the parameters going forward in the Kalman filter.

4.3.5 Detection Identification and Analysis

As discussed in section 4.2.1, error detection is required at each epoch to check for anomalous data and to remove the data following the DIA procedure (Kleusberg and Teunissen, 1998). Through testing, a critical value for the overall model test must be decided upon. It is critical to remove all erroneous observations that corrupt the solution, whilst not removing too much data that the accuracy of the solution is compromised due to lack of redundancy.

Experiments undertaken have shown that a critical T value of unity allows the erroneous data to be removed effectively, while also minimising the amount of data that is removed. If the T value exceeds the value of unity, the Kalman filter is rerun at that epoch with the bad observations removed.

Within the program, only one observation will achieve the maximum ω value required to remove that observation. However, when an observation is removed, its corresponding code and phase observations on both L1 and L2 for that satellite-station pair are also removed. At the following epoch if the satellite is still visible a full reset of the parameters associated with that observation is undertaken.

Chapter 5. Testing Methodology

5.1 Proposed GNSS Data

The measurement models, described in section 3.2.5 and 3.3, must be tested to assess their accuracy and precision. A series of tests will be established to estimate the UPDs and the satellite clocks, using a network of static receivers for use at a rover or user station. At the user station, the positional coordinates will be computed and the ambiguity parameters will be fixed to integer values.

The measurement models describe a method of estimating the position of an unknown kinematic rover in real time. However, to allow the accuracy of results to be calculated, it is not practical to test the models in a real-time kinematic mode to an unknown receiver. Instead, the models will be tested using historical static time series but in a pseudo real-time mode. The use of historical static data means that the 'true' position of the receiver will be known to a higher level of accuracy than predicted achievable using the methodology in this study. Therefore, it will be possible to test both the accuracy of the results as well as their precision.

Conversely, the data required to create the network capable of estimating the UPDs and satellite clocks must be derived from static receivers. These static receivers will need to have precise known coordinates so that the network parameters can be estimated accurately. For the UPD and satellite clock corrections to be relevant to the rover, the data must be from a similar geographical region and have been measured simultaneously, which would be the case in a RTK application.

The UPDs consist of both satellite dependent error and receiver dependent error (Ge *et al.*, 2008). The receiver dependent error is common to all receivers of the same type. Therefore, it is crucial when developing a network of receivers to ensure all stations are of the same receiver type. The satellite dependent parts are estimated by the network and can be utilised at the rover, provided the rover is receiving signals from the same subset of satellites.

The data used to test the measurement models will be downloaded from the British Isles GNSS Facility (BIGF) archive. This is a large collection of historical static data from about 160 CORS throughout mainland Britain (The University of Nottingham, 2017). Most of these CORS stations are part of OS Net maintained by Ordnance

Survey. This collection of data will allow numerous sites to be selected to act as both network and rover stations, ranging over distances from 10s km to 100s km. The station metadata will allow a check to be completed, guaranteeing all selected stations have the same receiver type. When choosing stations to use, a number of selection criteria will be considered.

5.2 Selected GNSS Data

There were a number of deciding factors when selecting which GNSS data to use for the measurement model.Firstly, as mentioned previously, receiver types were chosen to be consistent throughout the base network and rover station. After analysis of the various receivers in the OS Net and stored in the BIGF data archive it was concluded that the LEICA GRX1200 receiver type would be used due to its prevalence.

Secondly, all the stations needed to have 1 Hz epoch data available. This high rate, one observation per second data allows fast and accurate estimation of the UPDs and the satellite clocks within the network. It also allows the rover user to update position every second, which is vital in the offshore industry when the rover is in a kinematic mode, as the receivers are likely to be moving constantly. Fortunately, the majority of the data available through the BIGF archive was offered at the 1 Hz level, so this requirement did not limit station selection.

Finally, all the stations used in the tests must have where possible a 24 hour period of uninterrupted observations on the same Universal Time (UT) day. The day selected must also have IGS final orbits and clocks available. As discussed in section 2.1.9, these are not generally available for up to two weeks after the day of observation (International GNSS Service, 2017a). To provide a good sample of data with various atmospheric and multipath conditions, RINEX files were carefully selected. The RINEX files chosen were the first day of the month for each of the first 8 months of the year in 2014 (days of year 001, 032, 060, 091, 121, 152, 182 and 213). The approximate locations of the BIGF data files that were acquired and subsequently used to test the measurement models are shown in Figure 5-1.

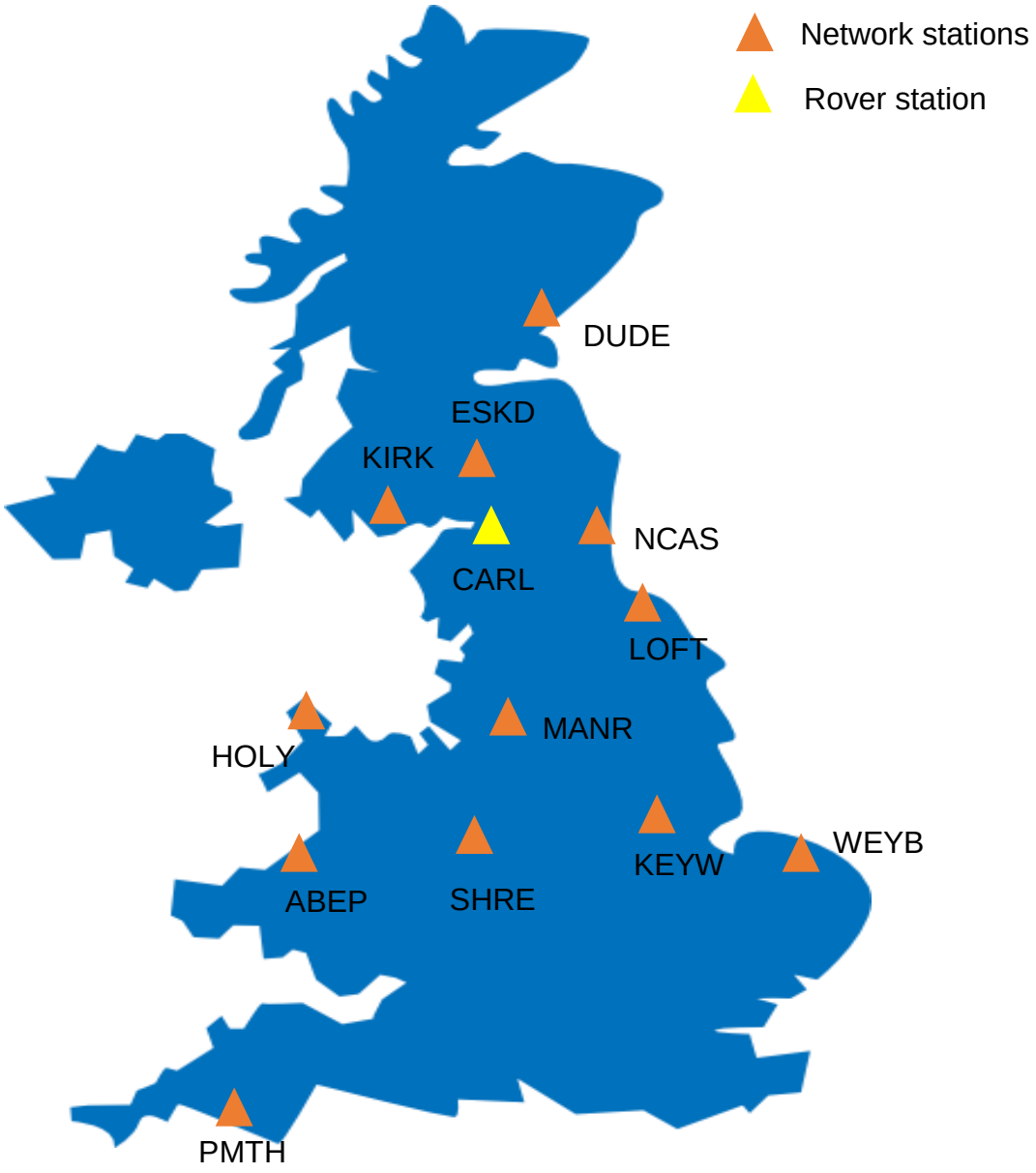

Figure 5-1 - Locations of GNSS Stations

5.3 Observed Minus Computed

As previously mentioned in section 4.3.1 the RINEX files will not be processed directly in with the testing methodology. Instead, OMC files will be generated through a program, GenOMC, developed and provided by Fugro Intersite. The program will read individual RINEX files together with precise coordinates, precise satellite clock and orbit information to determine the OMC values.

The major disadvantage of using the OMC program to obtain the input data files is that the satellite clock parameters have already been removed with the use of the IGS satellite clocks. Therefore, all that will remain in the OMC output is a small slowly varying residual satellite clock value. This slowly varying residual satellite clock will consequently have different stochastic properties to an actual satellite clock parameter, which tends to vary rapidly. Therefore, when estimating the parameters within the Kalman filter, the different stochastic properties will mean it is not an accurate representation of the method's ability to compute precise satellite clock values. An accurate representation can only be achieved when the stochastic properties are similar to those using raw observations and the process noise values within the Kalman filter are representative of the data.

To overcome this shortcoming, artificial satellite clock values will be added to the observations prior to the processing. To generate these artificial satellite clocks, a random number generator will be used to give each satellite, a clock error equivalent to a range error of between ±50 m. This random number will be generated at each epoch, allowing the satellite clock values to change both rapidly and unpredictably. The same satellite clock values will be used at each station in the network and at the user station to replicate the errors that would be present, if the OMC program were not to be used.

5.4 Number of Stations

The measurement model is capable of estimating UPDs and satellite clock parameters from a network of any number of static receivers. However, for double difference ambiguities to be calculated, for a fixed solution, at least two stations must be used to make up a minimum network. The number of stations employed in the network will have an effect on the redundancy within the model, i.e. the more stations used, the greater redundancy it creates. However, the greater the number of stations used, the more computational power is required to obtain a solution. Table 5-1 shows how the number of parameters estimated changes, as the number of stations in the network increases when using the measurement model presented in equation (3.58). This is based on nine satellites being visible at the current epoch as this is approximately the average number of GPS satellites in view at any one time.

Table 5-1 - Number of Network Stations Effect on Model Redundancy

Number of stations	Observations	Parameters	Redundancy
2	72	66	6
4	144	95	49
6	216	124	92
8	288	153	135

It is clear from Table 5-1 that the size of the network has a direct effect on the amount of redundancy. In theory, this should result in more accurately estimated UPDs and satellite clocks, therefore a better user solution. To test this theory, a series of networks will be processed varying from two stations to eight stations. The results will subsequently be compared to determine the optimum number of stations.

For a two station network, the CORS stations NCAS (Newcastle) and LOFT (Loftus) will be selected, with an interstation distance of 66 km. To increase the network to a four station network, the additional stations of ESKD (Eskdale) and KIRK (Kirkcudbright) will be added. The interstation distances between this network of stations will range between 66 km (NCAS-LOFT) and 206 km (LOFT-KIRK). The third test, involving six network stations, will employ the use of the stations HOLY (Holyhead) and MANR (Manchester) increasing the maximum interstation distance to 270 km. The location of all of these stations can be seen on the map in Figure 5-1.

In all tests, the user station will remain the same station to provide a consistent set of coordinate results for subsequent intercomparison. The user ‘rover’ station selected will be CARL (Carlisle) as the station is located most centrally to the network of stations used to compute the corrections. This station can also be seen in Figure 5-1.

5.5 Interstation Distances

In section 5.4, the optimum number of stations to include within the network was discussed. However, in this test all the stations were relatively close to each other and also close to the user station receiving the corrections. In many environments, especially offshore, it will not be possible to have such a dense network of static base stations close to the rover ‘user’. Therefore, further tests are required to ascertain whether the accuracy of the corrections degrades as the interstation distances are increased.

For this test, two, four, six and eight station networks will be selected. The first network will be a two station network consisting of DUDE (Dundee) and PMTH (Plymouth) with an interstation distance of 680 km. The four station network will consist of the two stations above with the addition of KEYW (Keyworth) and WEYB (Weybourne). The largest interstation distance will still be the 680 km between DUDE and PMTH but the network will now be denser. The test with six stations will have the additional stations HOLY and LOFT and finally the eight station network will include ABEP (Aberporth) and KIRK.

With all networks, station CARL will be retained as the user station due to its central location geographically. This approach will be adopted to ensure that the location of the user station within the network did not bias results.

5.6 User Location

Previously mentioned in section 5.5, the location of the user station within the network could potentially impact on the accuracy of the solution. In an ideal environment, the user would be located centrally between all the network stations being used to compute the corrections. However, in practice, rarely will it be possible to achieve this. It may be that the user is much closer to one station within the network or on the edge of the network. Additionally, it may be possible for the user station not to be within the network at all and to be located near the region of the network but outside of its bounds.

To test how much of an effect the user location can have, a series of four and six station networks will be again used. The first two networks will be a repeat of the tests outlined in section 5.5 with the stations DUDE, PMTH, KEYW and WEYB used in the four station network and DUDE, PMTH, KEYW, WEYB, HOLY and LOFT used in the six station network. For these two networks, the user CARL will remain in a central position. In the third and fourth networks, the user CARL will be outside of the extents of the network by approximately 250 km. The four station network will consist of PMTH, KEYW, WEYB, and ABEP. The six station network will utilise the four stations above with the addition of SHRE (Shrewsbury) and MANR.

5.7 Network Station Drop Out

All the testing will use historical data and by selection, minimal problems with a station becoming unavailable for a period of time were encountered. However, in a real time and a real life environment, a station may become either temporarily or permanently unavailable, for example, if the antenna is being changed or there is a power loss. Hence, it is important to test what effect this may have on the accuracy of the corrections and consequently the accuracy of the user position.

For this test, it is likely that the fewer stations there are in the network to begin with the more impact the loss of a station will have on the results. Therefore, to begin with, the network will comprise just four stations, DUDE, PMTH, KEYW and WEYB. For the first 18 hours, all four stations will be fully operational and for the remaining 6 hours the station WEYB will be removed from the observation list. The user CARL will then be assessed to see if the accuracy of the position is detrimentally affected by the loss of the fourth network station.

5.8 IAR at the Network

In the tests outlined in sections 5.4 to 5.7, the UPD and satellite clock corrections will be computed using a float solution. This means that the double difference ambiguities within the network are not fixed to their integer values. If these ambiguities are correctly fixed to their integer values, there are fewer parameters being estimated in the network solution and no error within the ambiguity parameter. Thus, theoretically making the solution more accurate.

This can be tested in part by analysing the T values described in section 4.2.1, which will show how well the solution fits to the data. If the T value decreases when ambiguities are fixed, it implies an improved fit to the data. However, this does not prove whether the UPD and satellite clock corrections computed are more accurate. To analyse this, the tests in section 5.5 will be repeated with a fixed network solution instead of a float solution. Therefore, the tests undertaken will use stations DUDE, PMTH, KEYW, WEYB, HOLY, LOFT, ABEP and KIRK. The corrections achieved will then be transmitted to the user to test whether the position of the rover is improved through the application of fixed corrections.

As described in section 4.3.4, the LAMBDA program is used to undertake IAR. However, there are multiple settings within the LAMBDA program, which can affect the reliability of the ambiguities being fixed.

Firstly, when using ILS with the ratio test it is important to select an appropriate critical value for the test. The critical value dictates how confident the LAMBDA program must be in its solution in order to fix the ambiguities to an integer. If the critical value is set too low, it will result in fewer ambiguities being fixed, therefore not realising the full potential of IAR. However, if the critical value is set too high, some ambiguities may be incorrectly fixed, which could result in large errors in other parameters. For these tests, a critical value of 0.2 will be used which means the most likely set of integers must be five times more likely than the second most likely set of integers for the program to accept the solution.

Secondly, it is not reliable to attempt to fix ambiguities to integer values at the first epoch as the solution needs time to converge. It is often advisable to wait a set number of epochs, before attempting any IAR for a given satellite, to allow the parameters associated with the given satellite to converge. In a similar manner to the ratio test, it is important to select an appropriate value for the number of epochs to wait before undertaking IAR. Too few epochs could result in incorrectly fixed ambiguities as the solution has not fully converged. Too many epochs will result in less ambiguities being fixed and therefore a sub optimal solution.

In these tests, a time of 1800 epochs or 30 minutes will be used to allow the ambiguities to converge. This value is a compromise between accuracy and speed of convergence. However, the ambiguities might not necessarily be fixed to integers after this number of epochs, as the ambiguities still have to pass the ratio test within the LAMBDA program.

5.9 IAR at the User

In all the tests outlined above, the ambiguities in the user solution will be computed based on a float value. As with the network solution, fixing ambiguities to their integer values should improve the solution and therefore improve the rover position. However, if any of the ambiguities are fixed incorrectly, this will cause a large error in the solution and hence the coordinated position. The implication here is that fixing

ambiguities may not always be advantageous. To ensure ambiguities are fixed to the correct values, it is critical that the UPD and satellite clock corrections are as accurate as possible.

To test the user's ability to correctly fix the ambiguities, the optimum float network and optimum fixed network solutions will be utilised. This is required to provide the rover with the best possible opportunity to undertake successful IAR. Again, the rover station will be retained as CARL throughout this test to aid comparison.

5.10 PPP-RTK Comparison

The existing methodology most comparable to that presented in this study is given by Zhang *et al.* (2011). To compare the accuracy of the corrections calculated here to those presented in the Zhang approach, this alternative approach will also be tested. The measurement models presented in Zhang *et al.* (2011), will be used alongside the approach in this thesis. Using the data obtained from BIGF, it will be possible to directly compare the two approaches.

The UPD and satellite clock corrections obtained from the two approaches will be different, due to the different parameterisations used in the methodologies. However, when used in conjunction with the different user measurement models, both will provide a user position solution. These user position solutions are comparable, so it will be possible to identify which methodology gives a significantly improved solution compared to the other.

To allow direct comparison with the models presented in this study, the tests outlined in section 5.5 will be repeated using this alternative measurement model. This includes processing the two, four and six station networks using the network stations DUDE, PMTH, KEYW, WEYB, HOLY and LOFT, whilst maintaining CARL as the rover receiver. Additionally, to aid direct comparisons, the same observation weightings, process noise values and initialisation periods will be used.

The comparison will also compare the two solutions abilities to fix integer ambiguities at the network and the rover. It can then be analysed to see if fixing these ambiguities has a positive impact on the accuracy of the rover position. The same three sets of network stations will be used to compute three fixed network solutions,

as in the float tests listed previously. Additionally, two of the networks will be used to analyse the rover ability to undertake IAR.

5.11 User Position

In the majority of the tests outlined in this chapter, the user position will be used to quantify the accuracy of the solution. To fully analyse the computed position, a statistical analysis needs to be undertaken for the east, north and up components. The correct user position is known to a higher degree of accuracy and the OMC program uses these coordinates to compute the OMC output file. Therefore, the computed user position should be equal to (0, 0, 0).

To analyse the position estimate accuracy, the Root Mean Square (RMS) value will be computed using the position components east, north and up separately to show which component is the most accurate. Additionally, a 3D RMS value will be computed to give an overall accuracy of the position over time.

The formula to compute the RMS for each component of position is given by equation (5.1):

$$RMSe = \sqrt{\frac{\sum (\mathrm{e} - \tilde{\mathrm{e}})^2}{n}} \tag{5.1}$$

where e is the east position at each epoch, $\tilde{\mathrm{e}}$ is the true east position, which will be equal to zero in these examples and n is the number of epochs. Similar expressions exist for north and up.

For the 3D RMS value the 3D error in positon will be first computed prior to application of equation (5.1). The 3D position error can be computed as shown in equation (5.2):

$$3D = \sqrt{e^2 + n^2 + u^2} \tag{5.2}$$

The 3D position error will then substituted for the east error in equation (5.1) to give the 3D RMS error, allowing direct statistical comparison between the different testing procedures.

Chapter 6. Results

6.1 Standard Settings

The results presented in this section test a number of different program settings, which affect the accuracy and precision such as number of network stations and interstation distance. However, there are a number of additional settings, which can have a significant impact on the results, including process noise and observational weight. These are not presented here, as these settings have been chosen based on previous literature and some basic tests within the program as outlined in Chapter 4. This has ascertained that the values chosen are sensible and provide the optimum solution.

Firstly, the observation weighting follows an elevation dependent weighting as outlined in section 4.3.3.2. Secondly, the process noise values have been tested to achieve the most appropriate values, which are outlined in section 4.3.3.3. Thirdly, the reference satellite is selected as the satellite at the highest elevation and the elevation mask is set as 7° as is common within literature (Fang *et al.*, 1998). Finally, the network solution is allowed a period of 12 hours to stabilise and compute accurate corrections, before the corrections are transmitted to the user. This stabilisation period does not affect the user convergence time as the network would be a constantly running program so this 12 hour period would only ever occur once on initialisation.

The observations that will act as the rover station are from static GNSS receivers. However, the coordinates of the receiver will be unconstrained within the Kalman filter. Therefore, this will simulate a kinematic solution being computed for the rover.

6.2 Baseline Computation

To assess how successful the measurement model is and how much of a difference applying UPD and satellite clock corrections makes, a series of baseline tests have been run. These tests use the OMC files generated with satellite clock and orbit corrections obtained from the IGS. Thus, the satellite clock and UPD corrections obtained from the network approach are not utilised and a conventional PPP solution is applied at the rover. These PPP solutions are obtained using the same program

and measurement model as the latter PPP-RTK tests to allow direct comparison. This will result in a solution where the ambiguities cannot be double difference integer values, and can be computed in a float solution. The rest of the measurement model stays the same as that presented in equation (3.60) in section 3.3.

To allow accurate comparison with the results in the remainder of this chapter, the user program is initialised after 12 hours to simulate the 12 hour stabilisation period of the network program. The positon is subsequently estimated at each epoch from 12 hours to 24 hours and the RMS values computed using the formula presented in section 5.11.

Figure 6-1 shows the results of the user position between 12 and 24 hours in east, north and up for DOY 001. The convergence time is approximately 1 hour, between 12 and 13 hours, before the positon estimate errors are below 5 cm in each respective direction. For the period between 13 and 24 hours, the RMS values for all the days tested are shown in Table 6-1.

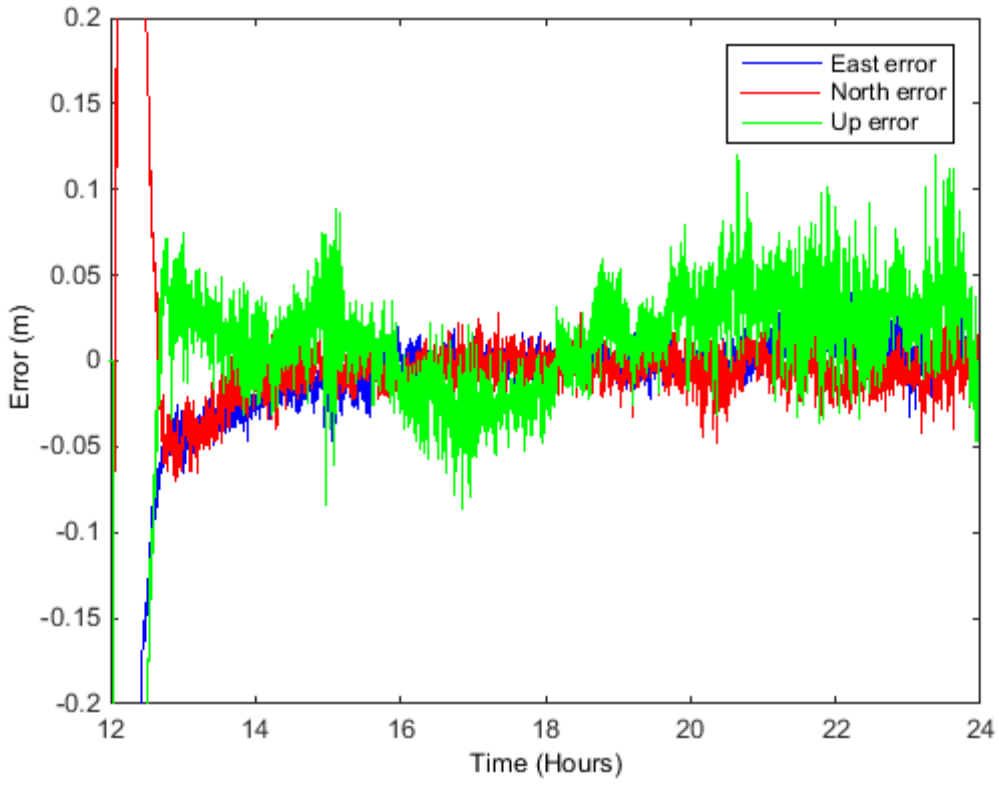

Figure 6-1 - Rover Positional Errors with No Corrections (DOY 001)

Table 6-1 - Rover Positional RMS Errors with No Corrections

DOY	East (mm)	North (mm)	Up (mm)	3D (mm)
001	12.1	10.5	29.3	33.4
032	12.5	15.3	23.4	30.7
060	13.3	10.2	35.9	39,7
091	21.2	20.8	34.5	45.5
121	20.4	19.3	23.1	36.4
152	75.8	18.2	52.3	94.4
182	30.3	26.7	48.0	62.7
213	9.9	17.5	29.5	35.7
Average	**28.9**	**15.7**	**33.1**	**48.1**

The RMS values in Table 6-1 show that for DOY 152 and DOY 182 the data quality is poor and not representative of the typical expected accuracies. Inspection of the RINEX files for these days reveals multiple data gaps of up to an hour in length. This causes the Kalman filter to restart and reconverge multiple times resulting in a much less accurate solution. As a result, DOY 152 and 182 will be omitted from all further testing to avoid biasing the results. Table 6-2 shows the average of the results once these two anomalies have been removed.

Table 6-2 - Rover Positional RMS Errors with No Corrections (No DOY 152 and 182)

DOY	East (mm)	North (mm)	Up (mm)	3D (mm)
001	12.1	10.5	29.3	33.4
032	12.5	15.3	23.4	30.7
060	13.3	10.2	35.9	39,7
091	21.2	20.8	34.5	45.5
121	20.4	19.3	23.1	36.4
213	9.9	17.5	29.5	35.7
Average	**15.9**	**15.2**	**29.2**	**36.5**

These positions estimated without UPD corrections are not directly comparable to real-time PPP positioning as the satellite clock and orbit corrections applied are final orbits and clocks, computed two weeks after the data is collected. Thus, the accuracies are equivalent to post processed results. If the following tests can provide user positions that are equivalent, or an improvement, on those presented in Figure 6-1 then it demonstrates that the measurement model presented in this thesis is a viable methodology for computing satellite clock and UPD corrections.

6.3 Network Results

Prior to presenting positioning for the user results, a series of results from the network processing are shown. The network results are visually similar for the majority of tests undertaken and will only be presented once. The graphs will follow the same pattern in subsequent tests, unless otherwise stated.

The network results presented here are a subset of the results from the six station network consisting of LOFT, NCAS, KIRK, ESKD, HOLY and MANR.

Figure 6-2 and Figure 6-3 are plots of the zenith tropospheric correction as computed from two stations within the network on DOY 001. The two stations are 105 km apart; therefore the plots should differ, as the troposphere will vary over such distances. There is a convergence period where the Kalman filter initialises. Initialisation only has to be done once as the network would run constantly after an initial set up. Consequently, the time the convergence takes is not relevant. Both plots are realistic estimates of the zenith wet troposphere component, with slow variance over the day and an overall change of less than 5 cm. In section 4.3.3.3 these troposphere estimates have been compared against independent processing software GIPSY-OASIS v6.4. The dry troposphere is not included in these plots as this has already been removed by the OMC program. However, there will be residual dry tropospheric error in the wet troposphere due to incorrect estimation of the pressure at the station within the OMC program. Similar plots can be obtained for the other four stations in the network but are not presented as they are similar to Figure 6-2 and Figure 6-3 and do not add any additional insight.

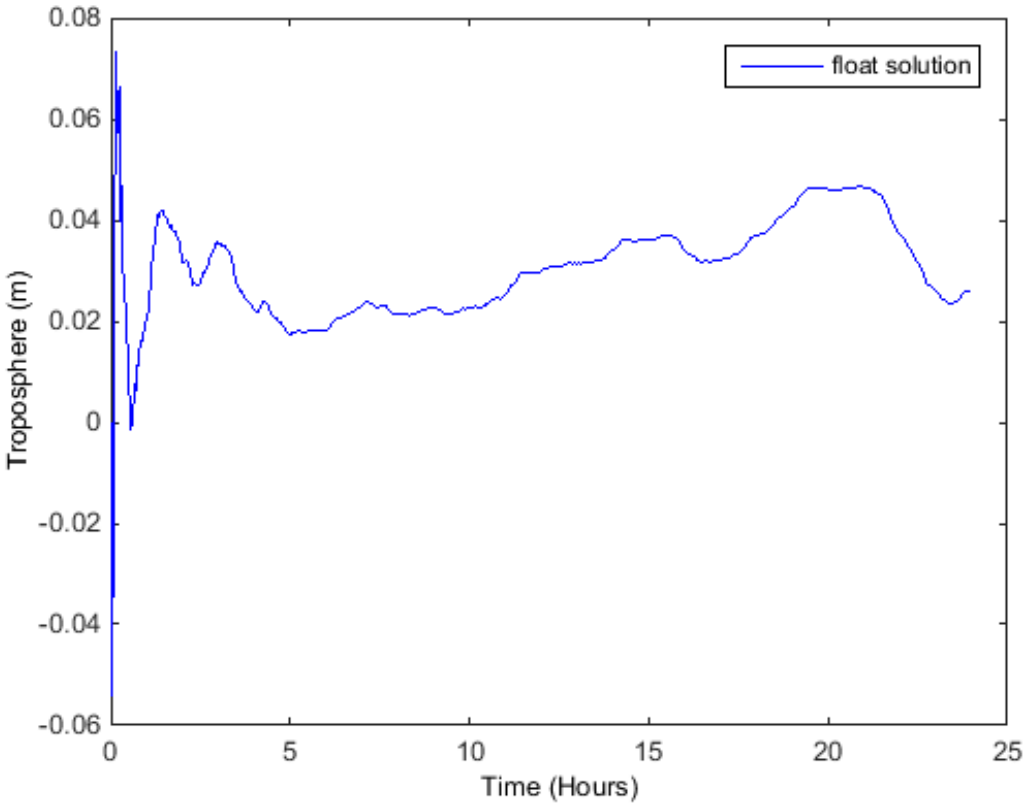

Figure 6-2 – Zenith wet troposphere delay of LOFT (DOY 001)

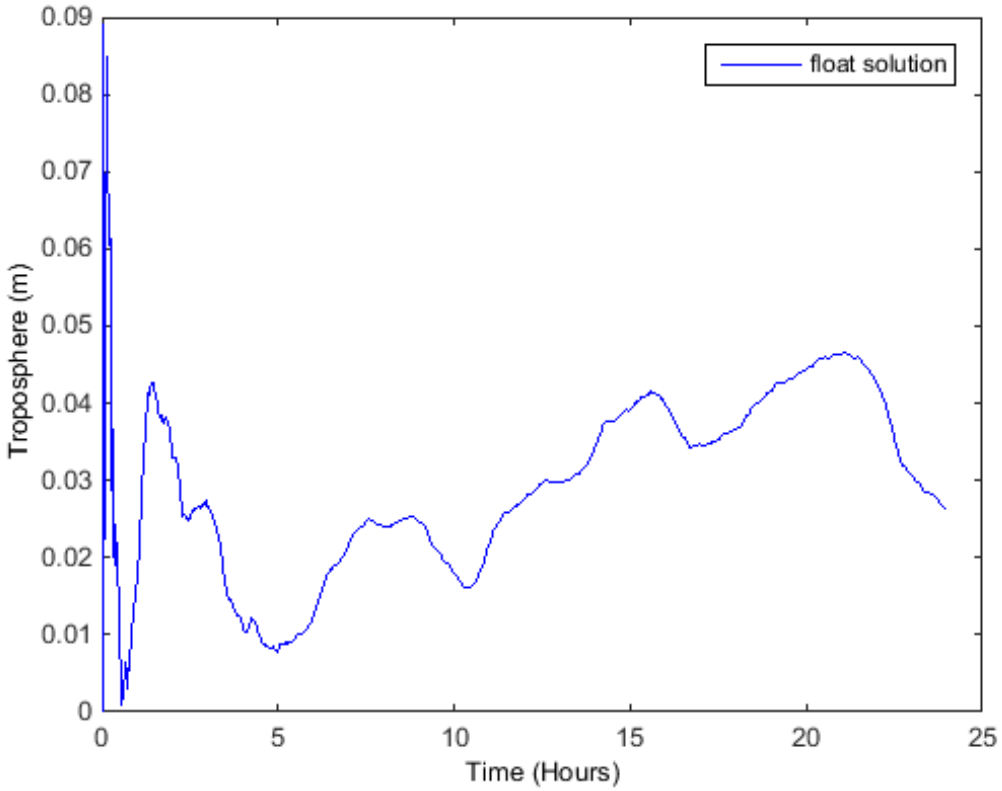

Figure 6-3 – Zenith wet troposphere delay of NCAS (DOY 001)

The estimate of the ionosphere from one network station, LOFT, to satellite Pseudo Random Noise 4 (PRN 4) is shown in Figure 6-4. Figure 6-4 shows a series of jumps in the time series, most notably between 12 and 17 hours. These jumps are caused by a change in reference satellite and not a change in the parameter. To aid visual inspection of the parameter estimation, the jumps can be removed to provide a smoother graph. The same jumps appear in parameter estimation of the UPDs, satellite clocks and ambiguities. For the remainder of the thesis, all the jumps will be removed to aid visual inspection. Finally, there are periods where the parameter estimation is equal to zero, for example, between 2 hours and 12 hours. These are periods where the satellite is not visible to the receiver and therefore no estimation is undertaken.

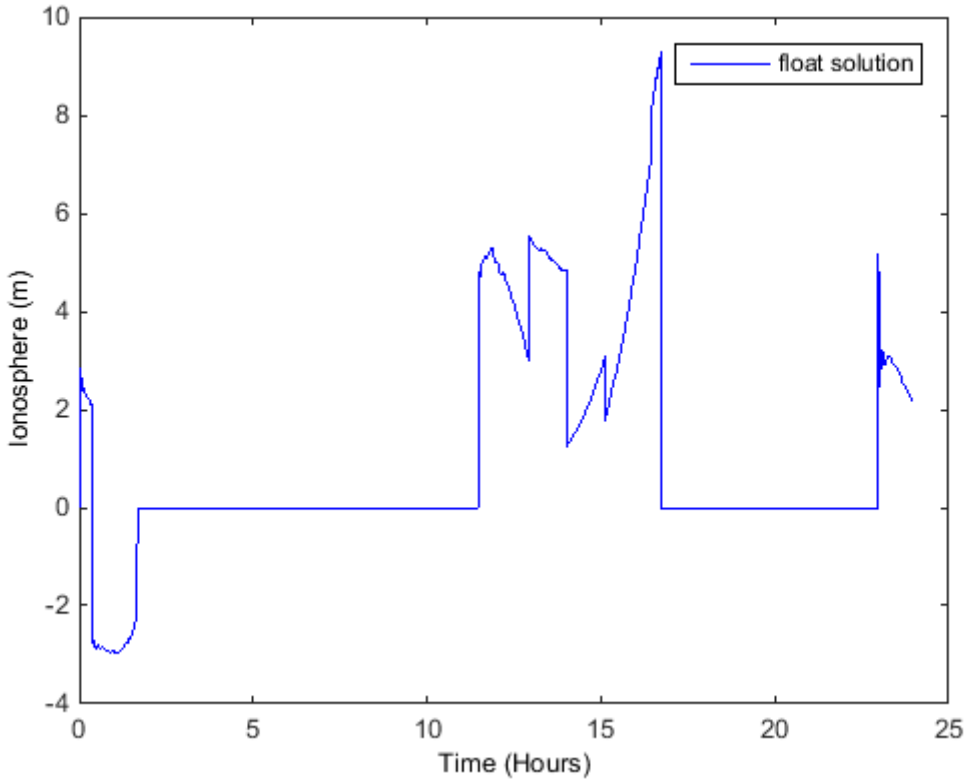

Figure 6-4 - Ionosphere delay at LOFT for Satellite PRN 4 (DOY 001)

Figure 6-5 has been smoothed to remove the jumps caused by the reference satellite changes. The plot now clearly shows the ionosphere change over time, with dependence on the elevation angle of the satellite. When the satellite rises in the sky, the ionosphere estimate decreases, due to the reduction in slant range. The ionosphere then increases again, as the satellite falls to the horizon.

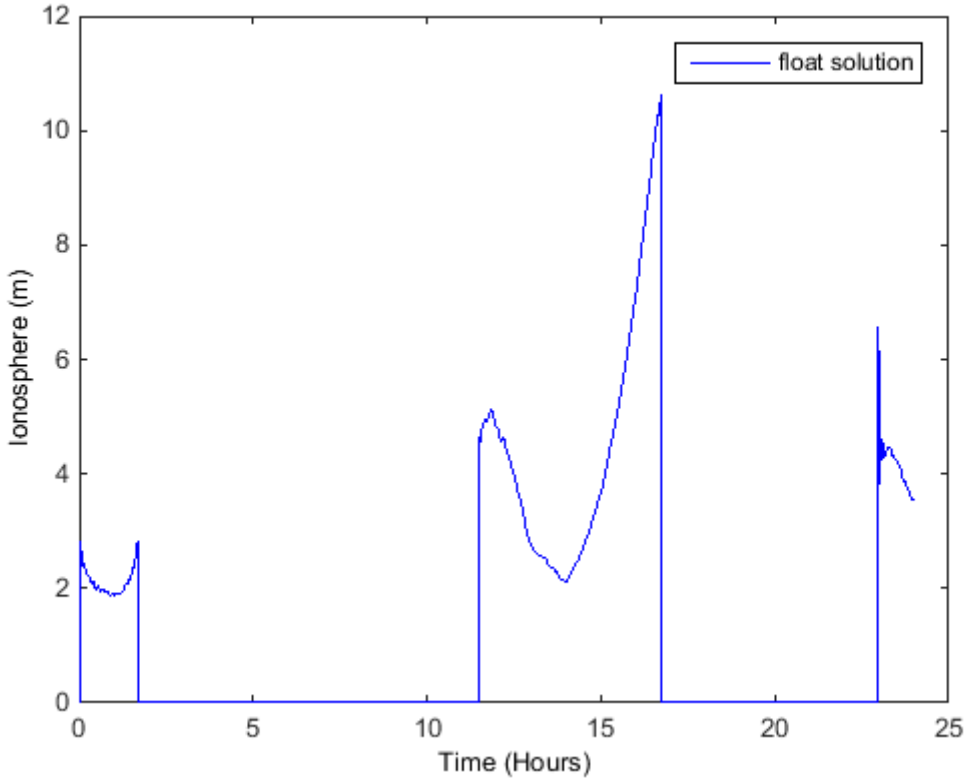

Figure 6-5 - Smoothed Ionosphere delay at LOFT for Satellite PRN 4 (DOY 001)

Figure 6-6 displays the smoothed float ambiguity estimates between network station LOFT and NCAS to satellite PRN 4. In this test, the ambiguity values remain float estimates throughout and no attempt is made to fix to integer values. It is important, however, to note the stability of the float estimates, as this will be key when trying to fix the values to integers. After initial convergence periods of approximately 30 minutes or 1800 epochs, the stability of the parameters is good. Figure 6-7 shows the period between 11 and 17 hours in more detail to show the convergence period and the parameter stability.

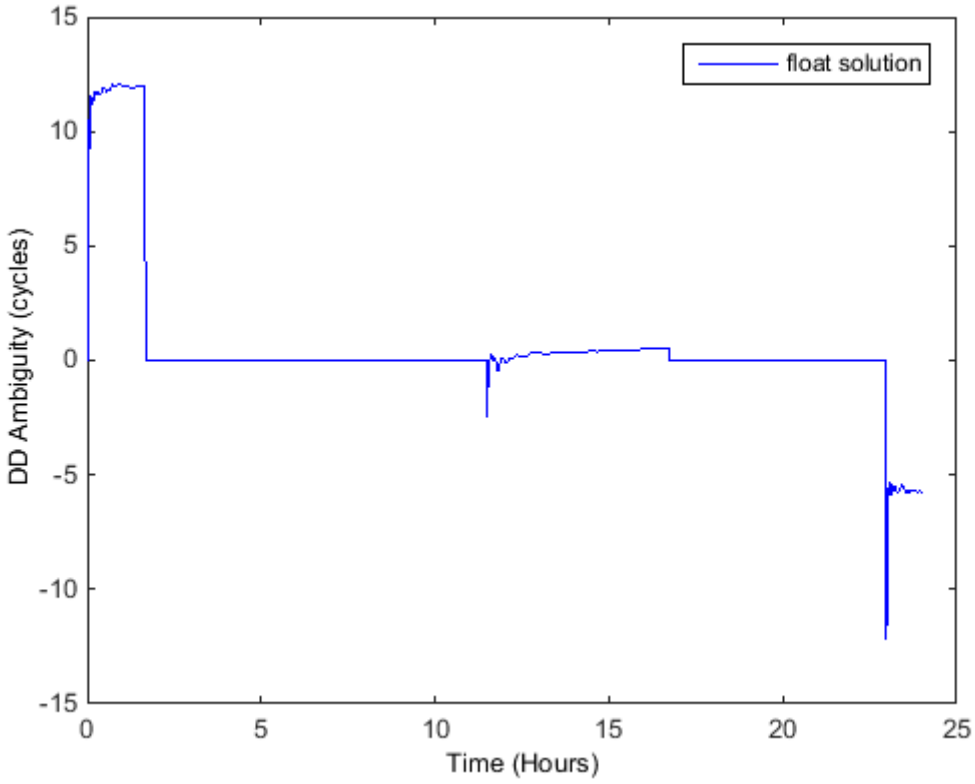

Figure 6-6 - Smoothed L1 Ambiguity between LOFT and NCAS for Satellite PRN 4 (DOY 001)

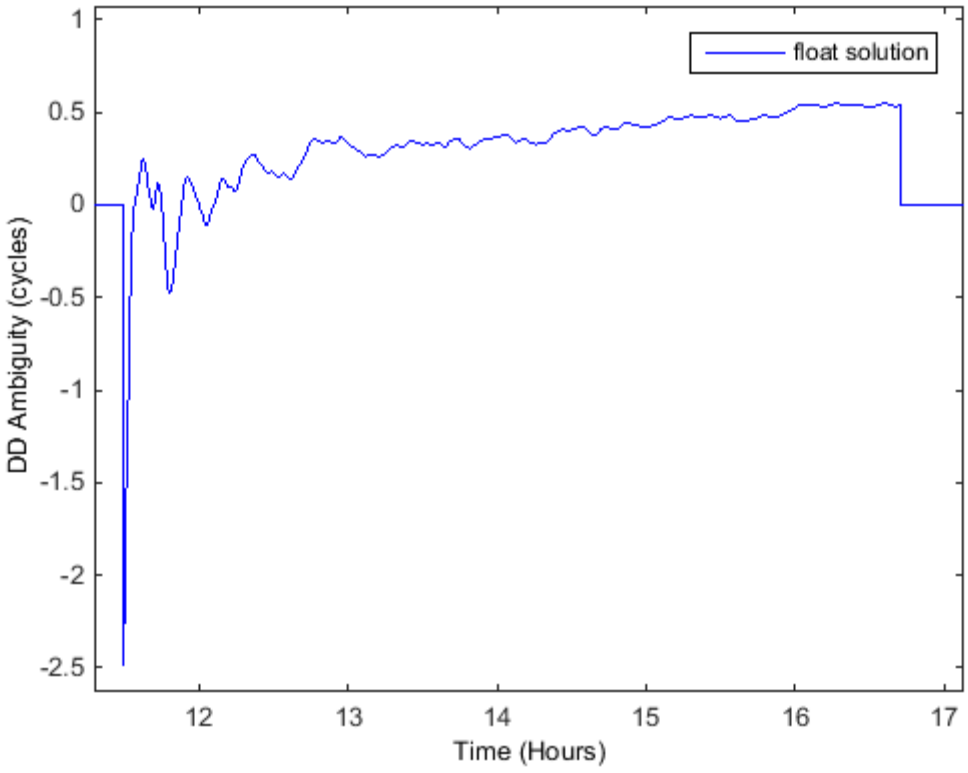

Figure 6-7 - Smoothed L1 Ambiguity between LOFT and NCAS for Satellite PRN 4 (11-17 hours) (DOY 001)

Figure 6-8 shows the satellite clock estimate for satellite PRN 4 over the day. The satellite clock parameter varies rapidly due to the applied random clock error. This rapid variation can be seen more clearly in Figure 6-9, which shows the estimation between 13 hours and 14 hours. Although the applied random clock error is between ±50 m, the parameter being estimated included a reference satellite. Consequently, Figure 6-9 has values in the region of ±65 m. Visually, it is hard to assess how accurately the measurement model is estimating the satellite clock correction. However, the rapidly changing values on the graph do show the Kalman filter is correctly modelling the parameter, as it allows the parameter estimation to freely move at each epoch, instead of being tightly constrained.

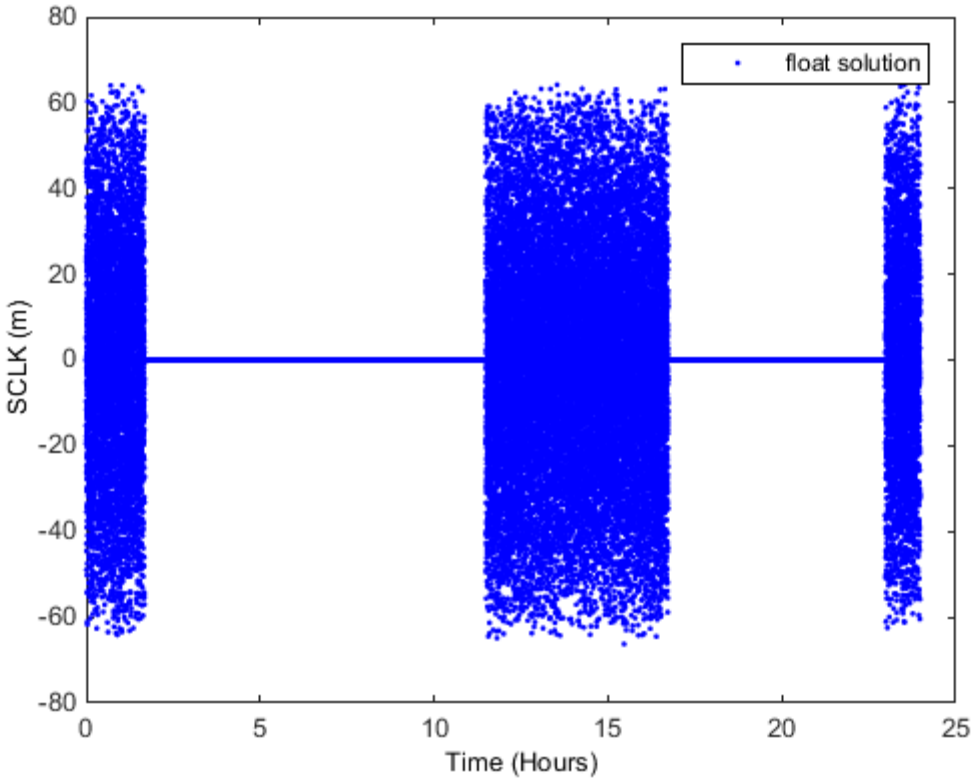

Figure 6-8 - Satellite Clock for Satellite PRN 4 (DOY 001)

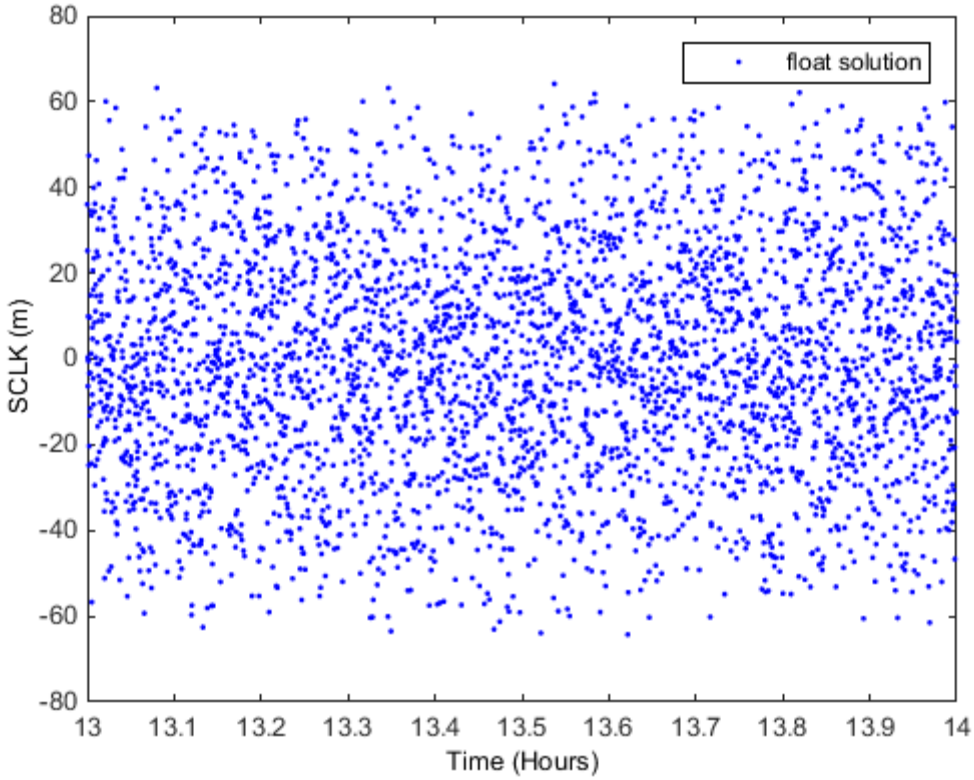

Figure 6-9 - Satellite Clock for Satellite PRN 4 (13-14 hours) (DOY 001)

Finally, Figure 6-10 shows the UPD estimates throughout the day. These estimates are slowly changing like the ambiguity estimates, but unlike ambiguities will never be fixed. A convergence time of approximately 30 minutes or 1800 epochs is again visible each time the satellite becomes visible to the receiver at 0 hours, 12 hours and 23 hours.

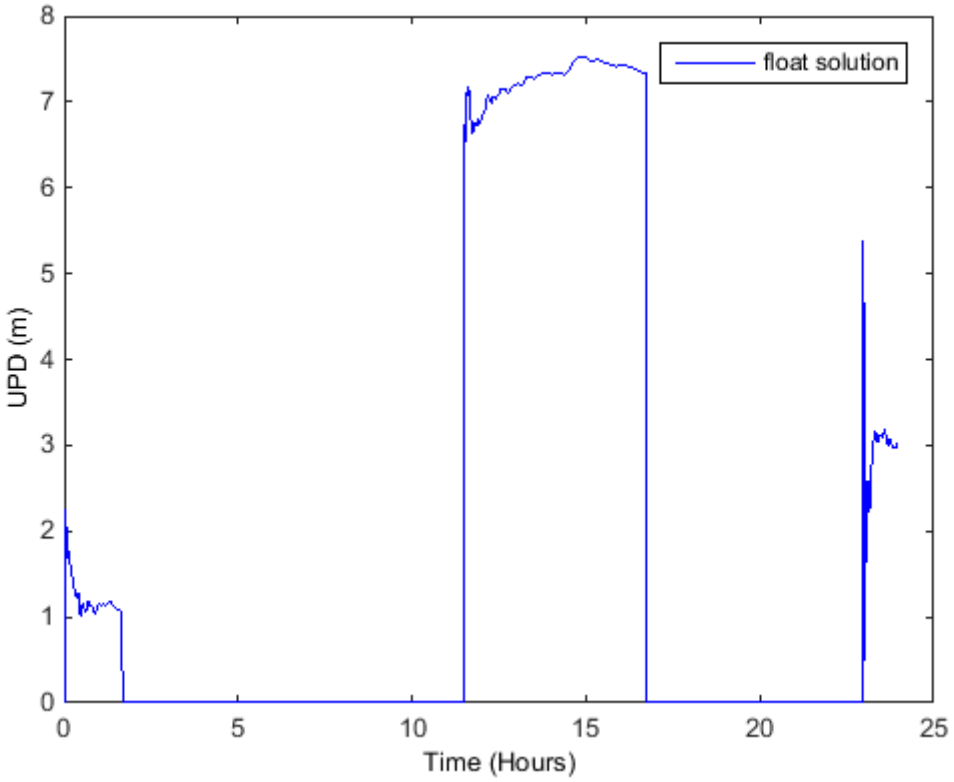

Figure 6-10 - Smoothed L1 UPD for Satellite PRN 4 (DOY 001)

Plots have been generated for each one of the parameters in the measurement model and to each satellite in the constellation but are not included here. For example, in a six station network there are over 600 parameters estimated, each with a corresponding graph. Instead, a selection of the results with respect to a randomly selected satellite, (PRN 4), have been shown to display the general pattern of the data.

6.4 Number of Network Stations

In section 5.4, it was discussed that the number of network stations can have an impact on the accuracy of the estimation of the satellite clock and UPD parameters. At this stage, the network stations selected were close to the rover and spread evenly about the rover to attempt to achieve the best possible results. For these reasons, the network will be referred to as a local network.

The first network used the two stations, NCAS and LOFT. Figure 6-11 shows the resultant differences to the station coordinates when the satellite clock and UPD corrections calculated from the network are applied to the rover on DOY 001.

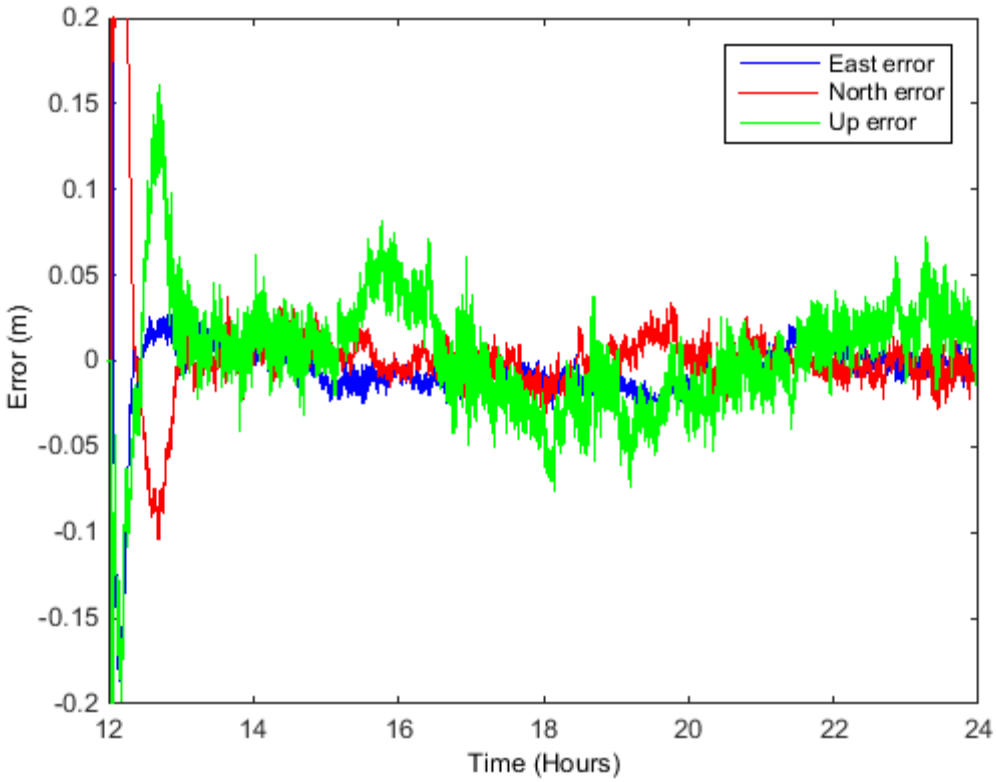

Figure 6-11 - Rover Positional Errors with Corrections from Two Local Stations (NCAS LOFT) (DOY 001)

The average RMS values computed for the rover are 13.7 mm, 14.2 mm and 30.3 mm in east, north and up respectively and can been seen in Table 6-3. The 3D RMS is calculated to be 36.4 mm between 13 hours and 24 hours. These results show no improvement or deterioration to the position, when compared to the baseline solution. Consequently, corrections from two network stations are not enough to improve the user's solution.

Table 6-3 - Rover Positional RMS Errors with Corrections from Two Local Stations (NCAS LOFT)

DOY	East (mm)	North (mm)	Up (mm)	3D (mm)
001	10.4	10.0	26.1	29.8
032	15.7	14.4	37.2	42.9
060	12.0	12.5	18.4	25.2
091	21.8	21.1	34.2	45.7
121	7.9	10.6	30.5	33.2
213	14.6	16.4	35.1	41.4
Average	13.7	14.2	30.3	36.4

To attempt to improve the position further, more redundancy is required in the network, which can be achieved by introducing additional stations. The local network stations KIRK and ESKD were added to enhance the network solution.

The results in Figure 6-12 are the rover error after using the corrections from four local stations on DOY 001. The RMS values show an improvement of approximately 12% compared to using no correction with values of 11.9 mm, 11.3 mm, 27.6 mm and 32.4 mm in east, north, up and 3D respectively as seen in Table 6-4.

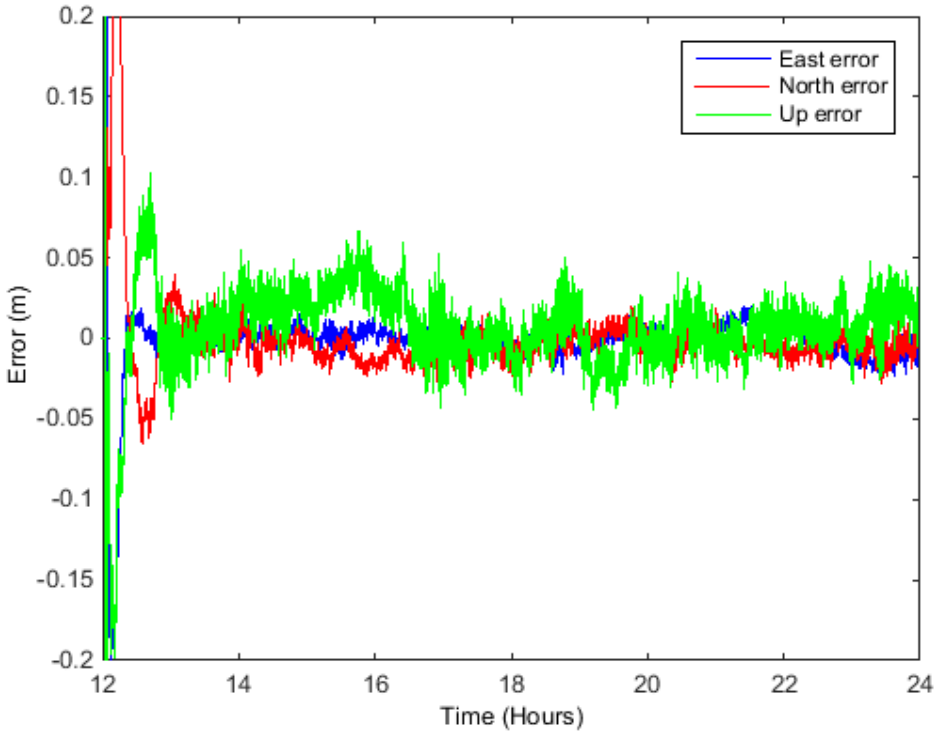

Figure 6-12 - Rover Positional Errors with Corrections from Four Local Stations (NCAS LOFT KIRK ESKD) (DOY 001)

Table 6-4 - Rover Positional RMS Errors with Corrections from Four Local Stations (NCAS LOFT KIRK ESKD)

DOY	East (mm)	North (mm)	Up (mm)	3D (mm)
001	7.0	8.6	18.8	21.9
032	11.8	12.4	36.1	40.0
060	7.2	7.8	27.7	29.6
091	18.3	10.6	24.4	32.3
121	11.9	9.1	27.3	31.1
213	15.4	19.1	31.1	39.6
Average	11.9	11.3	27.6	32.4

Further increasing the number of stations in the network to six, results in the rover position presented in Figure 6-13. It can be seen from Figure 6-13 that the convergence time has been improved compared to Figure 6-11 and Figure 6-12. This is due to the increased redundancy in the network and the reduction of some linear dependencies, which occur with a small number of network stations. For direct comparison, the RMS values have been computed over the same 13 to 24 hour range. The results of the average RMS are 13.4 mm, 13.0 mm, 24.2 mm and 31.2 mm and are presented in Table 6-5. There is no result available for DOY 032 due to network station MANR being unavailable on that day.

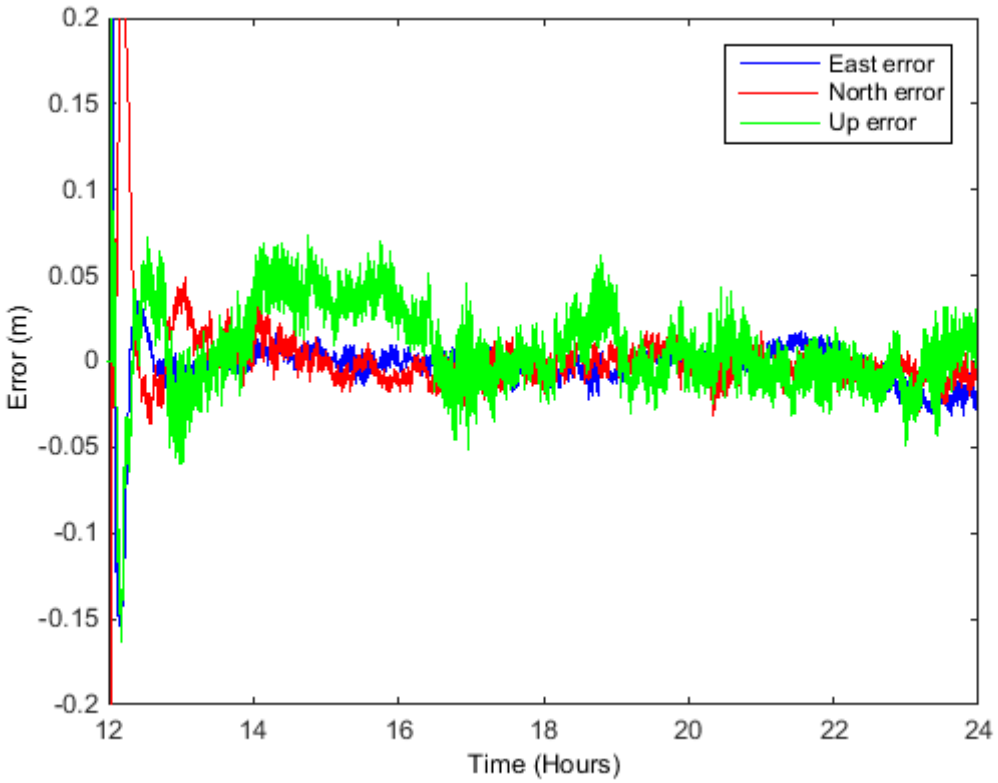

Figure 6-13 - Rover Positional Errors with Corrections from Six Local Stations (NCAS LOFT KIRK ESKD HOLY MANR) (DOY 001)

Table 6-5 - Rover Positional RMS Errors with Corrections from Six Local Stations (NCAS LOFT KIRK ESKD HOLY MANR)

DOY	East (mm)	North (mm)	Up (mm)	3D (mm)
001	8.9	8.5	22.9	26.0
032	NA	NA	NA	NA
060	6.0	7.8	24.2	26.1
091	26.4	20.2	26.5	42.5
121	11.9	9.2	24.8	29.0
213	13.6	19.1	22.6	32.6
Average	**13.4**	**13.0**	**24.2**	**31.2**

These RMS values are approximately 4% better than when applying corrections from four local stations. Therefore, the increased redundancy has further improved the solution. The results of this first series of tests are summarised in Table 6-6. The table shows that the number of stations in the network has a positive impact on the accuracy of the satellite clock and UPD corrections computed.

Table 6-6 – Rover Positional RMS Errors for Local Stations Summary

	No Corrections	Two Local Stations	Four Local Stations	Six Local Stations
East (mm)	15.9	13.7	11.9	13.4
North (mm)	15.2	14.2	11.3	13.0
Up (mm)	29.2	30.3	27.6	24.2
3D (mm)	36.5	36.4	32.4	31.2

6.5 Linear Dependencies

A major factor that causes an improvement to the satellite clock and UPD parameters when the number of network stations is increased is the reduction in the linear dependencies in the measurement model. Throughout testing it was apparent that there were strong correlations between certain parameters in the measurement model, mainly between the satellite clocks and the troposphere. The same correlation between the satellite clocks and the tropospheric mapping function was found in Zhang *et al.* (2011). This correlation implies that it is difficult to accurately estimate all parameters simultaneously. When more stations are included in the network, the leakage from one parameter to another within the measurement model is reduced, facilitating a solution for all parameters.

One way in which this aliasing can be visualised is with the variances within the Kalman filter. Each parameter is assigned an initial variance with additional process noise added at each epoch depending on the stochastics of the given parameter. For parameters such as the troposphere and the UPDs, the initial large variance should decrease rapidly and stabilise at a value just above the process noise. However, if correlations exist between parameters the initial large variance takes significantly longer to reduce, leading to longer convergence time and also less accurately estimated parameters. Figure 6-14 and Figure 6-15 show how the troposphere and UPD variances from the final variance covariance matrix, $Q_{\hat{x}_{k|k}}$, at each epoch change over the first hour of observations for a two station network compared to a six station network.

Figure 6-14 and Figure 6-15 show that the variances associated with the six station network reduce faster than those for the two station network. This pattern continues over the whole day of observations, resulting in the variances from the two station network always being higher than those in the six station network. Consequently, the accuracies of the parameters computed from the six station network are better than those from the two station network. The time taken to reduce the standard deviation also has an impact and demonstrates why the convergence time for the network parameters is improved, when more network stations are used.

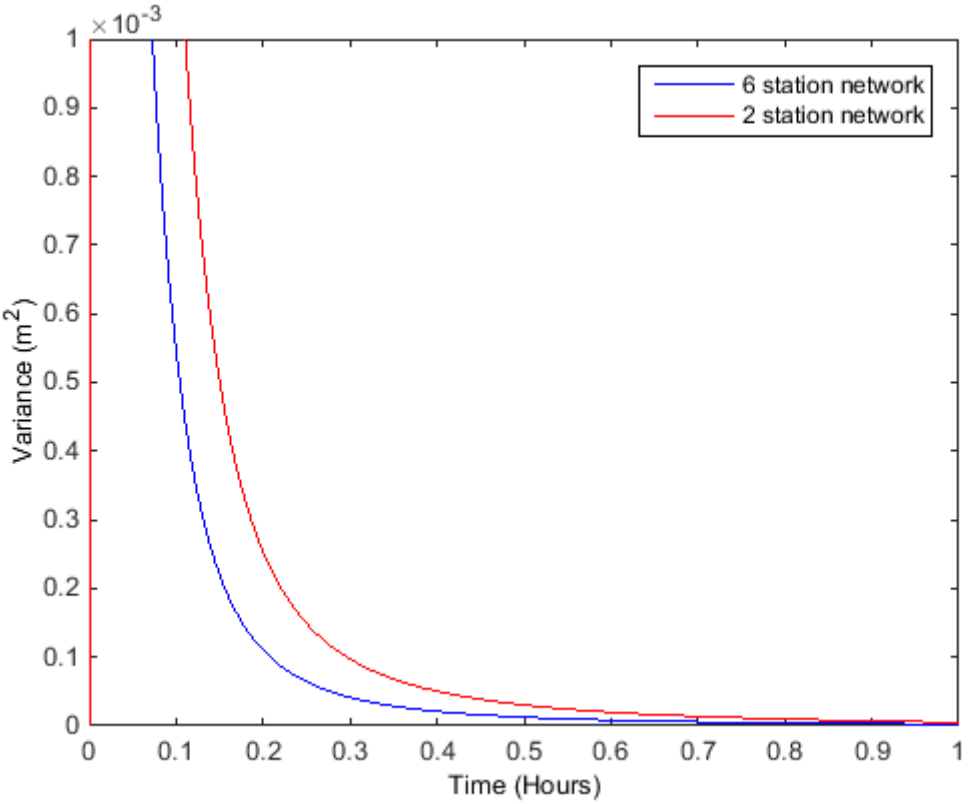

Figure 6-14 - Troposphere Variance Comparison (DOY 001)

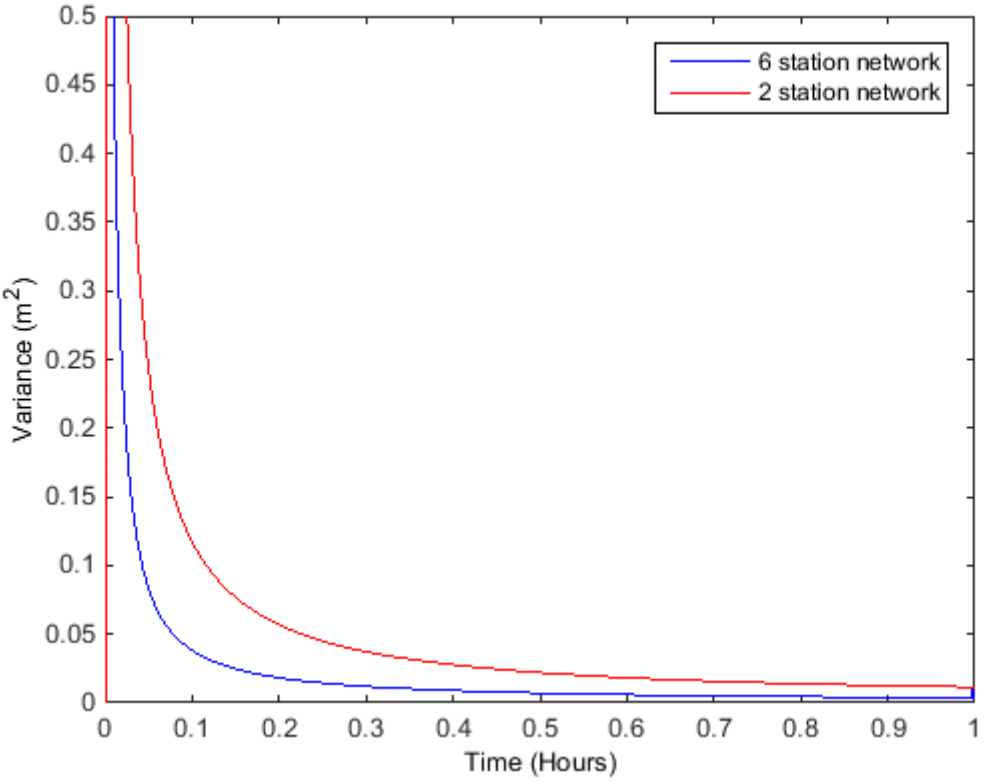

Figure 6-15 - UPD Variance Comparison (DOY 001)

6.6 Interstation Distances

It is unlikely in an offshore environment that it would be possible to utilise a local network with similar spatial distribution to those in the four and six station local network tests in section 6.4. Therefore, further tests will be carried out using a regional network, where the interstation distances are much larger.

In section 5.5, tests were outlined to assess the measurement model in a more realistic environment where the interstation distances must exceed 100-200 km. Consequently, a series of two, four, six and eight station networks were processed to compute satellite clock and UPD corrections. The stations used are outlined in section 5.5 and can be viewed in Figure 5-1. Due to the larger interstation distances, these networks will be referred to as regional networks.

The rover error for CARL, using corrections from a regional two station network, DUDE and PMTH, on DOY 001 can be viewed in Figure 6-16. The average RMS values computed from these results are 13.4 mm, 15.8 mm, 29.0 mm and 35.8 mm for east, north, up and 3D respectively and are also shown in Table 6-7. The

convergence time has increased to over one hour, although it is difficult to define an exact point where the position has converged. These results are similar to those with no corrections with just a 2% improvement compared to when no UPD corrections are sent. This is further indication that the correlations between the parameters are too high when only two network stations are used and the measurement model is too highly correlated.

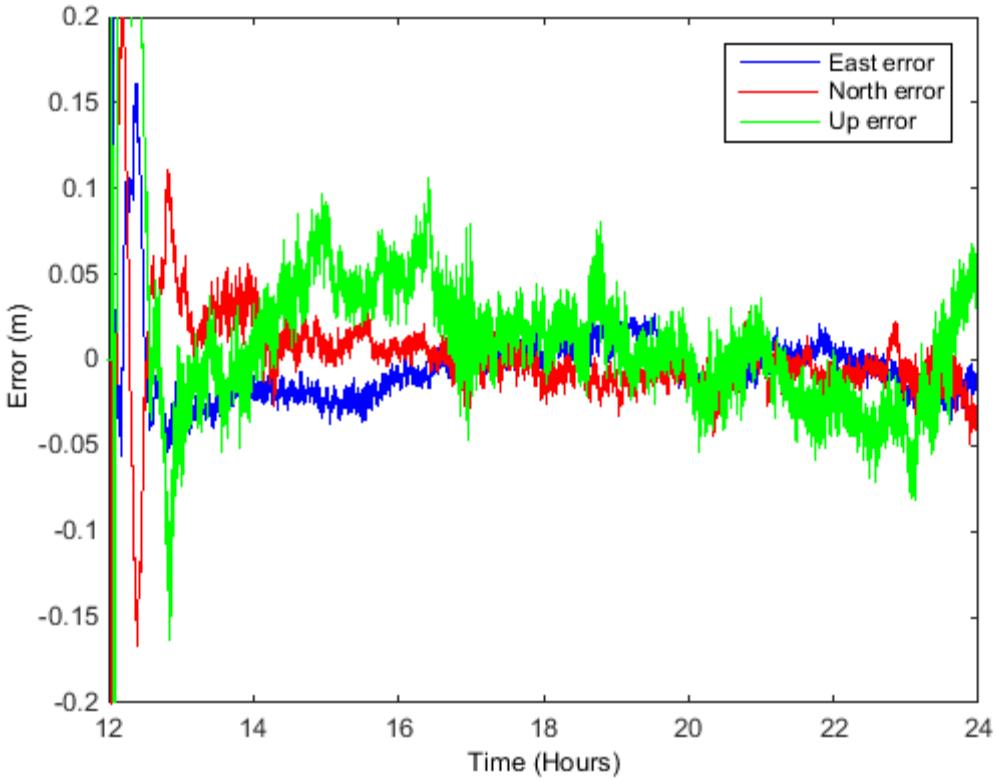

Figure 6-16 - Rover Positional Errors with Corrections from Two Regional Stations (DUDE PMTH) (DOY 001)

Table 6-7 - Rover Positional RMS Errors with Corrections from Two Regional Stations (DUDE PMTH)

DOY	East (mm)	North (mm)	Up (mm)	3D (mm)
001	14.4	13.7	32.7	38.2
032	17.5	13.6	24.4	32.9
060	7.3	9.6	21.3	24.5
091	17.9	21.0	35.8	45.2
121	10.9	15.0	29.3	34.7
213	12.6	22.0	30.3	39.5
Average	**13.4**	**15.8**	**29.0**	**35.8**

The results for a network of four stations, DUDE, PMTH, KEYW and WEYB, are shown in Figure 6-17. The average RMS values for four stations are approximately 19% improved compared to using only two regional stations with values of 11.3 mm, 12.4 mm, 25.0 mm, and 30.2 mm respectively as shown in Table 6-8. These results are an improvement on the baseline testing using no UPD corrections in section 6.2, with a 21% improvement. This demonstrates that with the measurement model presented in this thesis and a large regional network of at least four stations it is possible to improve the user position.

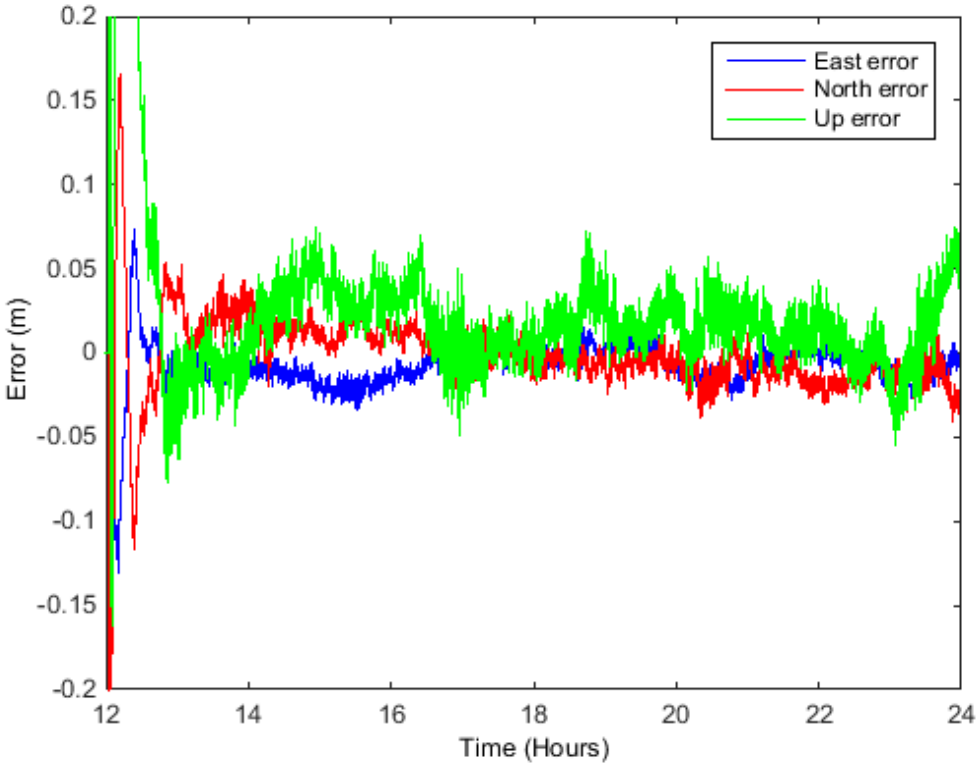

Figure 6-17 - Rover Positional Errors with Corrections from Four Regional Stations (DUDE PMTH KEYW WEYB) (DOY 001)

Table 6-8 - Rover Positional RMS Errors with Corrections from Four Regional Stations (DUDE PMTH KEYW WEYB)

DOY	East (mm)	North (mm)	Up (mm)	3D (mm)
001	11.2	13.8	25.4	31.0
032	8.7	9.4	21.6	25.1
060	6.2	7.4	15.9	18.6
091	15.4	15.0	35.6	41.6
121	11.4	12.4	22.1	27.8
213	15.1	16.6	29.4	37.0
Average	**11.3**	**12.4**	**25.0**	**30.2**

However, the improvement between the baseline test and the four station network could still be improved by adding further redundancy. Increased network redundancy should theoretically make the satellite clock and UPD estimates more accurate and consequently the user position more accurate. Therefore, the addition of further network stations will be tested to attempt to further improve the solution. Figure 6-18 shows the results when a network consisting of six network stations on DOY 001, DUDE, PMTH, KEYW, WEYB, HOLY and LOFT were used. The average RMS values computed for these results are 11.1 mm, 12.7 mm, 22.9 mm and 28.6 mm as shown in Table 6-9. This results in an approximate 6% improvement compared to the four station network and a 28% improvement from the baseline solution with no corrections applied.

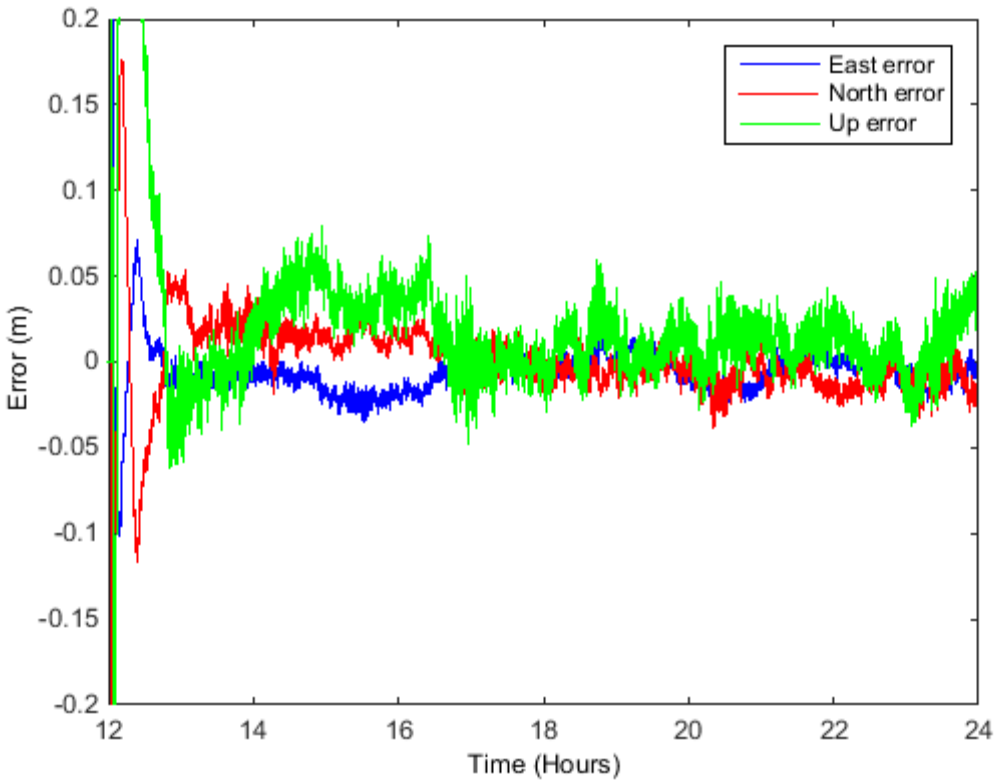

Figure 6-18 - Rover Positional Errors with Corrections from Six Regional Stations (DUDE PMTH KEYW WEYB HOLY LOFT) (DOY 001)

Table 6-9 - Rover Positional RMS Errors with Corrections from Six Regional Stations (DUDE PMTH KEYW WEYB HOLY LOFT)

DOY	East (mm)	North (mm)	Up (mm)	3D (mm)
001	10.1	13.1	24.0	29.4
032	8.6	9.4	22.4	25.8
060	6.2	8.5	14.4	17.8
091	16.0	14.6	25.9	33.7
121	11.1	13.2	21.5	27.6
213	14.7	17.2	29.4	37.1
Average	**11.1**	**12.7**	**22.9**	**28.6**

The final test in this section uses an eight station regional network. The results of the rover position using these corrections are presented in Figure 6-19. The RMS values show a minor improvement, approximately 1%, over the six station regional network with values of 10.2 mm, 12.7 mm, 23.1 mm and 28.3 mm respectively as shown in Table 6-10.

The small improvement between six and eight stations shows that although increasing the number of stations in the network does provide an improved solution there is a limit to the benefits. As additional stations are used in the network solution, the computational power required to obtain the solution increases. Therefore, this is a factor that must be considered when computing the network corrections. For this reason either six or eight stations appear sufficient to obtain an accurate solution without expending too much processing power. Consequently, the number of network stations tested in this study will not exceed eight.

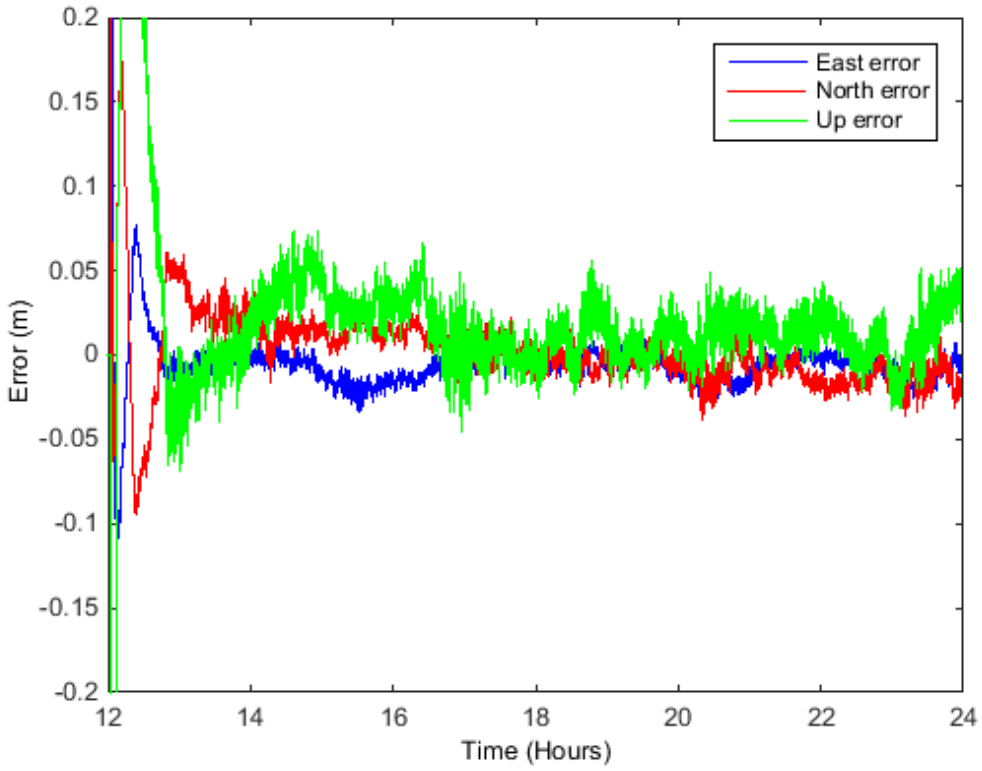

Figure 6-19 - Rover Positional Errors with Corrections from Eight Regional Stations (DUDE PMTH KEYW WEYB HOLY LOFT ABEP KIRK) (DOY 001)

Table 6-10 - Rover Positional RMS Errors with Corrections from Eight Regional Stations (DUDE PMTH KEYW WEYB HOLY LOFT ABEP KIRK)

DOY	East (mm)	North (mm)	Up (mm)	3D (mm)
001	10.2	14.7	22.8	29.0
032	8.5	9.7	24.3	27.5
060	6.6	9.5	15.9	19.7
091	10.9	12.1	26.2	30.8
121	13.8	15.4	25.4	32.7
213	11.2	14.6	23.9	30.2
Average	**10.2**	**12.7**	**23.1**	**28.3**

Table 6-11 summarises the results from the regional network. These 3D RMS results can be compared to those achieved in the local network tests in Table 6-12. When the results of the two, four and six station regional networks are compared to those achieved from the local networks the regional network results are better. However, the small difference between the results shows that the distance between the network stations and the user has little impact on the results. These results are to be expected as the UPDs are stable over large distances and the satellite clocks are not spatially variable.

Table 6-11 – Rover Positional RMS Error for Regional Stations Summary

	No Corrections	Two Regional Stations	Four Regional Stations	Six Regional Stations	Eight Regional Stations
East (mm)	15.9	13.4	11.3	11.1	10.2
North (mm)	15.2	15.8	12.4	12.7	12.7
Up (mm)	29.2	29.0	25.0	22.9	23.1
3D (mm)	36.5	35.8	30.2	28.6	28.3

Table 6-12 - Local and Regional Network RMS Comparison

	Local Network	Regional Network
Two Stations 3D RMS (mm)	36.4	35.8
Four Stations 3D RMS (mm)	32.4	30.2
Six Stations 3D RMS (mm)	31.2	28.6

6.7 User Location

So far the tests located the user near the centre of the network used to compute the corrections. However, it is not always possible when positioning offshore to have a good spatial distribution of network stations. Therefore, this section will examine whether the accuracy of the corrections is dependent on where the user is located in relation to the network.

This chapter previously established that the results from a two station network are not reliable. Therefore, a two station network will not be tested further. Instead, four and six station networks will be processed. In both cases, the user CARL is located approximately 250 km outside the extents of the network.

The user results for the four station network, PMTH, KEYW, ABEP and WEYB, on DOY 001 are presented in Figure 6-20. The average RMS values computed from the results are 21.2 mm, 17.5 mm, 39.5 mm and 48.8 mm for east, north, up and 3D respectively. These results can be compared to the four station regional network that surrounds the user, where the RMS values were 11.3 mm, 12.4 mm, 25.0 mm and 30.2 mm. Locating the user receiver outside of the extents of the network leads to the position estimates deteriorating by approximately 60%, compared to when the receiver is located centrally within the network.

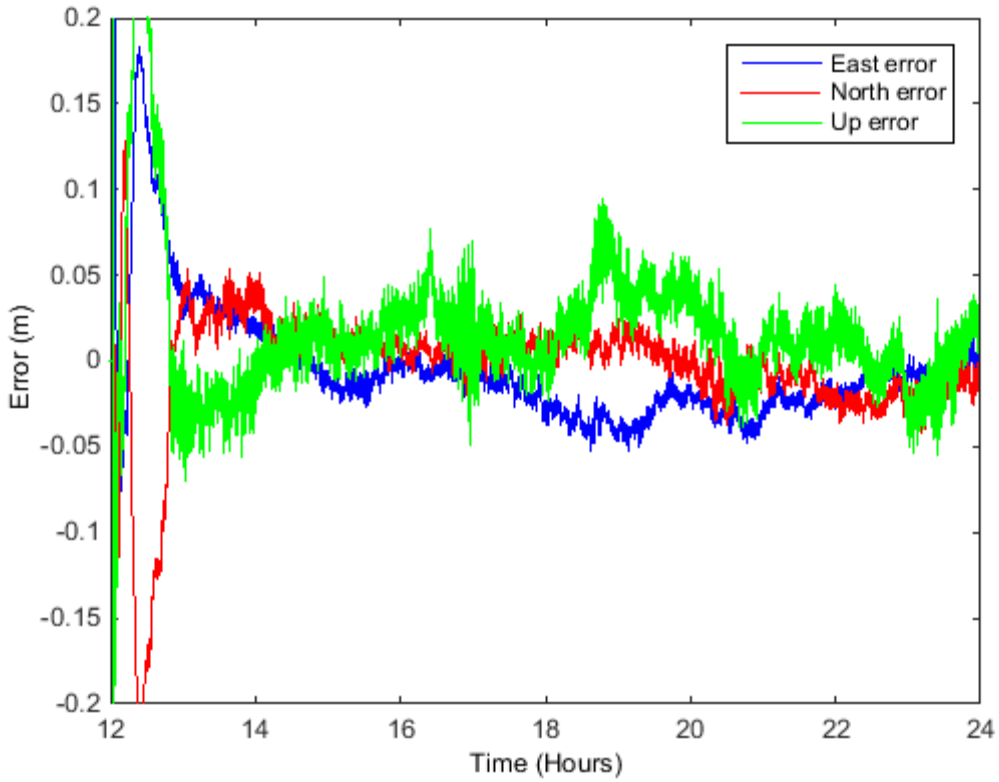

Figure 6-20 - Rover Positional Errors with Corrections from Four Regional Stations (not in close proximity to the user) (PMTH KEYW WEYB ABEP) (DOY 001)

Table 6-13 - Rover Positional RMS Errors with Corrections from Four Regional Stations (not in close proximity to the user) (PMTH KEYW WEYB ABEP)

DOY	East (mm)	North (mm)	Up (mm)	3D (mm)
001	22.5	17.2	25.6	38.2
032	20.5	13.5	53.8	59.2
060	15.2	14.1	20.9	29.4
091	20.7	19,8	49.1	56.9
121	26.2	18.1	40.2	51.3
213	22.4	24.4	47.3	57.7
Average	**21.2**	**17.5**	**39.5**	**48.8**

An assessment was undertaken for a theoretically more accurate six station network, PMTH, KEYW, ABEP, WEYB, MANR and SHRE. The results of the user using corrections from these six regional stations can be viewed in Figure 6-21. The RMS values for the rover in this test are 15.9 mm, 14.4 mm, 27.5 mm, and 35.2 mm in east, north, up and 3D. Again, as in the four station test the RMS values are worse than those achieved when the user was located centrally. An approximately 23% deterioration is seen compared to when the user to located centrally. Unfortunately, MANR data was not available for DOY 032 and SHRE data was unavailable for DOY 091 so these results have been omitted.

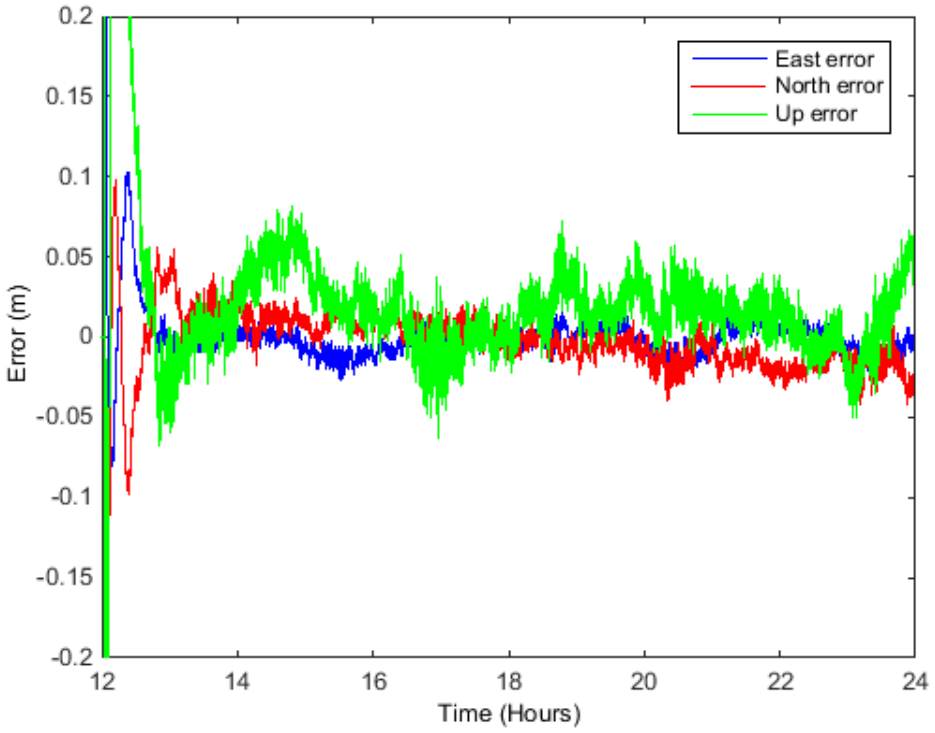

Figure 6-21 - Rover Positional Errors with Corrections from Six Regional Stations (not in close proximity to the user) (PMTH KEYW WEYB ABEP SHRE MANR) (DOY 001)

Table 6-14 - Rover Positional RMS Errors with Corrections from Six Regional Stations (not in close proximity to the user) (PMTH KEYW WEYB ABEP SHRE MANR)

DOY	East (mm)	North (mm)	Up (mm)	3D (mm)
001	7.6	14.2	25.2	29.9
032	NA	NA	NA	NA
060	15.7	12.5	19.9	28.3
091	NA	NA	NA	NA
121	23.6	15.6	36.4	46.1
213	16.7	15.3	28.6	36.5
Average	**15.9**	**14.4**	**27.5**	**35.2**

There are a number of potential reasons for the deterioration in the user results when the network is not located around the user. Firstly, any errors linked to the estimation of the troposphere and ionosphere are less likely to cancel when the network is further away from the user site. Secondly, the visibility periods of the satellites are likely to be different. When a satellite is not visible to the network, no corrections can be computed. Therefore, the observations from that satellite cannot be used by the rover. This will limit the number of satellites the user can use to compute the position, therefore reducing redundancy and potentially also accuracy. This limitation will be small for a regional network in the UK but will likely become significant for continental size networks. Finally, any residual orbit error in the IGS orbits will have a larger effect: the further the stations are apart as the angle of elevation will be different for each receiver.

For these reasons it is important to try to locate the network stations at the extents of the network where possible. This will result in the user never being outside of the network providing the corrections. If this is not possible, it is important to have a large number of stations in the network to mitigate these issues.

6.8 Network Station Drop Out

In section 5.7, it was discussed that it is important to assess the capabilities of the measurement model under real world scenarios. One such scenario is that a station in the network used to compute the satellite clock and UPD corrections, becomes non-operational. To test this scenario, a network is programmed to drop from four stations to three stations after 18 hours of the day.

One method of assessing the accuracy of the network solution is examining the T values computed using equation (4.10) in section 4.2.1. These T values computed each epoch show how well the observations fit the data. The lower the T value the better the estimated parameters fit the data. Figure 6-22 show the T value on DOY 001 computed for this network when one station drops out. Figure 6-23 shows the T value if the network had remained as four stations. It can be seen that the period after 18 hours has an average T value greater than the previous hours. This is confirmed by computing the average T value between 12 and 18 hours (0.31) and the average between 18 and 24 hours (0.42). This difference shows that the extra

station in the network contributes to additional redundancy and therefore allows the parameter estimates to fit to the data better.

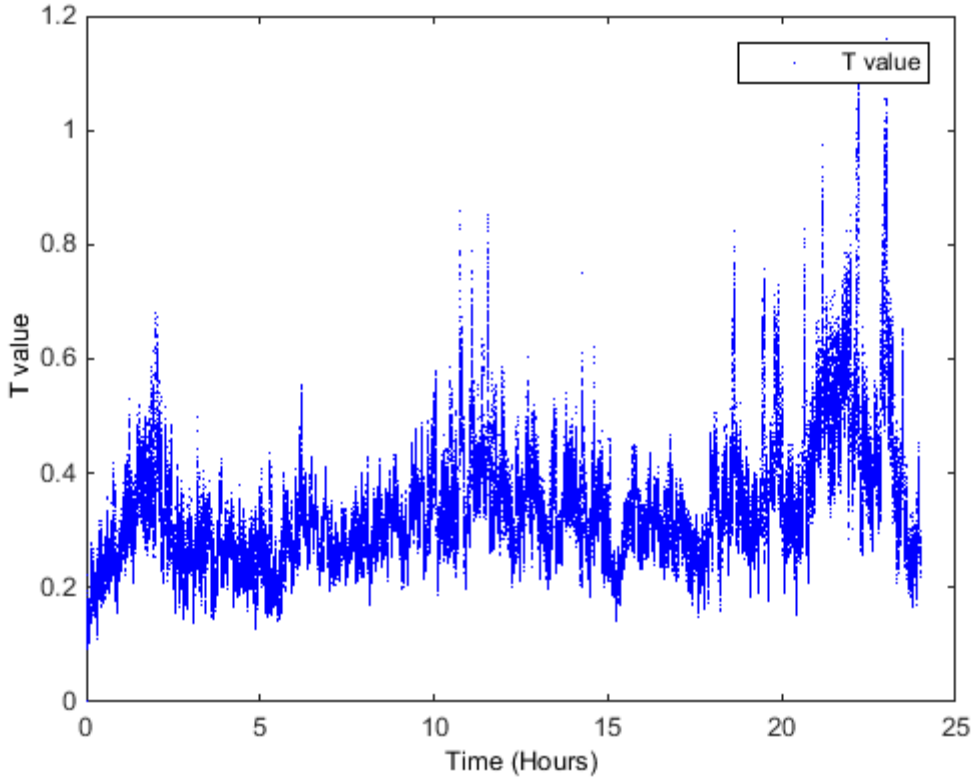

Figure 6-22 - T Value for Network of Four Stations Dropping to Three Stations (DUDE PMTH KEYW WEYB) (DOY 001)

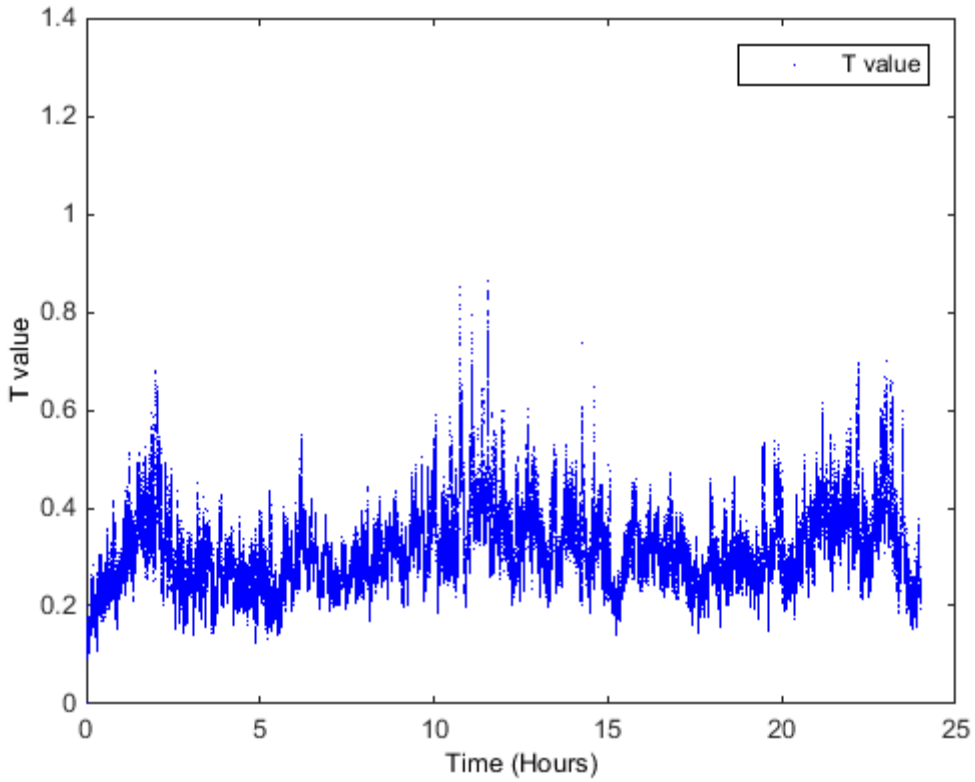

Figure 6-23 - T Value for Network of Four Stations (DUDE PMTH KEYW WEYB) (DOY 001)

The UPD and satellite clock corrections, computed from this network will be transmitted to the rover. The rover results for DOY 001 can be seen in Figure 6-24 and the RMS values in Table 6-15. The overall RMS values from 13 to 24 hours are 11.3 mm, 12.7 mm, 27.2 mm, and 32.2 mm respectively. These results can be subdivided in the period between 13 and 18 hours (Table 6-16), where four network stations are used to compute the corrections and between 18 and 24 hours (Table 6-17), when just three were used. For the period with four stations, the RMS values are 11.7 mm, 12.9 mm, 22.7 mm and 29.2 mm respectively, whereas, for the three station network, the RMS values were 10.7 mm, 12.4 mm, 28.5 mm and 33.1 mm respectively. Therefore, when the four station network was operational, a better solution was achieved, especially in the up direction. However, a point to note is that the measurement model and program were capable of a smooth transition from four stations to three. Previous tests have shown that larger station networks produce more accurate results. Therefore, the loss of a station will have a reduced effect on the accuracy of the corrections. If more stations are used to begin with, a loss of one station will not be 25% of the observations.

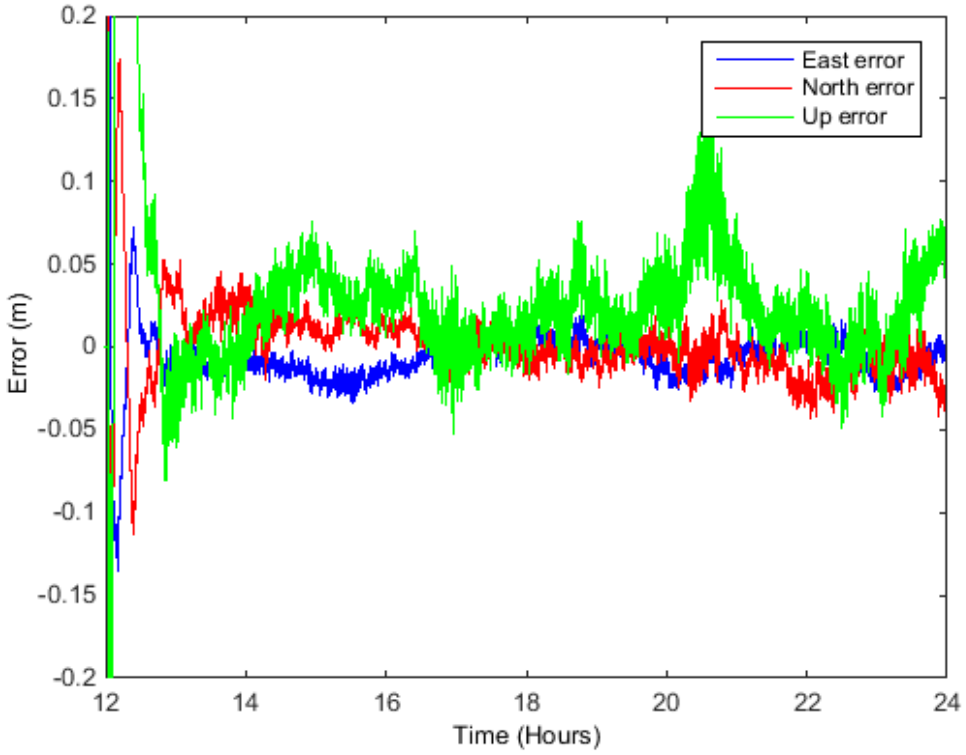

Figure 6-24 - Rover Positional Errors with Corrections from Four Stations Dropping to Three Stations (DUDE PMTH KEYW WEYB) (DOY 001)

Table 6-15 - Rover Positional RMS Errors with Corrections from Four Stations Dropping to Three Stations (DUDE PMTH KEYW WEYB) (13 – 24 hours)

DOY	East (mm)	North (mm)	Up (mm)	3D (mm)
001	11.6	14.3	33.6	38.3
032	8.7	9.5	22.0	25.5
060	6.7	7.6	17.7	20.4
091	15.7	15.8	39.1	45.0
121	9.9	12.7	21.7	27.1
213	15.3	16.2	29.2	36.7
Average	**11.3**	**12.7**	**27.2**	**32.2**

Table 6-16 - Rover Positional RMS Errors with Corrections from Four Stations Dropping to Three Stations (DUDE PMTH KEYW WEYB) (13 – 18 hours)

DOY	East (mm)	North (mm)	Up (mm)	3D (mm)
001	13.0	15.0	27.3	33.8
032	9.3	8.3	22.8	26.0
060	5.5	6.4	14.8	17.1
091	17.3	17.9	14.5	28.8
121	7.0	12.8	21.7	26.2
213	18.3	17.2	34.9	43.0
Average	**11.7**	**12.9**	**22.7**	**29.2**

Table 6-17 - Rover Positional RMS Errors with Corrections from Four Stations Dropping to Three Stations (DUDE PMTH KEYW WEYB) (18 – 24 hours)

DOY	East (mm)	North (mm)	Up (mm)	3D (mm)
001	10.3	13.6	38.1	41.7
032	8.1	10.5	21.4	25.1
060	7.3	8.1	19.1	22.0
091	14.7	14.4	47.7	52.0
121	12.0	12.7	21.7	27.9
213	12.0	15.2	22.7	29.8
Average	**10.7**	**12.4**	**28.5**	**33.1**

6.9 IAR at the Network

When the network consists of two or more stations, the measurement model creates ambiguities that are double differenced. The ambiguities can be fixed to integers, theoretically making the measurement model more accurate.

To assess whether fixing ambiguities to integer values resulted in a set of parameters that better fits the data, the T value can be examined. Figure 6-25 shows the T value for the two station fixed network on DOY 001. There is no IAR for the first 10 hours to initialise the Kalman filter, while each satellite must be visible for 1800 epochs before it is eligible for IAR. This 10 hour initialisation is not critical to the convergence times for users, as it will only have to be done once at the initialisation of the network. After this 10 hour initialisation, the T value decreases (Figure 6-25), showing the IAR has a positive impact on the solution in terms of fitting to the observations.

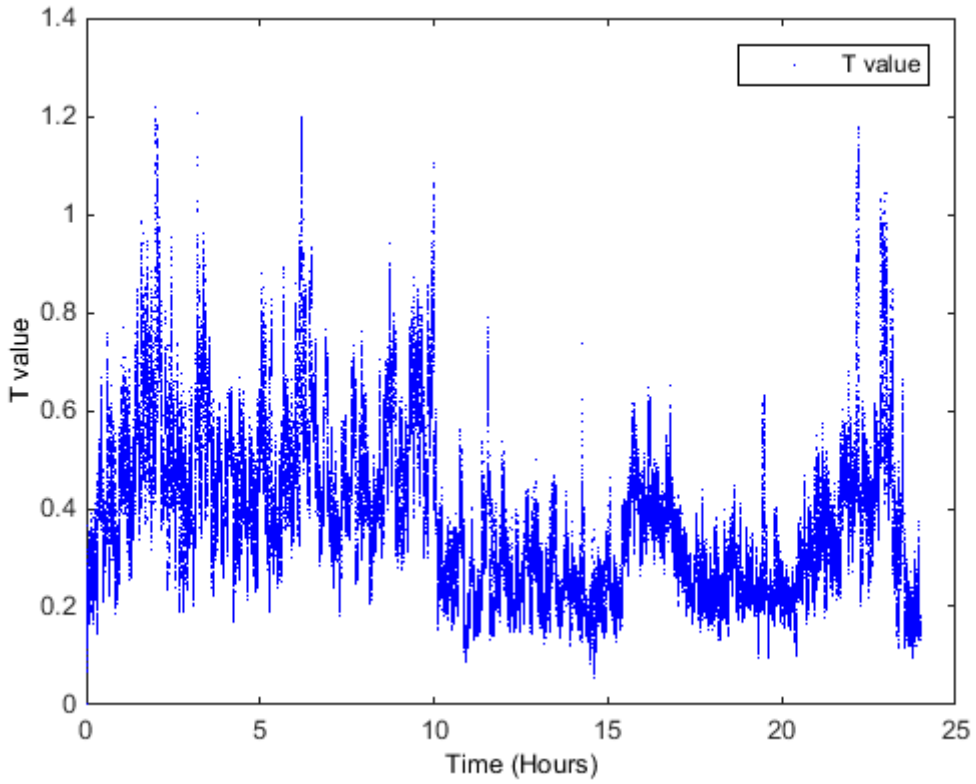

Figure 6-25 - T Value for Two Station Fixed Network (DUDE PMTH) (DOY 001)

Additionally, to assess how well the IAR has been undertaken, the percentage of ambiguities fixed can be computed. Ambiguities are not eligible for IAR until they have been visible for over 1800 epochs and have an elevation angle greater than

30°. The number of ambiguities fixed and the number eligible for IAR but not fixed at each epoch can be computed. These can then be combined to give a fixed percentage over the time series. For this two station network the percentage of fixed ambiguities is 36%. This percentage is lower than what would be ideal, due to the tight constraint applied on the LAMBDA program, with a critical value of 0.2. However, it was found that loosening the constraint to allow more ambiguities to be fixed, resulted in more incorrectly fixed ambiguities and consequently a less accurate solution.

The UPD and satellite clock corrections are used at the user in the same manner as if computed from a float solution. Figure 6-26 shows the user solution for DOY 001, which was computed using the corrections from the two station fixed network. However, as in all previous tests the user test does not undertake IAR, so this remains a float solution to aid comparison. The average RMS values obtained in this solution are 17.1 mm, 20.2 mm, 37.3 mm and 46.2 mm as shown in Table 6-18. If this is compared to the 13.4 mm, 15.8 mm, 29.0 mm and 35.8 mm obtained when using the two station float network, it can be seen to be less accurate by approximately 29%.

This lower accuracy shows that strong correlations between the parameters when only using a two station network can impact the undertaking of IAR. The correlations between the parameters make the estimation of the float ambiguity parameters difficult and consequently can lead to incorrect fixing of the ambiguities. Therefore, the potential to fix the ambiguities to the incorrect integer is high, making the solution unreliable.

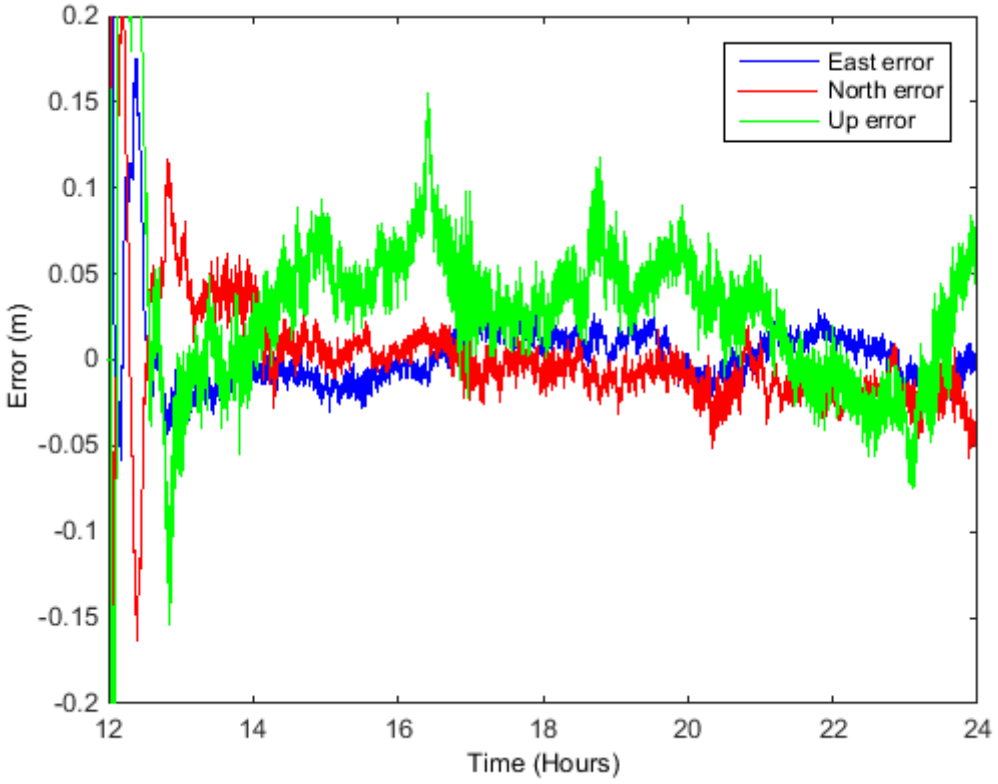

Figure 6-26 - Rover Positional Errors with Corrections from Two Fixed Stations (DUDE PMTH) (DOY 001)

Table 6-18 - Rover Positional RMS Errors with Corrections from Two Fixed Stations (DUDE PMTH)

DOY	East (mm)	North (mm)	Up (mm)	3D (mm)
001	12.8	19.2	43.6	49.3
032	17.5	13.6	24.4	32.9
060	12.5	15.7	44.3	48.6
091	21.1	26.8	41.3	53.6
121	16.8	19.1	37.8	45.5
213	22.1	26.5	32.5	47.4
Average	**17.1**	**20.2**	**37.3**	**46.2**

To reduce the correlations between the parameters and potentially make the ambiguity resolution more reliable, the network is increased to four stations. Figure 6-27, once again, shows how the T value is reduced, upon the start of the IAR process at 10 hours into the observations. Other peaks in the T value plot, such as between 15 and 17 hours correspond to when the fewest number of satellites are visible on DOY 001. Therefore, during this period, the Kalman filter struggles to fit the parameter estimates to the data with the same accuracy, as the redundancy in the measurement model is much lower.

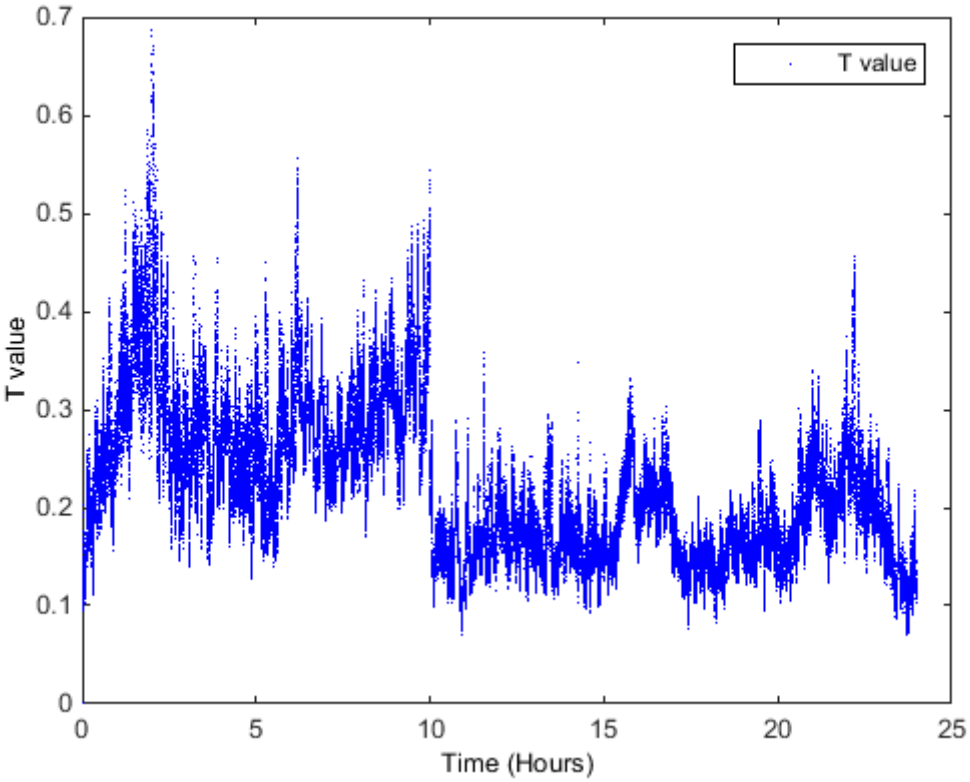

Figure 6-27 - T Value for Four Station Fixed Network (DUDE PMTH KEYW WEYB) (DOY 001)

The fixed corrections from the four stations, with an ambiguity fixed percentage of 40%, are utilised at the rover (Figure 6-28). The average RMS values associated with this network are shown in Table 6-19, with average values of 14.5 mm, 15.3 mm, 28.7 mm and 35.9 mm. Compared to the four station float solution, where RMS values were 11.3 mm, 12.4 mm, 25.0 mm and 30.2 mm, the fixed corrections give a worse user solution. The fixed user solution was approximately 19% worse than its float counterpart, using exactly the same four station network. This was not the anticipated result after undertaking IAR, but could have a number of causes.

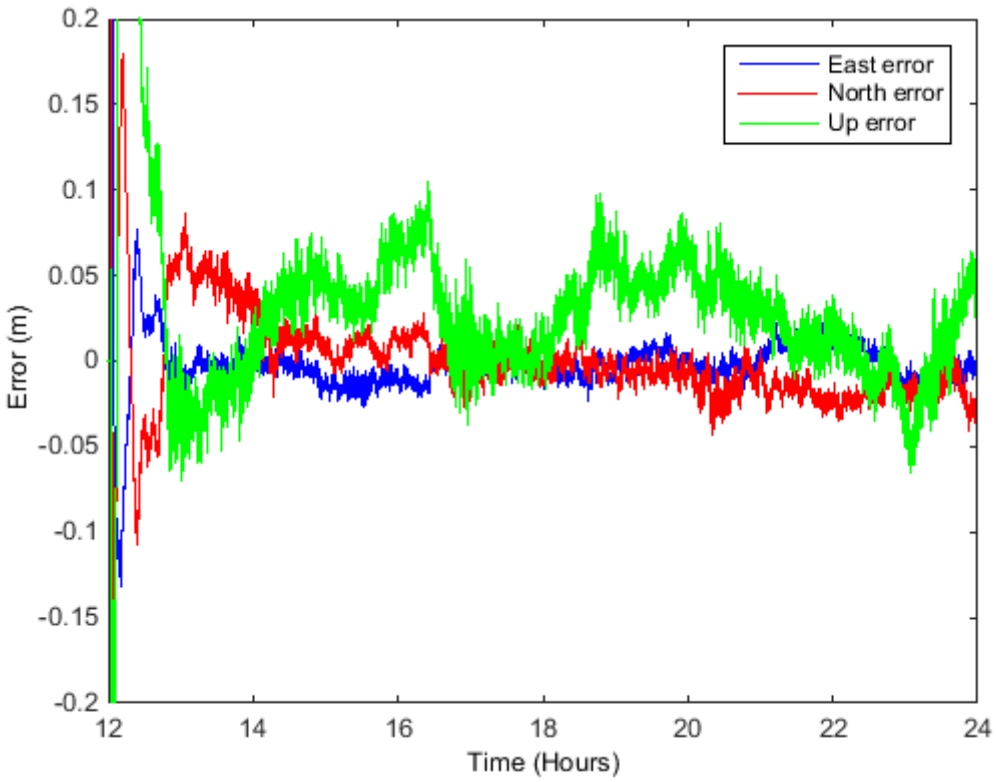

Figure 6-28 - Rover Positional Errors with Corrections from Four Fixed Stations (DUDE PMTH KEYW WEYB) (DOY 001)

Table 6-19 - Rover Positional RMS Errors with Corrections from Four Fixed Stations (DUDE PMTH KEYW WEYB)

DOY	East (mm)	North (mm)	Up (mm)	3D (mm)
001	8.9	20.1	37.7	43.6
032	14.3	11.6	24.5	30.6
060	9.7	8.8	19.6	23.6
091	14.0	14.9	30.5	36.7
121	19.5	15.4	23.5	34.2
213	20.5	20.7	36.4	46.7
Average	**14.5**	**15.3**	**28.7**	**35.9**

Firstly, one or more ambiguities in the network, could have been fixed to a wrong value, causing an error of at least 19 cm in those observations. There is no facility within the MATLAB program, created for this thesis, to further check whether previously fixed ambiguities are incorrectly fixed. This error will continue within the observations until the satellite in question no longer becomes visible. In more sophisticated software, this can be implemented as a method of error detection but this is beyond the scope of this study.

Secondly, when the ambiguities are fixed to an integer value the remaining parameters are updated, as described in section 4.3.4. This update step must take into account the correlations between the parameters, when trying to adjust the parameter estimations for the newly fixed ambiguities. As already discussed some correlations between parameters can be strong. Consequently, the update step can lead to unrealistic, centimetre level jumps in certain parameters, such as the troposphere. Due to the process noise values in the Kalman filter, any incorrect jump in parameters can take a number of minutes to resolve. This error in the troposphere estimation can directly lead to an error in the up component of the user position and may explain why the majority of the deterioration is in the up component.

Thirdly, the rover receiver is currently not undertaking any IAR in this test and consequently is just a float solution. When the rover attempts to undertake IAR, as shown later in this chapter, it may be shown that, although the fixed network corrections do not improve the float user solution, they may improve the user's ability to undertake IAR. Therefore, this could then lead to an improved user solution.

Finally, there are still errors that exist with all of the GPS observations and the parameter estimation, as the measurement model is not perfect. Therefore, some error is likely to be in the estimation of the float double difference ambiguities. If the ambiguities are fixed to the correct integer value the error within that parameter will be pushed into other parameters in the measurement model, for example the satellite clocks and the UPDs. However, this error is likely to small in most cases and will not be the main cause of the differences between the solutions.

The results from a six station network including IAR with an ambiguity fixed percentage rate of 45% are presented in Figure 6-29 and Figure 6-30. Similar to the previous two tests, Figure 6-29 shows the T value decreases upon the commencing

of the IAR at 10 hours. The average RMS values computed for the position are 13.9 mm, 17.4 mm, 31.4 mm and 38.8 mm as seen in Table 6-20. These values are approximately 8% worse compared to those in the previous four station fixed network test. As with the previous test, these results have a lower accuracy when compared to the float solution achieved in section 6.6, for the same reasons discussed previously.

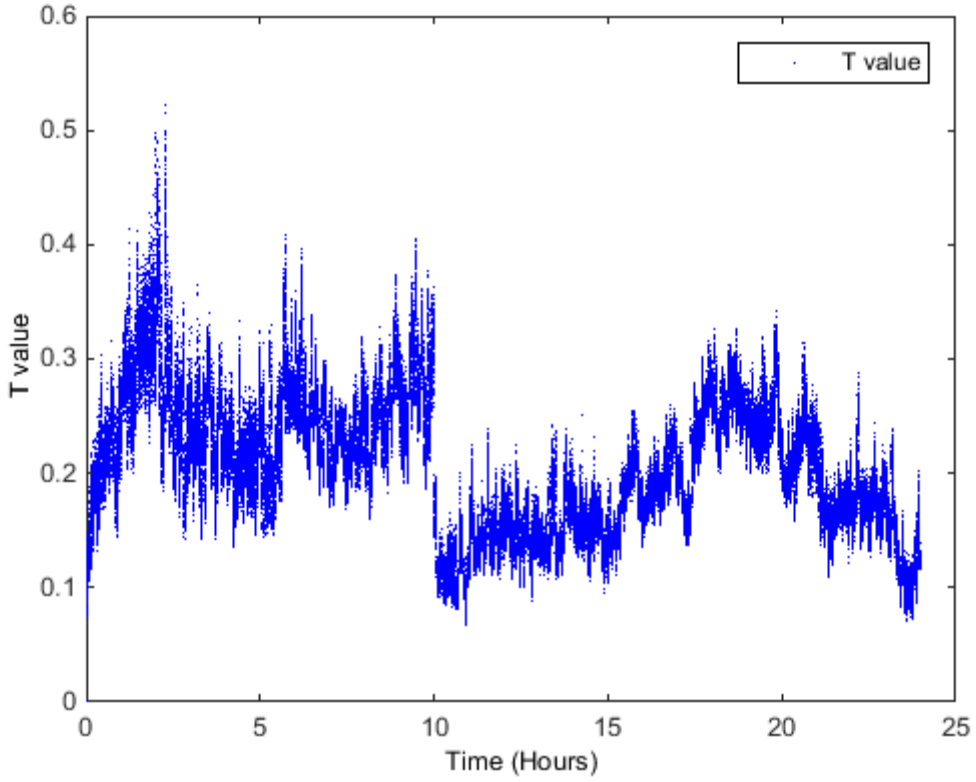

Figure 6-29 - T Value for Six Station Fixed Network (DUDE PMTH KEYW WEYB HOLY LOFT) (DOY 001)

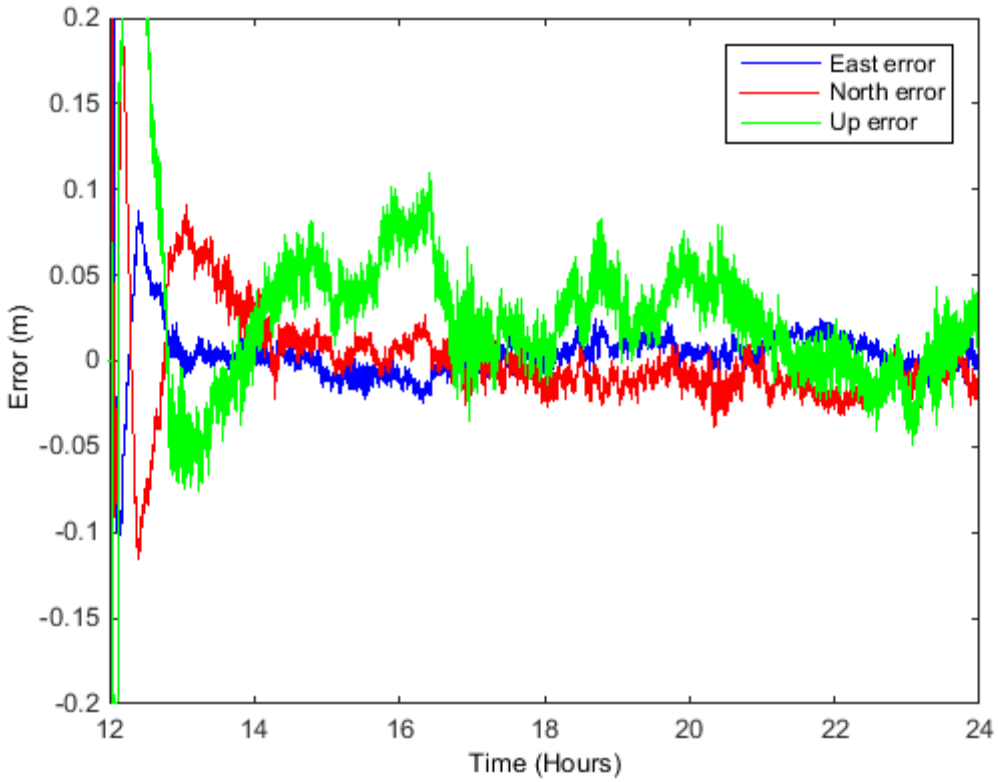

Figure 6-30 - Rover Positional Errors with Corrections from Six Fixed Stations (DUDE PMTH KEYW WEYB HOLY LOFT) (DOY 001)

Table 6-20 - Rover Positional RMS Errors with Corrections from Six Fixed Stations (DUDE PMTH KEYW WEYB HOLY LOFT)

DOY	East (mm)	North (mm)	Up (mm)	3D (mm)
001	8.8	20.0	37.4	43.3
032	12.5	11.7	27.1	32.0
060	10.5	11.5	22.0	26.9
091	10.2	14.2	31.6	36.1
121	21.5	16.6	30.1	40.5
213	20.0	30.1	40.4	54.2
Average	13.9	17.4	31.4	38.8

The tests using eight network stations while undertaking IAR with an ambiguity fixed percentage of 45% are presented in Figure 6-31 and Figure 6-32. The results follow the pattern established by the previous three tests. The T value decreases upon commencing of the IAR at 10 hours and the RMS values for the rover position are 13.6 mm, 17.0 mm, 30.5 mm and 38.2 mm as shown in Table 6-21. These results are highly comparable with the previous six station fixed network, with less than 1% improvement with the addition of the two extra stations. Finally, compared to the eight station float solution the results show an approximate 35% deterioration in the rover position.

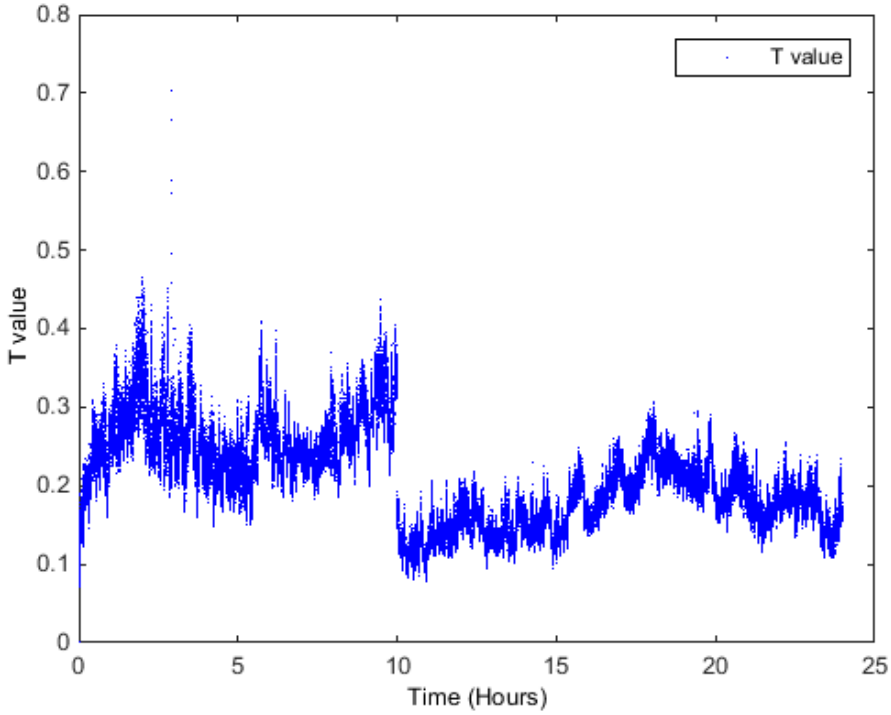

Figure 6-31 - T Value for Eight Station Fixed Network (DUDE PMTH KEYW WEYB HOLY LOFT ABEP KIRK) (DOY 001)

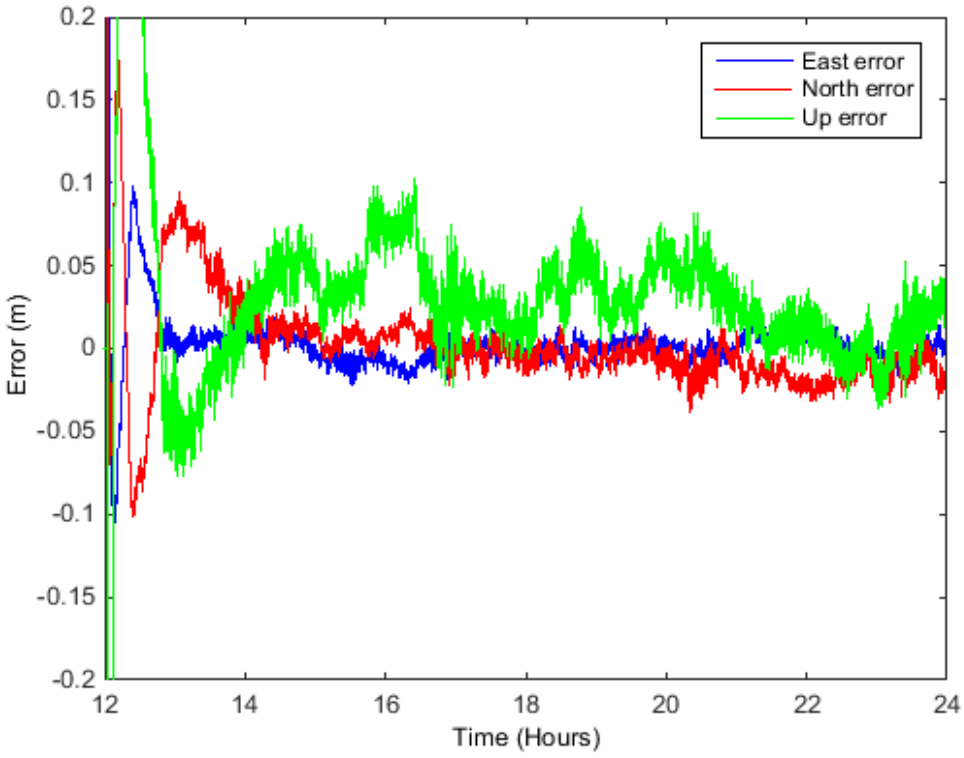

Figure 6-32 - Rover Positional Errors with Corrections from Eight Fixed Stations (DUDE PMTH KEYW WEYB HOLY LOFT ABEP KIRK) (DOY 001)

Table 6-21 - Rover Positional RMS Errors with Corrections from Eight Fixed Stations (DUDE PMTH KEYW WEYB HOLY LOFT ABEP KIRK)

DOY	East (mm)	North (mm)	Up (mm)	3D (mm)
001	6.9	20.6	37.4	43.2
032	10.4	11.9	33.0	36.6
060	14.3	15.3	29.8	36.4
091	12.7	17.6	31.4	38.2
121	23.9	18.3	20.5	36.5
213	13.6	18.1	31.0	38.4
Average	**13.6**	**17.0**	**30.5**	**38.2**

Despite all the tests showing that using an ambiguity fixed network provides inferior UPD and satellite clock corrections, the tests do show that using at least four stations in the network provides better results. Table 6-22 shows a summary of the results from this test compared to the float tests undertaken in section 6.6.

Table 6-22 - RMS Comparison of Float and Fixed Networks

	Float Network	Fixed Network
Two Stations 3D RMS (mm)	35.8	46.2
Four Stations 3D RMS (mm)	30.2	35.9
Six Stations 3D RMS (mm)	28.6	38.8
Eight Stations 3D RMS (mm)	28.3	38.2

6.10 IAR at the User

All the tests undertaken so far have used a rover solution without any attempt to undertake IAR. However, to realise the full potential of this study and potentially provide a further improvement to the rover position solution, the ambiguities need to be fixed to their integer values. However, it is critical that when IAR is undertaken the ambiguities are fixed correctly. Any ambiguities that are incorrectly fixed will adversely affect the rover position and provide a solution that will be inferior to the float solution.

For the user to correctly fix the ambiguities, precise UPD and satellite clock corrections must be used. In the tests outlined in this chapter, the best rover RMS values were obtained when using the eight station regional float network, with a 3D RMS of 28.3 mm.

The UPD and satellite clock corrections from the eight station float network are used at the rover in the same manner. As previous tests have shown convergence times of approximately one hour, the IAR process is not started until after one hour of observations, to limit the chances of incorrect ambiguity fixing. The same LAMBDA method of ILS with the ratio test is used to try to fix the user ambiguities, but with a critical value of 0.05. This value is a tighter constraint than in the network solution, as

the chance for incorrect fixing and the impact of incorrect fixing is higher in the user solution. The rover is a single receiver, so there is much less redundancy in the Kalman filter and consequently the chances of parameters being poorly estimated are higher.

The T value for the user during this test is shown in Figure 6-33. There is no noticeable drop in the T value when IAR commences, as occurs in the network tests. This shows that although IAR has been undertaken, it has not had a positive effect on the fit of the solution to the data. The peaks in the T value correspond to when there are fewer satellites visible to the receiver and therefore less redundancy.

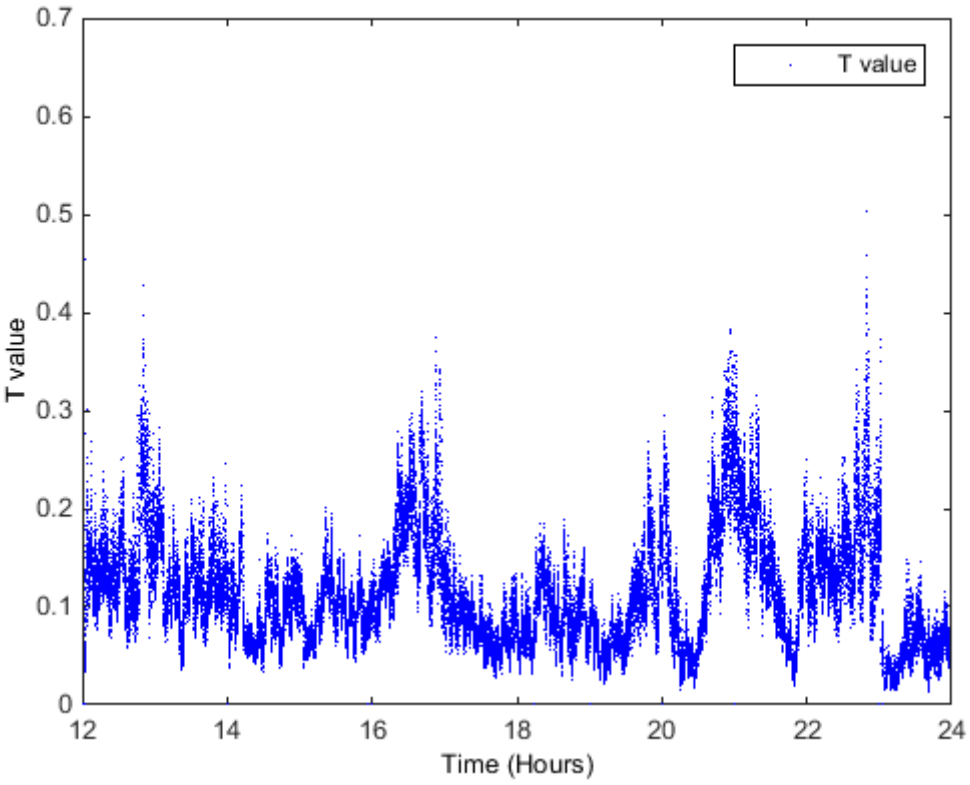

Figure 6-33 - T Value for User with Corrections from Eight Station Float Network (DUDE PMTH KEYW WEYB HOLY LOFT ABEP KIRK)

The results of the user position in this test are displayed in Figure 6-34. The ambiguity fixed percentage is 55%, which is higher than during the network tests. The RMS values from this test are 18.3 mm, 18.7 mm, 36.0 mm and 44.7 mm in east, north, up and 3D.

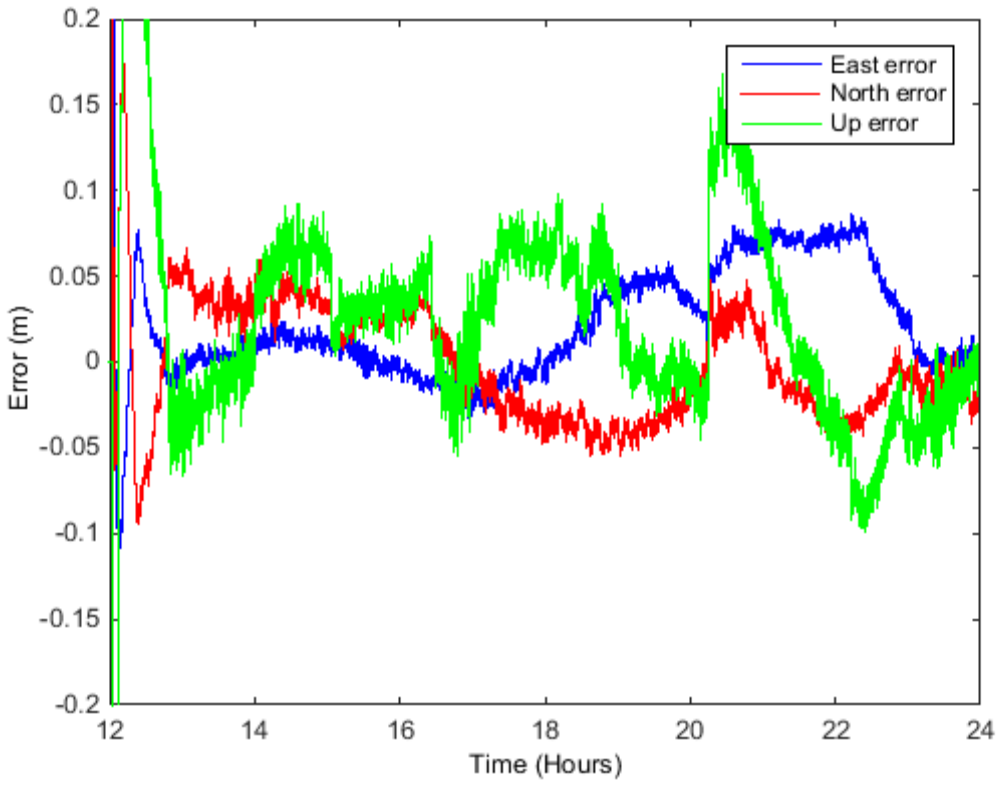

Figure 6-34 - Fixed Rover Positional Errors with Corrections from Eight Stations (DUDE PMTH KEYW WEYB HOLY LOFT ABEP KIRK) (DOY 001)

Table 6-23 - Fixed Rover Positional RMS Errors with Corrections from Eight Stations (DUDE PMTH KEYW WEYB HOLY LOFT ABEP KIRK)

DOY	East (mm)	North (mm)	Up (mm)	3D (mm)
001	35.8	34.2	71.9	87.3
032	8.7	9.7	23.5	26.9
060	6.6	9.5	15.9	19.7
091	19.4	25.3	36.1	48.2
121	14.8	15.7	28.3	35.6
213	24.3	17.8	40.2	50.2
Average	**18.3**	**18.7**	**36.0**	**44.7**

It is clear that these results are inferior to the float solution presented in section 6.6, where the RMS values were 10.2 mm, 12.7 mm, 23.1 mm and 28.3 mm. Figure 6-34 on DOY 001 shows some epochs where IAR has taken place and has a detrimental effect on the solution. For example, at 20 hours there is a jump in the up direction of approximately 20 cm, which directly corresponds to when an ambiguity is fixed. These jumps, caused by ambiguity fixing, result in the RMS values for the various days being much more varied. For example, DOY 060 3D RMS is 19.7 mm, whereas DOY 001 3D RMS is 87.3 mm, showing the detrimental effect incorrect ambiguity fixing can have on the results.

When a pair of ambiguities on the L1 and L2 frequencies are fixed, the difference between the float and fixed ambiguity values must be spread into different parts of the measurement model. If the difference between the L1 fixed ambiguity and its float counterpart and the difference between the L2 fixed ambiguity and its float counterpart is in the ratio of 1:1.649, then this jump can be absorbed within the ionosphere term. This is because the values in the measurement model for phase ionospheric terms are in this ratio. Additionally, the phase observations are precise compared to the code observations and a large error in code is not overly important. However, if the differences are not in this ratio, then additional parameters must accommodate some of the change. When this occurs, a jump in the troposphere or the east, north and up components can occur.

Theoretically, to undertake IAR at a user receiver the network providing corrections must also have fixed ambiguities. Therefore, despite the fixed network tests (discussed in section 6.9) providing inferior position estimates when using a float user solution, they may provide benefits when trying to compute a fixed user solution. Therefore, a second test was completed, using the six station fixed test described in section 6.9. The T value for this test is shown in Figure 6-35. When IAR commences at 13 hours, there is a drop in the T value, showing an improvement in the fit to the observations. The T value is maintained at this lower value, apart from some small peaks when fewer satellites are visible such as at 20 hours.

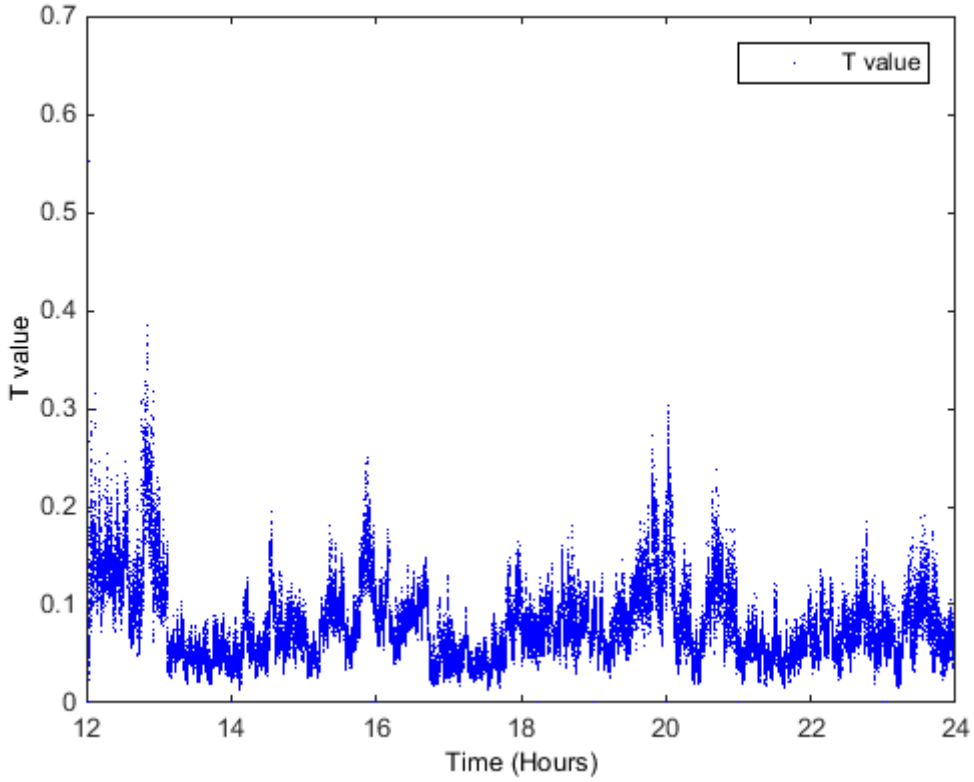

Figure 6-35 - T Value for User with Corrections from Six Station Fixed Network (DUDE PMTH KEYW WEYB HOLY LOFT) (DOY 001)

Figure 6-36 shows the rover position as a result of using these corrections on DOY 001. The ambiguity fixed percentage in this test is increased to 65% and the average RMS values were an improvement compared to the previous eight station float network with values of 13.2 mm, 13.2 mm, 27.1 mm and 33.0 mm. Compared to the RMS of 13.9 mm, 17.4 mm, 31.4 mm and 38.8 mm when using a float user solution with the same corrections there is a 17% improvement. This may show that to achieve a reliable fixed user solution, a fixed network is required to provide a double difference solution. However, these results are still inferior to using a float network solution and float user solution. Therefore, this indicates that although fixing ambiguities can have a positive impact on the user position, currently the number of incorrectly fixed ambiguities at either the network or the user is causing the solution to deteriorate.

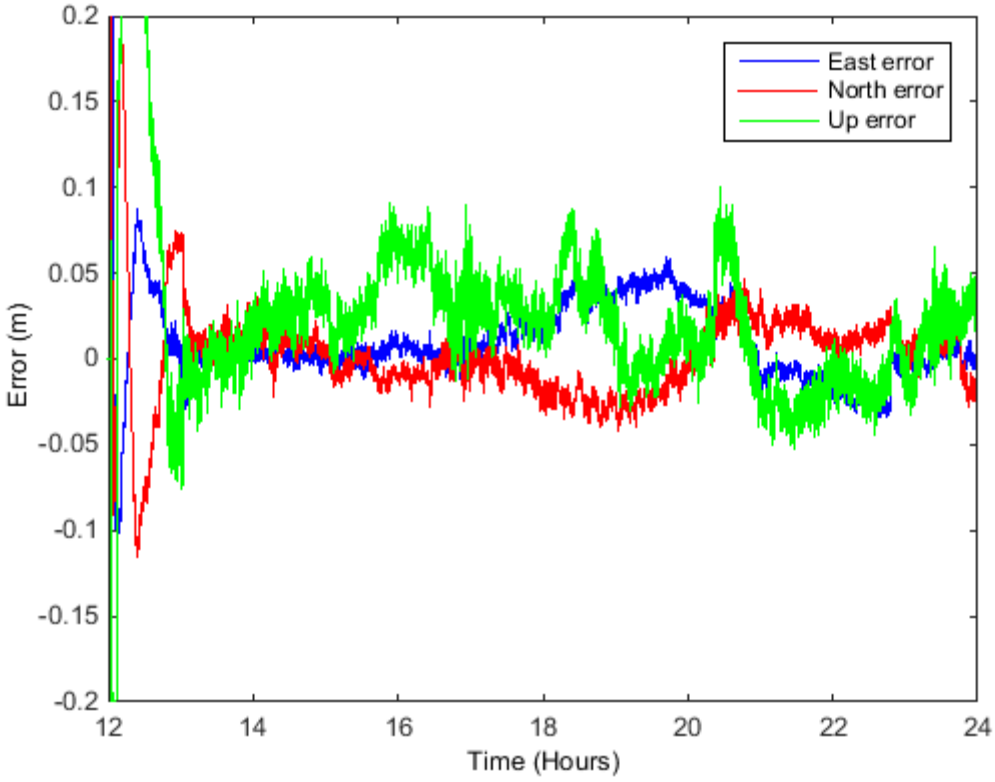

Figure 6-36 - Fixed Rover Positional Errors with Corrections from Six Fixed Stations (DUDE PMTH KEYW WEYB HOLY LOFT) (DOY 001)

Table 6-24 - Fixed Rover Positional RMS Errors with Corrections from Six Fixed Stations (DUDE PMTH KEYW WEYB HOLY LOFT)

DOY	East (mm)	North (mm)	Up (mm)	3D (mm)
001	21.0	17.1	33.0	42.7
032	8.7	9.8	21.9	25.5
060	6.2	8.5	14.4	17.8
091	16.0	14.6	35.9	42.0
121	12.6	13.5	24.8	30.9
213	14.6	15.8	32.7	39.1
Average	**13.2**	**13.2**	**27.1**	**33.0**

6.11 Proposed Measurement Model Results Summary

Table 6-25 shows a summary of the 3D RMS results presented in this chapter when testing the approach outlined in this thesis. Here it can be seen that using networks of more than two stations either locally or regionally can improve the user solution. However, it is clear that introducing IAR to either the network or the user can have a detrimental effect on the accuracy of the position.

Table 6-25 - Summary of Results from Proposed Measurement Model

	3D RMS (mm)
No Corrections	36.5
Two Local Stations	36.4
Four Local Stations	32.4
Six Local Stations	31.2
Two Regional Stations	35.8
Four Regional Stations	30.2
Six Regional Stations	28.6
Eight Regional Stations	28.3
Four Regional Stations (Away from User)	48.8
Six Regional Stations (Away from User)	35.2
Four Regional Stations (Dropping to 3)	32.2
Two Fixed Regional Stations	46.2
Four Fixed Regional Stations	35.9
Six Fixed Regional Stations	38.8
Eight Fixed Regional Stations	38.2
Eight Regional Stations – Fixed User	44.7
Six Fixed Regional Stations – Fixed User	33.0

6.12 PPP-RTK Comparison

A comparison with an alternative methodology (Zhang *et al.*, 2011), as described in section 5.10, was undertaken to assess the accuracy of this study. The measurement models developed in this approach are outlined in section 3.5. The first test used a two station float network, with the rover position for DOY 001 presented in Figure 6-37. The average RMS values computed from these results are 16.1 mm, 19.3 mm, 26.7 mm and 37.1 mm in east, north, up and 3D as seen in Table 6-26.

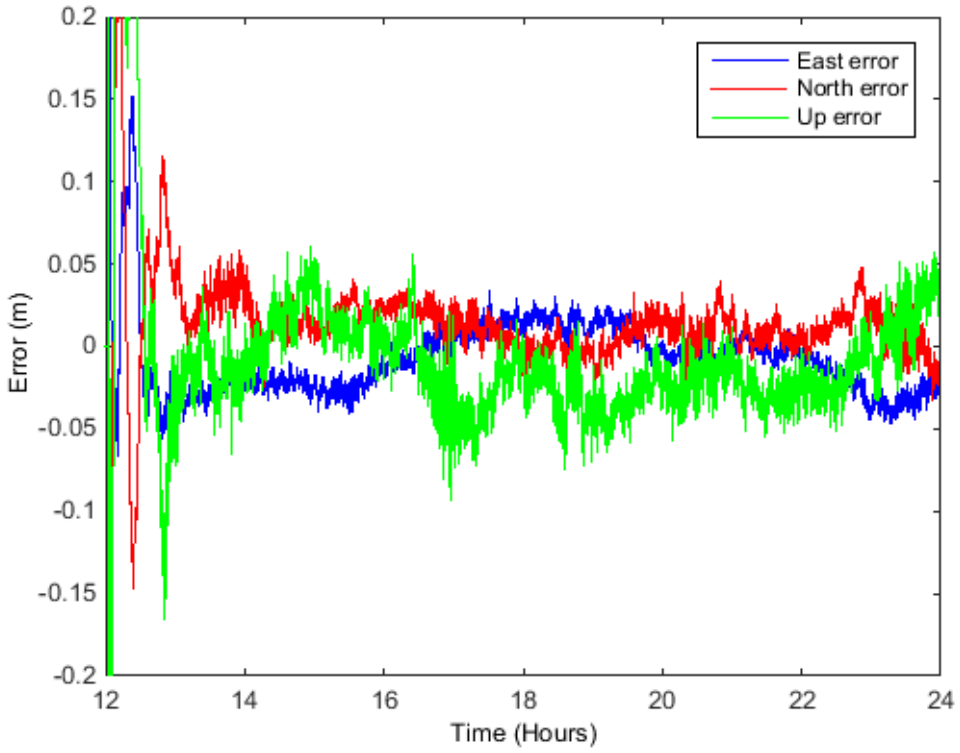

Figure 6-37 - Zhang Rover Positional Errors with Corrections from Two Stations & Alternative Model (DUDE PMTH) (DOY 001)

Table 6-26 - Zhang Rover Positional RMS Errors with Corrections from Two Stations & Alternative Model (DUDE PMTH)

DOY	East (mm)	North (mm)	Up (mm)	3D (mm)
001	19.2	17.7	26.9	37.4
032	8.3	12.0	19.6	24.4
060	22.8	29.2	32.7	49.4
091	15.7	21.0	27.5	40.0
121	12.3	15.6	24.9	31.9
213	18.2	20.4	28.3	39.3
Average	**16.1**	**19.3**	**26.7**	**37.1**

Figure 6-38 shows the same rover position but with satellite clock and UPD corrections computed from four network stations. The position estimates have improved by approximately 12% compared to those previously shown in Figure 6-37, with average RMS values of 15.0 mm, 16.3 mm, 24.3 mm and 33.0 mm as seen in Table 6-27.

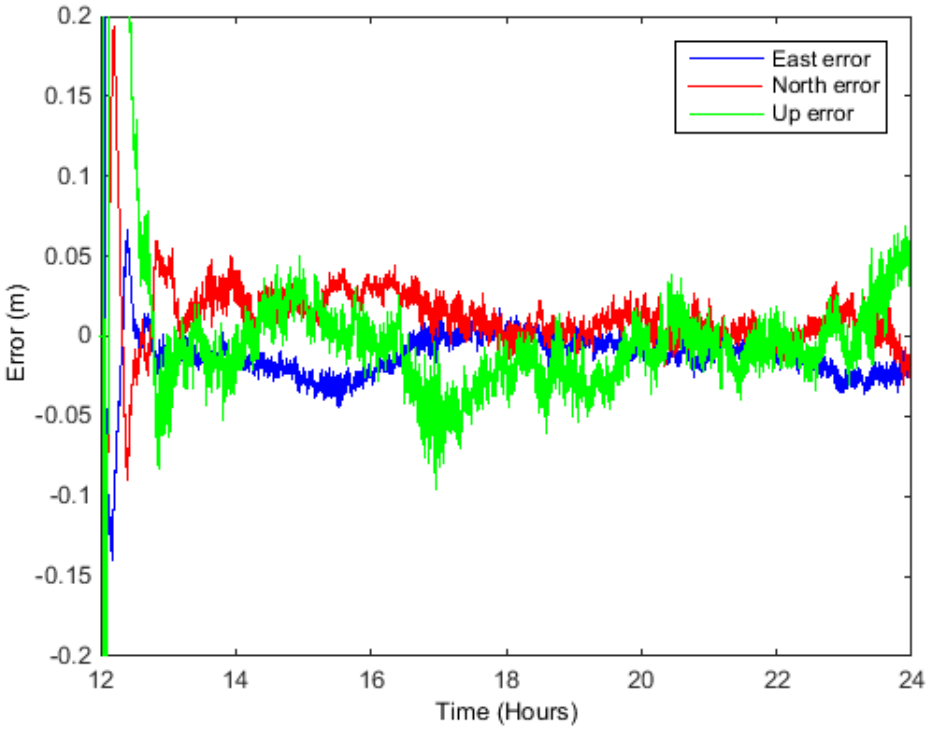

Figure 6-38 - Zhang Rover Positional Errors with Corrections from Four Stations & Alternative Model (DUDE PMTH KEYW WEYB) (DOY 001)

Table 6-27 - Zhang Rover Positional RMS Errors with Corrections from Four Stations & Alternative Model (DUDE PMTH KEYW WEYB)

DOY	East (mm)	North (mm)	Up (mm)	3D (mm)
001	16.2	17.3	23.2	33.1
032	9.0	11.8	19.4	24.4
060	21.2	17.9	28.9	40.1
091	14.2	15.6	25.6	33.2
121	19.3	20.4	27.1	39.0
213	10.1	14.9	21.3	27.9
Average	**15.0**	**16.3**	**24.3**	**33.0**

When the network is increased to include six stations, the RMS values remain similar to the previous four station test at 15.5 mm, 17.2 mm, 23.1 mm and 32.7 mm. The rover position, computed in this test for DOY 001, can be seen in Figure 6-39 and the RMS values in Table 6-28.

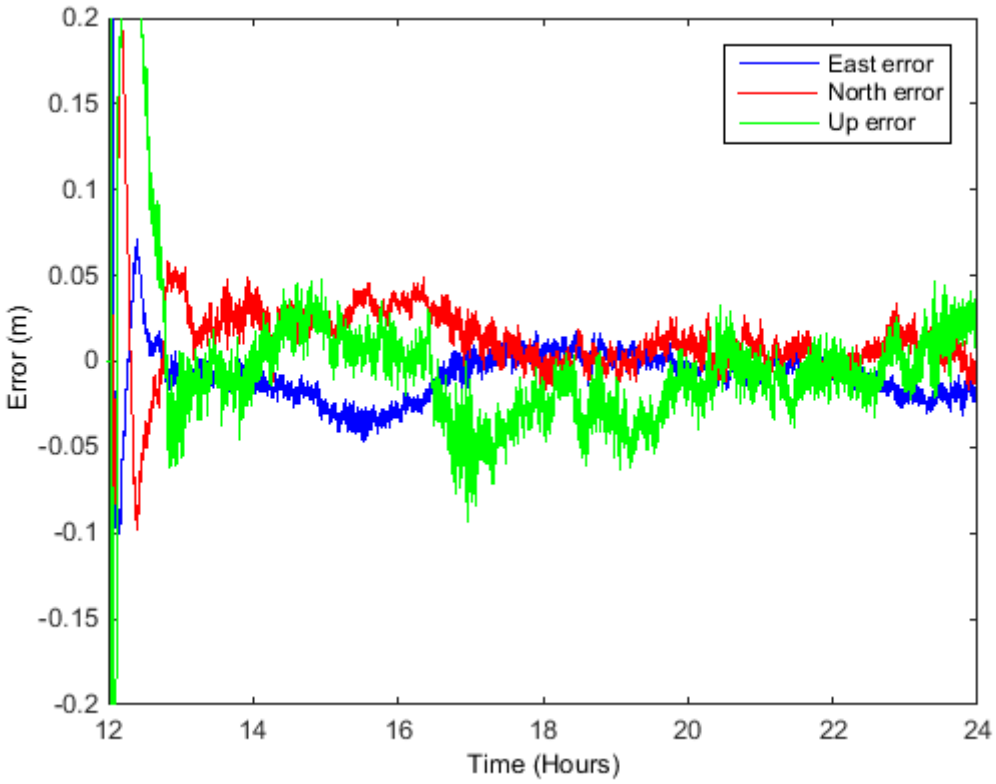

Figure 6-39 - Zhang Rover Positional Errors with Corrections from Six Stations & Alternative Model (DUDE PMTH KEYW WEYB HOLY LOFT) (DOY 001)

Table 6-28 - Zhang Rover Positional RMS Errors with Corrections from Six Stations & Alternative Model (DUDE PMTH KEYW WEYB HOLY LOFT)

DOY	East (mm)	North (mm)	Up (mm)	3D (mm)
001	15.3	18.6	23.5	33.6
032	10.3	12.1	19.1	24.9
060	19.2	17.6	26.7	37.3
091	17.2	21.0	22.3	35.1
121	18.5	19.6	26.1	37.5
213	12.3	14.5	20.6	28.0
Average	**15.5**	**17.2**	**23.1**	**32.7**

The three tests undertaken using this alternative measurement model, provide the results shown in Table 6-29. Similar to the results from the tests on the measurement model developed in this study, there is an improvement when more stations are included. However, there is little improvement when increasing the network from four to six. This shows that the measurement model developed in the Zhang study may not have the same correlation problem between parameters that exist in this study. Consequently, it appears that four stations is sufficient to achieve an optimum solution, as increasing to six stations has a minor deterioration in the results.

Table 6-29 - RMS for Zhang Methodology

	Two Regional Stations	Four Regional Stations	Six Regional Stations
East (mm)	16.1	15.0	15.5
North (mm)	19.3	16.3	17.2
Up (mm)	26.7	24.3	23.1
3D (mm)	37.1	33.0	32.7

It is important to compare the Zhang results to those in this study. Table 6-30 shows how the 3D RMS values computed in these three tests, compare to those achieved in section 6.6, using the same network stations. In all three comparative tests the methodology developed in this thesis outperformed the Zhang approach when comparing user accuracies. Additionally, the percentage of improvement that can be seen increases with the number of stations that were used in the network. A 4% difference in 3D RMS using just two network stations increases to 14% when six stations are used.

Table 6-30 - RMS Comparison between Methodologies

	Pearson	Zhang
Two Stations 3D RMS (mm)	35.8	37.1
Four Stations 3D RMS (mm)	30.2	33.0
Six Stations 3D RMS (mm)	28.6	32.7

6.12.1 PPP-RTK Comparison IAR at the Network

In section 6.9, it was shown that when using the measurement model developed in this study, the fixing of double difference ambiguities at the network had a detrimental effect on the user solution. However, in the Zhang method being compared, it has been demonstrated that fixing ambiguities can have a positive effect on the solution (Zhang *et al.*, 2011). Therefore, this section will test if a comparable solution can be achieved using the same data as in the previous tests.

To allow direct comparisons, the same two, four and six station networks were processed. The settings used within the Kalman filter and within the LAMBDA program were the same as in section 6.9.

The rover results when using corrections from the two station fixed network are presented in Figure 6-40 and Table 6-31. In this test the ambiguity fixed percentage is 40%. The corresponding RMS values were 25.7 mm, 29.1 mm, 43.2 mm and 58.1 mm. When this is compared to the 16.1 mm, 19.3 mm, 26.7 mm and 37.1 mm when using the same two network stations and not fixing ambiguities, IAR at the network adversely affects the solution, as it did in the tests for the measurement model in this study.

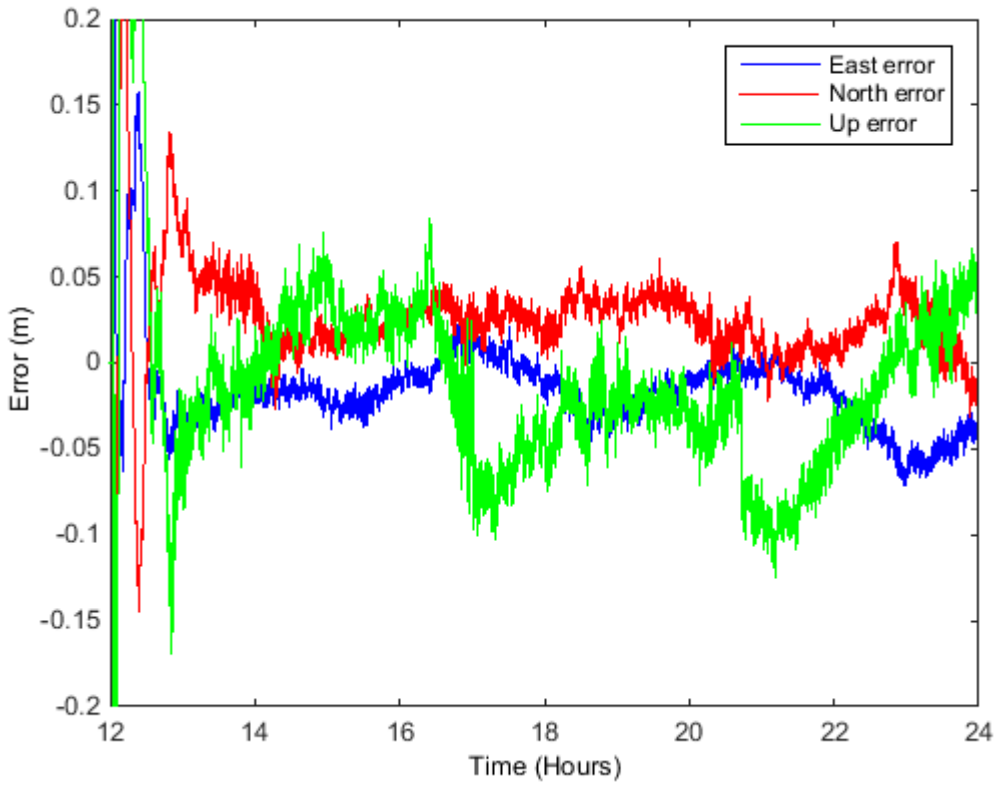

Figure 6-40 - Zhang Rover Positional Errors with Corrections from Two Station Fixed Network (DUDE PMTH) (DOY 001)

Table 6-31 - Zhang Rover Positional RMS Errors with Corrections from Two Station Fixed Network (DUDE PMTH)

DOY	East (mm)	North (mm)	Up (mm)	3D (mm)
001	25.7	29.1	43.2	58.1
032	12.7	13.9	22.3	29.2
060	20.2	31.5	44.7	58.3
091	23.5	19.4	34.5	46.0
121	27.3	24.1	38.9	53.3
213	19.0	28.3	41.8	53.9
Average	**21.4**	**24.4**	**37.6**	**49.8**

The results for the four and six station fixed networks are presented in Figure 6-41 and Figure 6-42. The ambiguity fixed percentages for these tests are 44% and 42% respectively. The average RMS values for these results were 15.7 mm, 20.9 mm, 24.7 mm and 36.1 mm for the four station network and 15.5 mm, 21.4 mm, 23.2 mm and 35.4 mm for the six station network, as shown in Table 6-32 and Table 6-33. These values are an approximate 37% improvement compared to the two station network, as would be expected, due to the increased redundancy. However, as in the two station test, these results are inferior to those presented for the float solution in section 6.12.

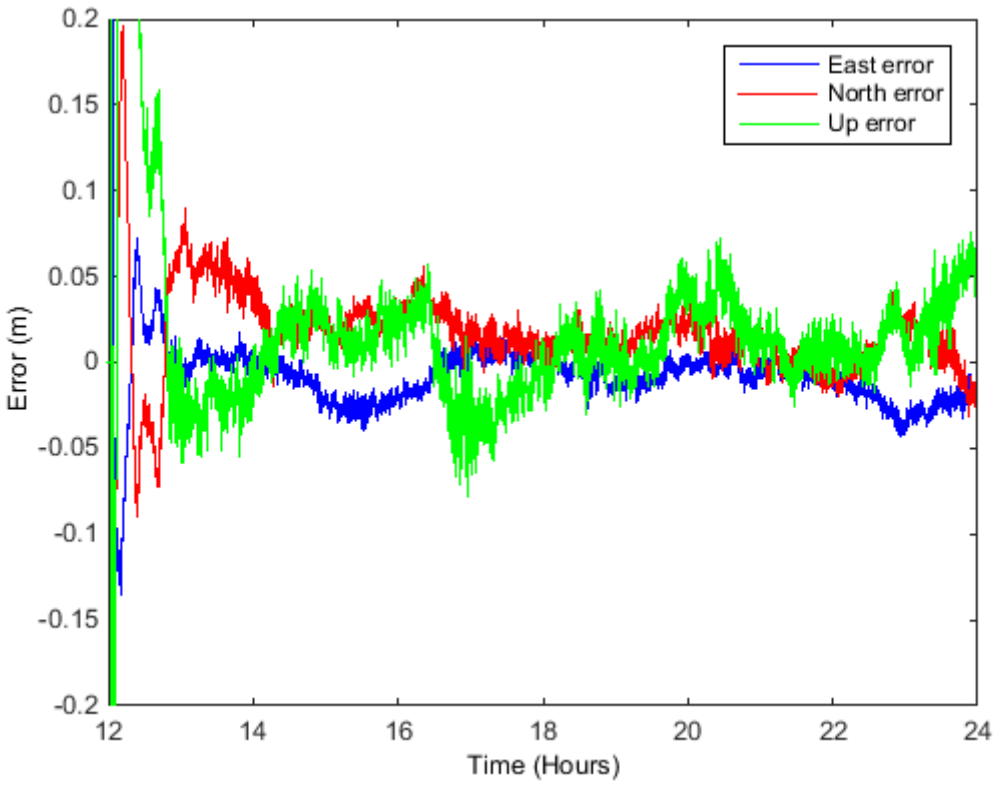

Figure 6-41 - Zhang Rover Positional Errors with Corrections from Four Station Fixed Network (DUDE PMTH KEYW WEYB) (DOY 001)

Table 6-32 - Zhang Rover Positional RMS Errors with Corrections from Four Station Fixed Network (DUDE PMTH KEYW WEYB)

DOY	East (mm)	North (mm)	Up (mm)	3D (mm)
001	14.6	24.7	24.8	38.0
032	10.6	17.4	21.4	29.5
060	21.4	19.2	21.6	35.9
091	18.2	22.9	29.8	41.8
121	15.6	19.7	25.2	35.6
213	13.7	21.2	25.3	35.7
Average	15.7	20.9	24.7	36.1

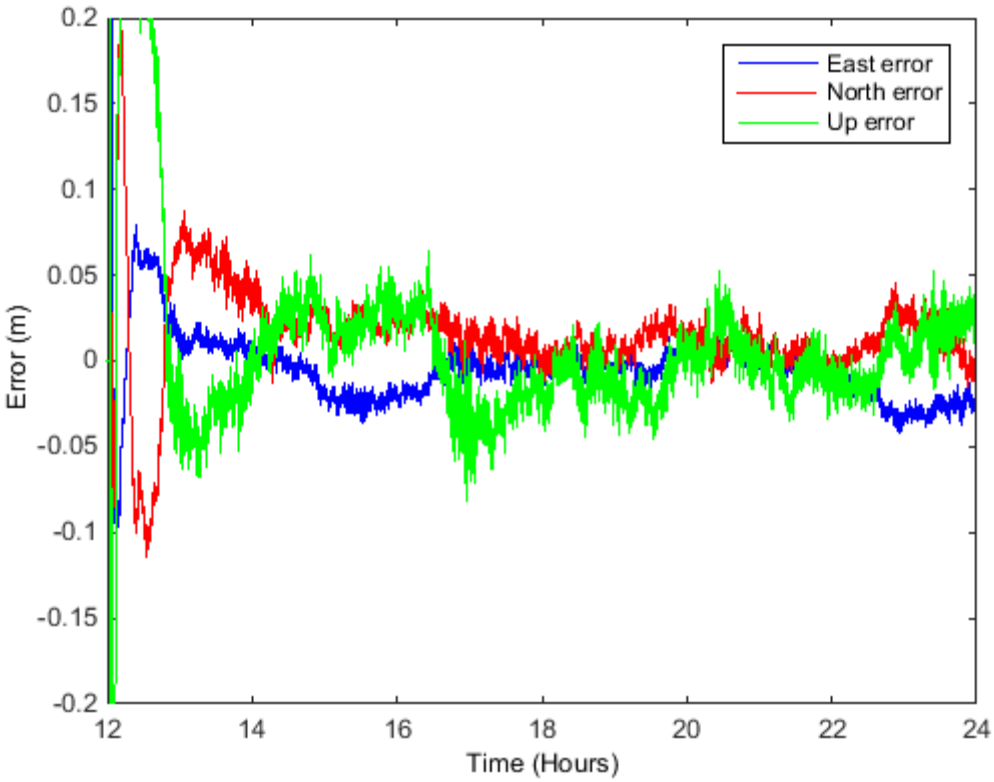

Figure 6-42 - Zhang Rover Positional Errors with Corrections from Six Station Fixed Network (DUDE PMTH KEYW WEYB HOLY LOFT) (DOY 001)

Table 6-33 - Zhang Rover Positional RMS Errors with Corrections from Six Station Fixed Network (DUDE PMTH KEYW WEYB HOLY LOFT)

DOY	East (mm)	North (mm)	Up (mm)	3D (mm)
001	14.5	23.9	23.4	36.5
032	10.6	16.7	22.0	29.6
060	21.1	20.3	18.6	34.7
091	18.1	26.3	29.1	43.2
121	16.1	21.3	24.5	36.2
213	12.7	19.8	21.6	31.9
Average	15.5	21.4	23.2	35.4

6.12.2 PPP-RTK Comparison IAR at the User

To compare how well the Zhang measurement model compares to the model in this study when undertaking IAR at the kinematic rover, two further tests will be undertaken. The six station networks that have been calculated, when ambiguities have been fixed and when they remain float, will be used to attempt an ambiguity fixed user solution.

The results presented in Figure 6-43 and Table 6-34 use the six station float network. It is clear that the rover position has deteriorated as a result of attempting to undertake IAR. In this test, 35% of the ambiguities were fixed. The average RMS values of 17.8 mm, 18.2 mm, 25.1 mm and 36.3 mm show that error in east, north, up and 3D has deteriorated by approximately 3% compared to the float solution using the same corrections.

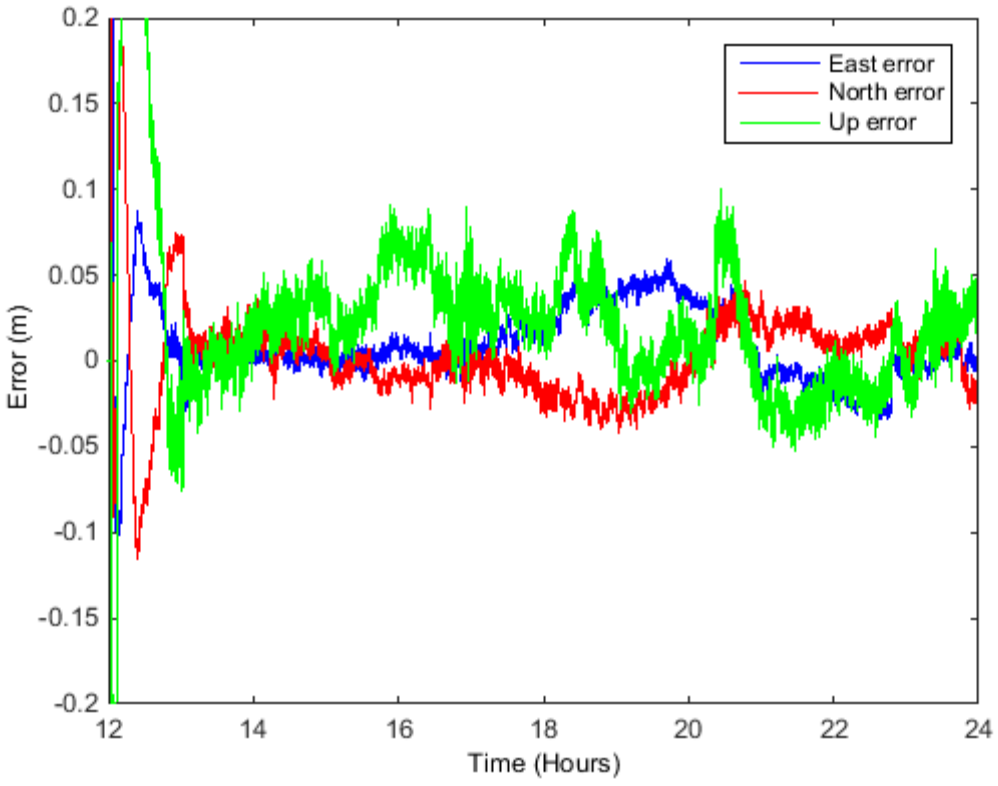

Figure 6-43 - Zhang Fixed Rover Positional Errors with Corrections from Six Station Network (DUDE PMTH KEYW WEYB HOLY LOFT) (DOY 001)

Table 6-34 - Zhang Fixed Rover Positional RMS Errors with Corrections from Six Station Network (DUDE PMTH KEYW WEYB HOLY LOFT)

DOY	East (mm)	North (mm)	Up (mm)	3D (mm)
001	23.7	21.2	33.4	46.1
032	10.2	13.9	18.8	25.5
060	19.0	17.7	24.8	35.9
091	21.3	19.2	28,9	40.7
121	17.8	16.4	21.8	32.6
213	14.5	20.7	26.9	36.9
Average	**17.8**	**18.2**	**25.1**	**36.3**

The ambiguity fixed rover position when using the six station fixed network can be seen in Figure 6-44 for DOY 001 and Table 6-35. The RMS values for these results were 18.3 mm, 20.2 mm, 31.1 mm and 41.6 mm when 34% of the ambiguities were fixed. These results show deterioration compared to when using the six station float network in the previous test, approximately 15%, and when using a fixed six station network solution but a float user, approximately 18%.

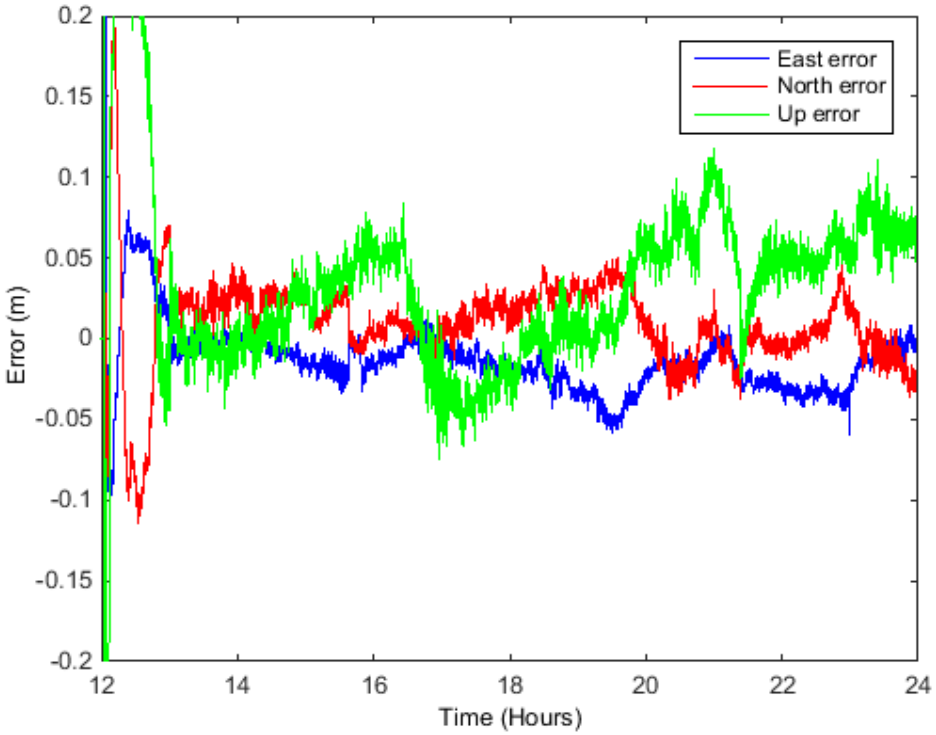

Figure 6-44 - Zhang Fixed Rover Positional Errors with Corrections from Six Station Fixed Network (DUDE PMTH KEYW WEYB HOLY LOFT) (DOY 001)

Table 6-35 - Zhang Fixed Rover Positional RMS Errors with Corrections from Six Station Fixed Network (DUDE PMTH KEYW WEYB HOLY LOFT)

DOY	East (mm)	North (mm)	Up (mm)	3D (mm)
001	21.4	19.7	44.4	53.1
032	11.0	16.9	24.4	31.7
060	21.6	20.7	25.8	39.5
091	18.5	23.4	31.2	43.2
121	20.4	22.4	35.6	46.7
213	16.8	18.3	25.1	35.3
Average	**18.3**	**20.2**	**31.1**	**41.6**

These tests show that, as with the approach developed in this study, the Zhang approach does not provide an improvement with IAR. Instead, at the rover, the results are better when ambiguities are left as float values. This is contrary to what is shown in literature (Zhang *et al.*, 2011).

There could be a number of reasons why both methods have been unable to reliably fix integer ambiguities. Firstly, the data obtained from BIGF may contain some additional errors, which cause the ambiguities to be incorrectly estimated. However, this is unlikely as various stations have been used and there is no metadata indicating any problems with the data.

Secondly, the process noise values applied in the Kalman filter may be incorrect and result in parameter estimates that are under or over constrained. However, various values have been tested throughout this study based on existing literature, as discussed in section 4.3.3.3. The values used in these tests were found to provide the best results.

Thirdly, the fixing of the ambiguity parameters to integers, in the LAMBDA program, may be causing errors. Settings, such as the critical value, affect the number of ambiguities fixed and hence affect the potential accuracy. Various critical values have been tested and the ones used here provided the most realistic solutions.

Finally, the manner in which the remaining parameters are updated after IAR could introduce errors. As previously discussed, if the ambiguity parameters change on the L1 and L2 frequencies and they are not in the ratio of 1:1.649, unrealistic jumps in other parameters, such as the troposphere can occur. This could lead to errors in the estimation of parameters after undertaking IAR.

This alternative PPP-RTK approach was previously tested with a four station network in China, with interstation distances of 60 – 100 km and a 30 sec sampling rate. During the Zhang approach, ambiguity fixed positioning achieved accuracies of about 1 cm and 5 cm for the horizontal and vertical components respectively. While ambiguity float positioning accuracies were in the range of 2 – 4 dm (Zhang *et al.*, 2011). The results presented in this thesis during ambiguity float testing, show similar accuracies to the ambiguity fixed positioning outlined in the previous Zhang study.

However, as discussed, the improvement shown when undertaking IAR could not be replicated.

6.13 PPP-RTK Comparison Results Summary

Table 6-36 shows a summary of the 3D RMS results presented in section 6.12. These results show that increasing the number of stations in the network has a positive impact on the accuracy of the user position. However, IAR has a negative effect on the solution.

Table 6-36 - PPP-RTK Comparison Summary of Results

	3D RMS (mm)
Two Regional Stations	37.1
Four Regional Stations	33.0
Six Regional Stations	32.7
Two Fixed Regional Stations	49.6
Four Fixed Regional Stations	36.1
Six Fixed Regional Stations	35.4
Six Regional Stations – Fixed User	36.3
Six Fixed Regional Stations – Fixed User	41.6

Chapter 7. Conclusions and Future Work

This study set out to present a novel method for computing high rate UPD and satellite clock corrections from a network of reference receivers. It was then anticipated that these corrections could then be used to improve the position estimates of an unknown kinematic receiver. By using these corrections the ambiguities at the kinematic rover receiver should become integer in nature. Therefore, allowing IAR and consequently a further improvement in the position estimate of the unknown rover.

7.1 Conclusions

Chapter 6 outlined the results of a number of tests, which showed that it is possible to compute satellite clocks and UPDs simultaneously, using a large regional network of reference stations. Using these computed values as corrections at a rover site also showed that using these corrections provides an improvement to the rover position estimate, compared to using IGS final orbits alone and no UPDs. This is a major advance and of real benefit to the offshore community, as it could realise potentially faster centimetre level precision, on a global scale.

PPP requires precise satellite orbits and clocks. The orbits are derived by a number of external agencies and can be predicted ahead by 12 hours due to the long wavelength characteristics of orbital perturbations. However, availability of real-time clocks is more of an issue. The IGS provide a real-time service but this is not guaranteed nor is its integrity ensured. An offshore provider needs in-house capability to provide real-time GNSS clocks. The fact they can be computed along with UPDs, for transmission to customers, will have highly significant impact.

Section 6.6 showed that the number of stations used to compute the UPD and satellite clock corrections can have an impact on the results. It has been determined that at least four stations are required in the network to compute accurate corrections, which will provide a benefit to the rover positon. However, increasing the number of stations to six provides a further 5% improvement compared to four stations. Once the number of stations included in the network has reached six, little improvement can be seen by adding further stations. The six station network

provided RMS values for the rover position of 11.1 mm, 12.7 mm, 22.9 mm and 28.6 mm in east, north, up and 3D respectively.

The tests in section 6.4 confirmed that the distance between the network stations does not have a negative impact on the kinematic rover's position. Using a six station local network, with interstation distances of approximately 150 km, provided RMS values of 13.4 mm, 13.0 mm, 24.2 mm and 31.2 mm in east, north, up and 3D. Therefore, these results are actually 9% inferior to the six station regional test. For many applications, it will not be possible to have such a dense network so close to the rover, so it is important that it does not have a detrimental effect on the result.

Further testing showed that it is also beneficial to locate the rover centrally within the network. However, as the number of stations in the reference network is increased, the location of the user becomes less important to the accuracy of the position. Hence, there was 23% deterioration in the rover position solution when the user was located outside of the network when using a six station network compared to 60% when using a four station network.

If the methods proposed here were to be used to provide corrections to users in real time, it is important that the system is robust. One factor to this is that the system must be capable of losing the observations from one or more stations, while continuing to seamlessly compute satellite clock and UPD corrections. Tests showed that it is possible to continue computing the corrections. However, it must be noted that due to the reduction in observations and therefore the decrease in redundancy, the accuracy of the corrections may be negatively affected.

One main objective of the project was to improve both the accuracy of the corrections and the user position using IAR. However, multiple tests have shown that this has not been possible using the existing program. In all tests undertaken at the network and user components the fixing of ambiguities to integer values had a negative effect on the rover position. Potentially, there were multiple reasons for this deterioration, which were set out in section 6.9. However, in this instance, it is unclear what the exact reason for the failure is. Therefore, this is one area where further work would be required to improve the application of this study.

Comparisons with a similar PPP-RTK approach (Zhang *et al.*, 2011) were made in section 6.12. These showed that when undertaking ambiguity float solutions on both approaches, the measurement model developed in this study performed favourably. For the same six station network, the measurement model presented in this study performed over 14% better when the RMS values were compared.

During the comparisons with the alternative PPP-RTK approach, IAR was also undertaken on this measurement model. The ability to undertake IAR had already been proven to be possible using a four station network in China. However, the positive impact that would be expected when undertaking IAR could not be replicated. Undertaking IAR on this approach had the same negative impact on the results, as occurred when undertaking IAR on the measurement model developed in this study.

A further aim of the project was to develop an approach that could result in similar convergence times to those in existing approaches. Existing approaches have convergence times of several tens of minutes at a mobile receiver (Laurichesse *et al.*, 2008; Mervart *et al.*, 2008; Geng *et al.*, 2011). During testing of the approach in this study, a convergence time of one hour was assumed for all tests to allow comparable statistics to be computed. In some cases, such as when corrections were computed from just a two station network, the convergence time required nearly the full hour to create a fully converged solution. However, in other tests when additional network stations were used, the convergence time was reduced, to approximately 45 minutes. Further work could lead to improved process noise values, which could in turn improve the convergence. In addition, the reliable undertaking of IAR could reduce convergence times, if explored further in the future.

7.2 Future Work

There are a number are factors that could further improve this study. Some of these are elements of the study that currently could be improved upon and others are factors that have been beyond the scope of this study.

Firstly, the successful integration of IAR has not been possible. One reason for this may be the unsophisticated error detection within the program. DIA is used to detect if each observation fits to the parameter estimates. However, there are no tests to

see if ambiguities have been correctly fixed to integers, once they have been initially fixed. This means if the ambiguities are incorrectly fixed, they will remain so until the satellite disappears from view. More sophisticated software has a second Kalman filter running alongside the initial filter, which permanently runs an ambiguity float solution. This can be used to constantly check if the ambiguities in the primary Kalman filter have been correctly fixed.

Secondly, as previously mentioned the convergence time for the rover solution is sub optimal, compared to similar existing methods. It is likely that this can be improved upon, especially if the successful integration of IAR can be undertaken. Further testing with different process noise values may also lead to small improvements to the convergence times of the user solution.

Thirdly, the testing undertaken in Chapter 6 showed that the satellite clock and UPD corrections can be computed and transmitted over 100s of km. If the network of reference stations could be increased sufficiently across the globe, it would theoretically be possible to compute a global solution. This global set of UPD and satellite clock estimates could then be used to correct a rover position anywhere on the globe. However, testing would have to be done to assess the level of accuracy these corrections could achieve. Additionally, if this approach was taken, the amount of computational power required to process a global set of network stations would have to be considered.

One benefit of the methodologies presented in this study is the use of the L1 and L2 frequencies independently, instead of the LC linear combination. By using these GPS frequencies separately, the integration of additional frequencies becomes easier. The L5 frequency that is currently being phased into the GPS constellation, would deliver additional observations and redundancy to the measurement model, therefore providing the potential for increased accuracy. Further to this, additional GNSS, such as Galileo, could be utilised easily with their frequencies added to the measurement model. This would result in the receivers in the network and at the user, receiving observations from more satellites. Consequently, adding further redundancy to the measurement model.

Finally, all the testing undertaken in this study has used static GNSS sites acting as a kinematic rover, to allow the accuracy of the corrections to be easily testing against

the known truth. However, to fully test the methodology's capability to correct a kinematic rover receiver, observations would have to be collected for a kinematic receiver. If the true position of the kinematic receiver could be computed, this could subsequently be tested against the GPS computed rover solution.

References

Allinson, C. (2012) *Hydrofest*. Available at: http://www.ths.org.uk/documents/ths.org.uk/downloads/hydrofest_2012_(1)_overview_-_survey_support_in_the_o&g_industry.pdf.

Awange, J.L. (2012) 'Environmental monitoring using GNSS global navigation satellite systems'. New York ; London: New York ; London : Springer.

Bertiger, W., Desai, S.D., Haines, B., Harvey, N., Moore, A.W., Owen, S. and Weiss, J.P. (2010) 'Single receiver phase ambiguity resolution with GPS data', *Journal of Geodesy*, 84(5), pp. 327-337.

Blewitt, G. (1989) 'Carrier Phase Ambiguity Resolution for the Global Positioning System Applied to Geodetic Baselines up to 2000 Km', *Journal of Geophysical Research-Solid Earth and Planets*, 94(B8), pp. 10187-10203.

Bona, P. (2000) 'Accuracy of GPS phase and code observations in practice', *Acta Geodaetica et Geophysica Hungarica*, 35(4), pp. 433-451.

Clarke, P.J. and Penna, N.T. (2010) 'Ocean Tide Loading and Relative GNSS in the British Isles', *Survey Review*, 42(317), pp. 212-228.

Dai, L., Wang, J., Rizos, C. and Han, S. (2003) 'Predicting atmospheric biases for real-time ambiguity resolution in GPS/GLONASS reference station networks', *Journal of Geodesy*, 76(11), pp. 617-628.

de Jong, C.D. (2013) *Satellite clocks and UPDs*. Fugro Intersite, Internal Document.

de Jong, K., Goode, M., Liu, X. and Stone, M. (2016) 'New Developments in Precise Offshore GNSS Positioning', in Zerr, B., Jaulin, L., Creuze, V., Debese, N., Quidu, I., Clement, B. and Billon-Coat, A. (eds.) *Quantitative Monitoring of the Underwater Environment: Results of the International Marine Science and Technology Event MOQESM´14 in Brest, France*. Cham: Springer International Publishing, pp. 3-12.

De Jonge, P. and Tiberius, C. (1996) 'The LAMBDA method for integer ambiguity estimation: implementation aspects', *Publications of the Delft Computing Centre, LGR-Series*, 12(12), pp. 1-47.

Dekkiche, H., Kahlouche, S. and Abbas, H. (2010) 'Differential ionosphere modelling for single-reference long-baseline GPS kinematic positioning', *Earth, planets and space*, 62(12), pp. 915-922.

Doherty, P., Raffi, E., Klobuchar, J. and El-Arini, M.B. (1994) *Proceedings of ION GPS-94, part*.

Fang, P., Bevis, M., Bock, Y., Gutman, S. and Wolfe, D. (1998) 'GPS meteorology: Reducing systematic errors in geodetic estimates for zenith delay', *Geophysical Research Letters*, 25(19), pp. 3583-3586.

Fugro (2017) *Starfix*. Available at: https://www.fugro.com/our-services/marine-asset-integrity/satellite-positioning/starfix (Accessed: 12/4/17).

Ge, M., Gendt, G., Rothacher, M., Shi, C. and Liu, J. (2008) 'Resolution of GPS carrier-phase ambiguities in Precise Point Positioning (PPP) with daily observations', *Journal of Geodesy*, 82(7), pp. 389-399.

Geng, J., Meng, X., Teferle, F. and Dodson, A. (2010a) 'Performance of precise point positioning with ambiguity resolution for 1 to 4 hour observation periods', *Survey Review*, 42(316), pp. 155-165.

Geng, J., Shi, C., Ge, M., Dodson, A., Lou, Y., Zhao, Q. and Liu, J. (2012) 'Improving the estimation of fractional- cycle biases for ambiguity resolution in precise point positioning', *Journal of Geodesy*, 86(8), pp. 579-589.

Geng, J., Teferle, F.N., Meng, X. and Dodson, A.H. (2011) 'Towards PPP-RTK: Ambiguity resolution in real- time precise point positioning', *Adv. Space Res.*, 47(10), pp. 1664-1673.

Geng, J.H., Meng, X.L., Dodson, A.H. and Teferle, F.N. (2010b) 'Integer ambiguity resolution in precise point positioning: method comparison', *Journal of Geodesy*, 84(9), pp. 569-581.

Gurtner, W. (2007) *RINEX: The Receiver Independant Exchange Format Version 2.11*. Available at: ftp://igs.org/pub/data/format/rinex211.txt (Accessed: 11/12/17).

Hadas, T. and Bosy, J. (2015) 'IGS RTS precise orbits and clocks verification and quality degradation over time', *GPS Solutions*, 19(1), pp. 93-105.

Hofmann-Wellenhof, B. (2008) *GNSS--global navigation satellite systems GPS, GLONASS, Galileo, and more*. Wien ; New York: Wien ; New York : Springer.

International GNSS Service (2017a) *IGS Product Avaliability*. Available at: https://igscb.jpl.nasa.gov/components/prods_cb.html.

International GNSS Service (2017b) *Products*. Available at: http://www.igs.org/products.

Kalman, R.E. (1960) 'A New Approach to Linear Filtering and Prediction Problems', *Journal of basic engineering.*, 82(1), pp. 35-45.

Kleusberg, A. and Teunissen, P.J.G. (1998) *GPS for geodesy*. 2nd, completely rev. and extended ed.. edn. Berlin ; New York: Berlin ; New York : Springer.

Kouba, J. (2009) *A Guide to Using International GNSS Service Products*.

Kouba, J. and Héroux, P. (2001) 'Precise point positioning using IGS orbit and clock products', *GPS solutions*, 5(2), pp. 12-28.

Laurichesse, D. (2011) 'The CNES Real-time PPP with undifferenced integer ambiguity resolution demonstrator', *Proceedings of the 24th International Technical Meeting of the Satellite Division of the Institute of Navigation (Ion Gnss 2011)*, pp. 654-662.

Laurichesse, D., Mercier, F., Berthias, J. and Bijac, J. (2008) *Proceedings of the 2008 National Technical Meeting of The Institute of Navigation*.

Leick, A. (2015) *GPS satellite surveying*. Fourth edition / Alfred Leick, Lev Rapoport, Dmitry Tatarnikov.. edn. Hoboken : John Wiley & Sons.

Li, P. and Zhang, X. (2014) 'Integrating GPS and GLONASS to accelerate convergence and initialization times of precise point positioning', *GPS Solutions*, 18(3), pp. 461-471.

Li, X.X., Ge, M.R., Zhang, H.P., Nischan, T. and Wickert, J. (2013) 'The GFZ real-time GNSS precise positioning service system and its adaption for COMPASS', *Advances in Space Research*, 51(6), pp. 1008-1018.

Liu, X. (2010) *Global PPP IAR: GFZ approach*. Fugro Intersite, Internal Document.

Lyard, F., Lefevre, F., Letellier, T. and Francis, O. (2006) 'Modelling the global ocean tides: modern insights from FES2004', *Ocean Dynamics*, 56(5), pp. 394-415.

Matsumoto, K., Takanezawa, T. and Ooe, M. (2000) 'Ocean Tide Models Developed by Assimilating TOPEX/POSEIDON Altimeter Data into Hydrodynamical Model: A Global Model and a Regional Model around Japan', *Journal of Oceanography*, 56(5), pp. 567-581.

Melbourne, W. (1985) *Proceedings of the First Symposium on Precise Positioning with the Global Positioning System, Positioning with GPS-1985, Ed. CC Goad, Rockville, Maryland, pub. US Department of Commerce, NOAA*.

Mervart, L., Lukes, Z., Rocken, C. and Iwabuchi, T. (2008) *Proceedings of ION GNSS*.

Odijk, D., Verhagen, S., Teunissen, P., Hernandez-Pajares, M., Juan, J.M., Sanz, J., Samson, J. and Tossaint, M. (2010) *Proceedings of the 2010 International Technical Meeting of the Institute of Navigation*.

Ordnance Survey (2017) *OS Net*. Available at: https://www.ordnancesurvey.co.uk/business-and-government/products/os-net/ (Accessed: 12/4/17).

Øvstedal, O., Kjørsvik, N. and Gjevestad, J. (2006) 'Surveying using GPS precise point positioning', *XXII International FIG Congress, Munich, Germany*.

Sanz Subirana, J., Juan Zornoza, J.M. and Hernandez-Pajares, M. (2011) *Ionosphere-free Combination for Dual Frequency Receivers*. Available at: http://www.navipedia.net/index.php/Ionosphere-free_Combination_for_Dual_Frequency_Receivers.

Sideris, M.G. (2009) *Observing our changing earth*. Springer.

Teunissen, P. (1993) *Invited lecture, section IV theory and methodology, IAG general meeting, Beijing, China*.

Teunissen, P.J. (1994) *Position Location and Navigation Symposium, 1994., IEEE*. IEEE.

Teunissen, P.J. (1995) 'The least-squares ambiguity decorrelation adjustment: a method for fast GPS integer ambiguity estimation', *Journal of geodesy*, 70(1-2), pp. 65-82.

Teunissen, P.J.G., Odijk, D. and Zhang, B. (2010) 'PPP-RTK: Results of CORS network-based PPP with integer ambiguity resolution', *Journal of Aeronautics, Astronautics and Aviation*, 42(4), pp. 223-230.

The University of Nottingham (2017) *BIGF - NERC British Isles continuous GNSS Facility*. Available at: http://www.bigf.ac.uk/ (Accessed: 20/4/17).

Verhagen, S.a.L., B. (2012) *LAMBDA - Matlab implementation version 3.0. Delft University of Technology and Curtin University* [Computer program].

Wanninger, L. (2004) *Introduction to Network RTK*. Available at: http://www.wasoft.de/e/iagwg451/intro/introduction.html (Accessed: 23/6/16).

Wells, D.E., N. Beck, D. Delikaraoglou, A. Kleusberg, E.J. Krakiwsky, G. Lachapelle, R.B. Langley, M. Nakiboglu, K.P. Schwarz, J.M. Tranquilla and P. Vanicek (1986) *Guide to GPS positioning*. Fredericton, New Brunswick: Fredericton, New Brunswick : Canadian GPS Associates.

Xu, G. (2003) *GPS : theory, algorithms, and applications*. New York: New York : Springer.

Zhang, B.C., Teunissen, P.J.G. and Odijk, D. (2011) 'A Novel Un-differenced PPP-RTK concept', *Journal of Navigation*, 64, pp. S180-S191.

Zhang, Y., Wang, Q. and Jiang, X. (2017) 'Property Analysis of the Real-Time Uncalibrated Phase Delay Product Generated by Regional Reference Stations and Its Influence on Precise Point Positioning Ambiguity Resolution', *Sensors*, 17(5), p. 1162.